VIBRATIONAL SPECTROSCOPIC STUDY OF STRUCTURAL PHASE TRANSITIONS IN SOME PEROVSKITE TYPE LAYERED COMPOUNDS

by

PINNELLI SEETHA RAMA PRASAD
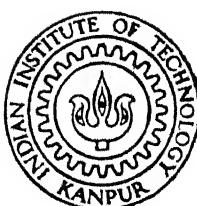
DEPARTMENT OF PHYSICS

INDIAN INSTITUTE OF TECHNOLOGY KANPUR

MAY 1990

VIBRATIONAL SPECTROSCOPIC STUDY OF STRUCTURAL PHASE TRANSITIONS IN SOME PEROVSKITE TYPE LAYERED COMPOUNDS

A Thesis Submitted
in Partial Fulfilment of the Requirements
for the Degree of
DOCTOR OF PHILOSOPHY

by

PINNELLI SEETHA RAMA PRASAD

to the

DEPARTMENT OF PHYSICS

INDIAN INSTITUTE OF TECHNOLOGY KANPUR

MAY 1990

CERTIFICATE

It is certified that the work contained in the thesis entitled **Vibrational Spectroscopic Study of Structural Phase Transitions in Some Perovskite Type Layered Compounds** by Mr Pinnelli Seetha Rama Prasad, has been carried out under my supervision and that this work has not been submitted elsewhere for a degree.

(H D Bist)

May, 1990

Thesis Supervisor
Department of Physics
IIT Kanpur

SYNOPSIS

Name of Student: **PINNELLI SEETHA RAMA PRASAD**   Roll #: **8410966**

Degree for which submitted: **Ph.D**   Department: **Physics**

Thesis Title: VIBRATIONAL SPECTROSCOPIC STUDY OF STRUCTURAL PHASE TRANSITIONS IN SOME PEROVSKITE TYPE LAYERED COMPOUNDS

Name of thesis supervisor: **H D Bist**

Light scattering studies have played an important role in understanding the dynamics of molecules in condensed state of matter. The scattering of light occurs due to the fluctuations in the dielectric tensor of the scattering medium. Near phase transition the fluctuations in some of these quantities are enhanced. This makes light scattering an important tool for the study of structural phase transitions. Infrared, Raman and neutron spectroscopic techniques are complementary and provide an insight into the microscopic origin of structural transitions. Careful measurements of spectral variations in few thermosensitive modes provide useful information about the structure and dynamics near the transition.

Di(alkylammonium) tetrachlorometalates of general formula $(C_nH_{2n+1}NH_3)_2 MCl_4$ where M is a divalent metal ion and n = 1, 2, 3 *etc.*, are known to crystallize in a two dimensional perovskite type layered structure. The planes in these crystals are made up of the corner-shared MCl_6 octahedra and the

alkylammonium ions fill the gaps. The intra-layer interactions are stronger than the inter-layer interactions. These crystals undergo several structural transitions in a wide range of temperature and are mainly due to the reorientational motion of the organic ion. Their structural similarities with phospholipids and the important role of the organic ions in the phase transition sequence have also attracted the attention of bio-physicists. A systematic study of few of the crystals with M = Cd, Zn, Hg are reported in this thesis.

Chapter I of the thesis deals with the introduction to vibrational spectroscopy and phase transitions. The role of the Raman (RS) and infrared (IR) spectroscopic techniques to probe the transitions are briefly reviewed.

A brief description of the Raman and IR instrumentation is given in Chapter II. The design/details of the low/high temperature cells used in the present study are also described. The procedure of estimating the *true widths* from the observed spectra to get the information about the relaxation process is given in this chapter. The adopted procedure to deconvolute the overlapped bands is described at the end of this chapter.

In Chapter III a systematic and detailed study of phase transitions in $(CH_3NH_3)_2MCl_4$ (M = Cd, Zn, Hg) systems (abbreviated as C_1MCl) in the range 80 - 420 K is presented. The tetragonal (TLT) to monoclinic (MLT) transition at 160 K in M = Cd crystal is studied by IR and Raman. In IR spectra, abrupt spectral variations in the CH_3, NH_3 rocking modes (ν_{12}

and ν_{11}) are observed around 160 K indicating the transition. The ν_{12} mode shows an abrupt frequency and linewidth jumps around 160 K while ν_{11} mode is observed to split into two components with a dramatic variation in linewidth. These parameters can well be explained by soft-hard mode coupling model, from which the value of order parameter exponent (β) is calculated to be 0.26 $\pm$ 0.05. Temperature evolution of RS spectra in the CH_3 stretching (ν_2) mode region show a split and the intensity ratio follow an Arrhenius type variation. The calculated activation energy (0.036 eV) is in agreement with NMR results. The change in H-bonding strength is demonstrated by the variations in few IR and Raman modes involving NH_3 groups. The vibrational assignments are proposed using the Raman, IR and FIR spectra in M = Zn and Hg systems at room temperature (RT). The phase transitions are studied by RS and differential scanning calorimetry (DSC)/differential thermal analysis (DTA). The doublet of ν_5 (CN stretching) mode in C_1ZnCl merges at 411 K and the activation energy (0.08 eV), is estimated from the intensity ratio variations. Additionally, the intensity of $\nu(ZnCl)$ stretching mode also decreases corroborating the transition. DTA study of C_1HgCl reveals two transitions at 335 and 432 K. The transition at 335 K is further analyzed by means of RS. The temperature dependence of ν_5 and $\nu(HgCl)$ modes reveal the transition at 335 K. The linewidth variations of these modes seem to be affected by the reorientational motion. The activation energy of 0.13 eV is estimated from the linewidth variations of ν_5. The variations of frequency and reduced peak

intensities of ν_5 mode scales with η and η^2 (η — order parameter) respectively. These observations give a consistent value of $\beta \cong 0.35 \pm 0.04$.

The parent ethylammonium chloride (C_2Cl) and di(ethylammonium) tetrachlorocadmate (C_2CdCl) are studied and the results form Chapter IV of the thesis. Two transitions at 221 and 345 K are reported earlier based on DSC studies in C_2Cl. In the sub-ambient temperature side the translational modes involving halogen ion split near 223 K whereas, $\nu(CC)$ and $\nu(CN)$ modes do not show any anomalies. The linewidths of these modes show linear variation up to 340 K and diverge near 345 K. The entire lattice spectrum disappears around 345 K and reappears on cooling. Broad structure of the observed spectra show that the ethylammonium ions are disordered in high temperature phase. The Raman polarization studies in 20 - 3300 cm^{-1} in C_2CdCl, are used to assign the modes. At RT both the Raman and IR spectra in this compound show many common bands, indicating the effective symmetry of ethylammonium ion as C_s. To probe low temperature transitions, the Raman in X(ZZ)Y polarization and IR (thin crystal) spectra are studied in the range of 100 - 300 K. The anomalous linewidth changes around 216 K, for $\rho(CH_2)$, $\rho(CH_3)$ and $\rho(CH_3)$ (rocking modes) in IR; and $\nu(CC)$ mode in the Raman spectra are attributed to the disorder effects of ethylammonium ion. From the thermal evolution of the linewidths of these modes, the activation energy associated with the transition is calculated to be 0.06 eV, which is consistent with the NMR results. Discontinuous changes in spectral parameters of $\delta(CCN)$

(bending) in the Raman and 1192 cm^{-1} (combinational) mode in IR spectra confirm the first order nature of the transition. Calculated β ($\simeq$ 0.27 ± 0.04) from these variations compares well with the birefringence studies (0.3). The change in H-bonding strength is reflected in IR spectra through the $\delta_{asy}(NH_3)$ + $\tau(NH_3)$ mode.

Chapter V contains the temperature variation studies in propylammonium chloride (C_3Cl) and di(propylammonium) tetrachlorocadmate (C_3CdCl). Two transitions are known at 188 and 408 K from DSC studies in C_3Cl. The Raman spectra of C_3Cl is studied using a powdered sample in the range of 80 - 385 K. Sample changes its colour around 385 K and decomposes. The spectral parameters of $\nu(CC)$ and $\nu(CN)$ modes show dramatic variations around 186 K. A singlet and broad $\nu(CN)$ mode splits into two around the same temperature. The reduced peak intensity of these modes shows a large increase which is proportional to η^2 in 98 - 186 K region. The exponent value is calculated to be 0.35 ± 0.04. The Rayleigh wing decreases and new bands appear corroborating the transition. The Raman spectra in different polarization along with IR spectra are used to assign the modes of C_3CdCl at RT. IR spectra using a thin plate of C_3CdCl are recorded in the rocking and $\delta_{asy}(NH_3)$ + $\tau(NH_3)$ mode region down to 100 K. No strong anomalies are found near 183 K where a transition is reported to occur. Near 158 K rocking modes become sharp and a sudden jump in the combinational mode is observed. At about 113 K where a first order transition is reported to occur, many bands split and

became sharp. At still lower temperature ($\leq$ 113 K) the platelet sample became polycrystalline. The linewidth of ν(CC) mode in **X(ZZ)Y** and **X(YY)Z** polarizations, does not show any exponential increase, like in C_2CdCl, around 158 K where a order-disorder transition occurs. The linewidth shows a linear variation in this temperature range. The librational mode of the propylammonium ion also shows similar changes. These results suggest that the dominant process for the transition may not be ordering of propylammonium ion in C_3CdCl. The transition at 113 K has been characterized by a split in ν(CC) mode along with many newly appeared lattice modes.

It is concluded from the present study that the SPTs in $(C_nH_{2n+1}NH_3)_2MCl_4$ type family of crystals are mostly due to the reorientational motion of alkylammonium ions. A careful study of certain thermosensitive modes has provided useful information regarding the transition mechanism. The scope for the future work along with the generalities deduced from the present study have been discussed in Chapter VI.

ACKNOWLEDGMENTS

To
my parents

TABLE OF CONTENTS

CHAPTER II

EXPERIMENTAL

CHAPTER III

VIBRATIONAL SPECTROSCOPIC STUDY OF STRUCTURAL PHASE TRANSITIONS
IN $(CH_3NH_3)_2MCl_4$ CRYSTALS: M = Cd, Zn AND Hg

CHAPTER V

VIBRATIONAL SPECTROSCOPIC STUDY OF $C_3H_7NH_3Cl$ AND $(C_3H_7NH_3)_2CdCl_4$ CRYSTALS

Phase Transitions

CHAPTER VI

CONCLUDING REMARKS

LIST OF TABLES

LIST OF FIGURES

CONCEPTS OF VIBRATIONAL SPECTROSCOPY AND PHASE TRANSITIONS IN SOLIDS

1.0 GENERAL

Existence of matter in its different states *i.e.*, gaseous, liquid, solid or plasma is determined by the forces acting on its constituent entities. A precise knowledge of both inter- and intra-molecular forces in the matter is required to solve a wide variety of problems in Physics, Chemistry and Biology. These interactions determine the properties of the matter. Thermodynamic and kinetic studies essentially delineate the bulk properties. However, spectroscopic techniques elucidate the properties of the individual entities [1,3]. The molecules in a solid are different from those in a gas. They occupy relatively fixed positions in the crystal and produce many variations in their properties. Vibrational spectroscopy opens a channel of studying the molecular arrangements in solids. The lineshape analysis of both the Raman and infrared spectra, though difficult to interpret, contains valuable information about the dynamical nature [4,5].

Under the influence of external parameters like temperature and pressure the equilibrium configuration of the

matter may be disturbed and ultimately may transform into another phase. The most fascinating aspect of phase transitions is that the condensed phase breaks the inherent symmetry of the problem *i.e.*, the system becomes less symmetric at lower temperatures. Phase transitions are not simply marked by a sudden onset of a new phase, but they exhibit anomalies both in thermodynamic and response functions in the critical region [6,8]. Within the solid phase, matter exists in different symmetries at various temperature and pressures. These changes mainly occur because of the variations in their molecular arrangements. The modes which vanish at T_c (called *soft modes*) proved convenient and attractive to characterize the transitions through spectroscopic techniques. Additionally, certain other modes could split and/or new modes could appear during the phase changes. A careful spectral measurements of such modes are helpful in understanding the nature of phase transitions [9,12].

1.1 CLASSIFICATION OF SOLIDS

Solids are broadly classified as *crystalline* and *amorphous*. In solids the constituent atoms/molecules execute small vibrations about their equilibrium positions called crystal sites. In crystalline solids the arrangement under thermal equilibrium must be regular. However, in amorphous solids they vibrate about randomly situated points, representing a metastable state. Eventually, they must become crystalline. However, because of

the large relaxation times the amorphous solids behave as if they are stable for an almost unlimited time. The fact that a sharp melting point does not exist for amorphous solids, distinguishes the two kinds of solids broadly [13,15].

Usually the crystalline solids are divided into four categories based on the extent of loss of molecular identity. Only salient features of each kind are described below.
(i) Complete non-existence of identity of the constituent molecules form a class of crystals known as *metallic* crystals. The metals usually absorb the infrared radiation. (ii) The other extreme class of crystals in which to a good approximation, the individual identity is retained are known as *van der Waals* crystals. The internal vibrations of the constituent molecules undergo little variations under condensation in these crystals. The presence of the weak inter-molecular interactions could be seen in the lattice modes. The lattice motions can arise either from quasi-translational or quasi-rotational motions of molecular groups. They usually occur at low frequencies, quite separated from that of the internal modes. (iii) The third class of solids which fall in the middle of above two are known as *covalent* or *ionic* crystals. In covalent crystals, electron pair establishes a bond between each pair of the neighbouring nuclei. If one of the nuclei has more electron affinity, the electron bond pair will have the proportionate polarity. In the extreme case, if the electron pair is localized towards one member in the bond, it gives rise to what is known as *ionic* nature of the crystal. (iv) The fourth class of crystals which

do not fit well with the above classification are the *Hydrogen-bonded* crystals possessing some important properties. In these crystals, bonding involves three-centers, out of which one is of proton and the other two could be same or different nuclei. The nature of hydrogen bonding has been well understood.

1.2 CLASSIFICATION OF MOLECULAR MOTION

The classification of molecular vibrations in a crystal using group theoretical methods is well known [16-21]. Two such approaches are briefly described in the following.

1.2.1 Unit Cell Approach

It is the first method developed by Bhagavantam and Venkatarayudu, which provides a systematic classification of molecular vibrations in solid state [22,23]. According to this model, the unit cell of the crystal is treated as a giant molecule. The space group operations are applied in order to classify the modes. The classification of 3nN degrees of freedom of the crystal which contains n molecules in its unit cell has been reduced to 3N modes of the unit cell. It is based on the assumption that the atoms/molecules situated at an equivalent lattice sites in different unit cells will be in same

state of motion without any phase difference. But one should have complete knowledge about the arrangement of atoms in the unit cell. For example, the modes of methylammonium ion under point group symmetry C_{3v} classified using this method are summarized in Table 1.1.

1.2.2 Site Symmetry Approach

The unit cell approach becomes troublesome while dealing with a unit cell containing a large number of atoms. One can overcome this difficulty by using the site symmetry approach put forth by Halford and Horning [24,25], which is simpler. Utility of this approach depends on the selection of the site group [26]. It is chosen in such a way that it should be a sub-group of both the free ion and factor groups. After knowing the normal mode distribution in the free ion symmetry group, it is correlated to the factor group using the standard correlation tables [21,27]. In this thesis this method is extensively used.

1.3 VIBRATIONAL SPECTRA

Vibrational spectroscopy has been a standard method to study the molecular structure. Even though the subject is very old, still there is a lot of interest [28,32]. Basic concepts of the process and the influence of anharmonicity and Fermi resonance on the spectral profiles are briefly described here.

A system absorbs (or emits) radiation by virtue of periodic changes in its dipole moment. The frequency of absorption is equal to that of the oscillating dipole and lies in the infrared region. So, the crystal can absorb the incident radiation whenever the frequency matches with that of the normal mode frequency. The dipole moment is generally a function of normal coordinates (Q_k) and can be expanded in Taylor series as,

$$\mu = \mu_o + \sum (\partial\mu/\partial Q_k)_o \, Q_k + \sum (\partial^2\mu/\partial Q_k \partial Q_l)_o \, Q_k Q_l + \qquad 1.1$$

where μ_o is the permanent dipole moment. The Einstien summation convention is followed in the thesis for simplicity. Assuming that the contribution from the higher order terms in Q is small, then eqn 1.1 can be written as,

$$\mu = \mu_o + \sum (\partial\mu/\partial Q_k)_o \, Q_k \qquad\qquad 1.2$$

The transition moment from a state i to f with eigen functions ψ_i and ψ_f can be defined as,

$$\mu_{if} = \int \psi_i \, \mu \, \psi_f \, d\tau . \qquad\qquad 1.3$$

Substituting eqn 1.2 in eqn 1.3, we get

$$\mu_{if} = \mu_o \int \psi_i \, \psi_f \, d\tau + \sum \left\{ (\partial\mu/\partial Q_k)_o \int \psi_i \, Q_k \, \psi_f \, d\tau \right\} \qquad 1.4$$

using the properties of Hermite Polynomials, infrared absorption is permissible if, and only if, the vibrational quantum number (Δv_k) of all but one of the normal modes must remain unchanged and that of the remaining should change by unity. Further, $(\partial\mu/\partial Q_k)_o$ should be non-vanishing. These selection rules are restrictive in the sense that their derivation is based on the assumptions that (i) system is a collection of simple harmonic oscillators and (ii) μ can be expanded as a Taylor series. But in a real system these assumptions are not valid strictly.

1.3.2 RAMAN SCATTERING

A complementary method to IR absorption is the Raman scattering. The incident field (E) produces an induced polarization (P) which is responsible for the process. P and E are related by,

$$P = \alpha E \qquad 1.5$$

where α is a polarizability tensor. Recalling the two earlier assumptions of § 1.3.1, α can be expanded in Taylor series as,

$$\alpha = \alpha_o + \sum(\partial\alpha/\partial Q_k)_o \, Q_k + \sum(\partial^2\alpha/\partial Q_k \partial Q_l)_o \, Q_k \, Q_l + \dots \qquad 1.6$$

$$\rightarrow P = \alpha_o \cdot E + \sum \left\{ (\partial\alpha/\partial Q_k)_o \, Q_k \right\} \cdot E + \dots \qquad 1.7$$

Since α_o is a simple molecular constant, first term represents a condition where P oscillates at the frequency ν_o like E which leads to Rayleigh scattering. The next term contributes to Raman scattering. So, one obvious condition is that $(\partial\alpha/\partial Q_k)_o$ should be non-zero. Now the transition moment is defined as,

$$P_{if} = \int \psi_i \, P \, \psi_f \, d\tau$$
$$= E \sum (\partial\alpha/\partial Q_k)_o \int \psi_i \, Q_k \, \psi_f \, d\tau \qquad 1.8$$

which gives non-zero contribution for $\Delta\upsilon_k = \pm 1$. So, under these selection rules it is imperative that only fundamental vibrations $(0 \longrightarrow 1)$ are allowed in a crystal. But in practice one observes many more transitions because the system behaves like an anharmonic oscillator.

1.4 INFLUENCE OF PERTURBATIONS ON MOLECULAR SPECTRA

1.4.1 Anharmonicity

There are two main sources of anharmonicity. Deviations from the harmonic potential (V) lead to *mechanical anharmonicity* whereas asymmetric vibrations of a molecule lead to *electrical anharmonicity* [16,28,29].

$$\left. \begin{aligned} V &= \sum (\frac{\partial^2 V}{\partial Q_k \partial Q_l})_o \quad Q_k Q_l \quad + \sum (\frac{\partial^3 V}{\partial Q_k \partial Q_l \partial Q_m})_o \quad Q_k Q_l Q_m \quad + \\ &\quad \sum (\frac{\partial^4 V}{\partial Q_k \partial Q_l \partial Q_m \partial Q_n})_o \quad Q_k Q_l Q_m Q_n \quad + \ldots \\ \mu &= \mu_o + \sum (\frac{\partial\mu}{\partial Q_k})_o Q_k \quad + \sum (\frac{\partial^2\mu}{\partial Q_k \partial Q_l})_o Q_k Q_l \quad + \sum (\frac{\partial^3\mu}{\partial Q_k \partial Q_l \partial Q_m})_o Q_k Q_l Q_m \quad + \ldots \end{aligned} \right] \quad 1.9$$

Immediate manifestations of anharmonic terms are readily observed in vibrational spectra. The transitions which involve the change in single quantum number by ± 2 and change in more than one quantum number simultaneously are allowed. They are called the overtones and combinational modes respectively. The origin of these transitions have already been explained in great detail [33,35]. Both these anharmonicities exist in real systems. A simple non-rigorous way of identifying these two kinds in vibrational spectra is - if overtones/combinations along with its fundamentals are present, it indicates mechanical anharmonicity and if their presence does not depend on fundamentals, it indicates electrical anharmonicity. Using the observed spectral profiles it is possible to calculate cubic, quartic and higher order dipole moment derivative constants [36,37].

1.4.2 Fermi Resonance

The energy levels in polyatomic molecules are much more perturbed which is not explainable by anharmonicity and are due to the phenomenon known as *Fermi Resonance*. Two or more vibrational levels of a polyatomic molecule belonging to different vibrations may have nearly same energy *i.e.*, they may be accidentally degenerate. Such a resonance causes repulsion in the energy levels. One of these states which is very weak in normal conditions, would appear as strong as a fundamental [28,38-40].

Formation of the hydrogen bond (H-bond) also affects the vibrational frequencies. The H-bond is defined as the bond between an atom (Y) and the hydrogen atom of a covalent bonded molecule AH and is represented as A-H...Y. Atoms A and Y have electro negativity values greater than H; for example C, N, P, O, S, Se, F, Cl, Br, I *etc*. Both inter- and intra-molecular H-bonding are possible [41,42]. Diffraction and spectroscopic studies are necessary in order to get complete information about the bond. Spectroscopic methods mainly provide the information needed to understand the strength of H-bond by which quantitative interpretation of the data is not an easy task [43-45]. But the changes can be interpreted qualitatively.

The modes which are affected by the formation of H-bonds are ν_{AH} (stretching), δ_{AH} (bending), ν_{AY} and τ_{AH} (torsional). Both ν_{AH} and δ_{AH} modes are also present in the absence of H-bond. However, these would undergo a drastic frequency shift in the presence of H-bond. The torsional modes occur only if A is a polyatomic molecule. Though the presence of ν_{AY} and τ_{AH} (usually very weak) inevitably indicates the formation of H-bond, however, it is much more convenient and reliable to use the observed variations in ν_{AH} and δ_{AH} for qualitative understanding [20,41]. A large number of studies on H-bonded systems show that the ν_{AH} decreases and δ_{AH} increases in frequency as H-bond becomes stronger. Also, the intensity

and linewidths of ν_{AH} increase with the increase in H-bond strengths. Typical linewidths of ν_{AH} for a weak, medium and strong H-bonded systems are of the order of 10, 10^2 and 10^3 cm^{-1}, respectively [42-46].

1.5 RELAXATIONAL PROCESSES IN SOLIDS

The dynamical nature of molecules produces some obvious and subtle variations in vibrational spectral data. A careful study of the spectral profile as a function of external parameters (like temperature, pressure, concentration etc) provides an insight into the dynamical nature. There exist two types of relaxations called vibrational and rotational (reorientational) relaxations [1-5]. A relaxation generally refers to a process by which the energy associated with the corresponding degree of freedom of a molecule is transported to the system.

Vibrational Relaxation

The vibrational relaxation of a mode (ν) of a molecule i may be due to one or all of the following mechanisms: (i) vibrational energy transfer to the lattice by means of rotational or translational degrees of freedom, (ii) energy redistribution between internal modes, (iii) resonance vibrational energy transfer, coupling of adjacent molecules via particular coordinate and (iv) band broadening occurring due to the lack of

phase coherence of the excited vibrations in a particular mode. The effects (i) and (ii) are essentially due to depopulation of the vibrational states and are collectively known as *energy relaxations*. The last two are known as *inhomogeneous broadening* mechanisms [4]. In solids, these relaxations are very fast. The variations in spectral profiles as a function of temperature are very marginal and therefore the interpretation of the results becomes tedious and complicated. Different mathematical models to explain these relaxational processes are based on the anharmonic interaction and predicts very weak temperature dependence. In fact, the linewidth of the mode increases linearly with temperature in many systems [4,47-50].

Rotational Relaxations

A molecule in a crystal can perform angular rotations in an equivalent minima of a potential called the orientational potential or single particle potential, which is due to the result of interactions with the other molecules situated at different orientations [47]. The potential is given by,

$$V = V_o + \Delta V \qquad\qquad 1.10$$

where the static part V_o depends on the interaction strength with other molecules, while fluctuating part ΔV is temperature

dependent. The relative magnitude of these quantities alongwith the moment of inertia ($\mathscr{I}$) of the molecular group determines different types of rotational motions. Free rotations which are very rare in condensed state (except solid hydrogen) are possible if $\hbar^2/2\mathscr{I} \gg V_o$ and ΔV. Rotational diffusion occurs if $V_o > \hbar^2/2\mathscr{I}$ and $V_o \approx \Delta V$; and then the molecules undergo Brownian motion in the orientational space, for example, motion in plastic crystals. Classical reorientations are possible if $V_o \gg \hbar^2/2\mathscr{I} > \Delta V$. At lower temperatures, molecules stay at one of the minima; however, by raising the temperature sufficiently high they can go to other minimum by means of thermal reorientations [47,51].

1.5.1 Spectral Manifestation of Molecular Motion

Spectral data carries the information about molecular dynamics. But interpretation is not a simple task. However, in a few simpler cases (isotropic), the contributions from vibrational and orientational relaxations can be separated. Following the quantum mechanical treatment, the lineshapes in the Raman scattering and infrared absorption processes, respectively, is given by [48-54].

$$I(\omega) \propto \int dt\ e^{i\omega t} < \varepsilon_i\ \alpha(t)\ \varepsilon_s \varepsilon_i\ \alpha(o)\ \varepsilon_s> \qquad 1.11$$

$$I_{IR}(\omega) \propto \frac{1}{2\pi} \int dt\ e^{i\omega t}\ <\mu(t)\ \mu(o)> \qquad 1.12$$

where ε_i and ε_s are the unit vectors along the polarization directions of the incident and scattered light. In the Raman scattering two experimental situations arise, *i.e.*, $\varepsilon_s \parallel \varepsilon_i$ and $\varepsilon_s \perp \varepsilon_i$. The isotropic and anisotropic contributions to the Raman lineshapes is defined as [53,63],

$$I_{iso} = I_{\parallel} - (4/3)\ I_{\perp} \qquad\qquad 1.13$$

$$I_{aniso} = I_{\perp} \qquad\qquad 1.14$$

Using eqn 1.6 and assuming phases of vibrations on neighbouring molecules are uncorrelated, then eqns 1.13 and 1.14 can be written as [48],

$$I_{iso}(\omega) \propto \left|\frac{\partial\alpha}{\partial Q}\right|^2 \int dt\ e^{i\omega t}\ \langle Q_i(t)Q_i(o)\rangle \qquad\qquad 1.15$$

$$I_{aniso}(\omega) \propto \int dt\ e^{i\omega t}\ \langle P_2(\cos\theta_i(t))Q_i(t)Q_i(o)\rangle \qquad\qquad 1.16$$

Here $\theta_i(t)$ is the angle between the polarizability at time $t = 0$ and $t = t$ and P_2 is the second order Legrendre polynomial. Thus anisotropic part of the vibrational line contains the information about both vibrational and rotational relaxations. Similar analysis for IR absorption gives,

$$I_{IR}(\omega) \propto \int dt\ e^{i\omega t}\ \langle P_1(\cos\theta_i(t))Q_i(t)Q_i(o)\rangle \qquad\qquad 1.17$$

It is clear that both the Raman and IR spectra gives similar information regarding the relaxations. The combined experiments

can provide the information about vibrational and rotational relaxations.

1.5.2 Experimental Probes

With the advent of tunable and pico-second lasers this area of study has gained momentum [55,56]. The infrared absorption and spontaneous Raman scattering techniques are stillextensively used in experimental and theoretical research [57-62]. Various experimental probes for the relaxation processes can be categorized into two classes *viz.*, those which employ the scattering and/or absorption of electromagnetic radiation and those which do not. All the spectroscopic methods form the former and ultrasonic absorption studies form second class of studies.

The former class consists of both spectral lineshape analysis in IR absorption and spontaneous Raman scattering *etc* and coherent pico-second excitation studies. The first set of experiments are easier to perform but the interpretation is ambiguous. From § 1.5.1 it is clear that these techniques inherently carry the information about the molecular motions. In some suitable condition the information about the vibrational and rotational relaxations can be separated conveniently. However, it is not generally true. The infrared and the anisotropic parts of the Raman bands are affected by the vibrational dephasing with the corresponding time correlation functions approximately given as,

$$C_n(t) \cong \langle P_n(\cos\theta_i(t)) \, Q_i(t)Q_i(o) \rangle \qquad 1.18$$

where n = 1 for infrared and n = 2 for Raman spectra. From eqn 1.18 it is clear that spectral profiles carry the information about reorientational and vibrational relaxational processes. In order to extract the information about a particular process, the other contribution must somehow be eliminated. If we are interested in reorientational relaxation in the crudest approximation, the contribution from vibrational process must be ignored. However, this is valid only in the range where the vibrational relaxation is much slower than reorientational. Bartoli and Litovitz [63]; and Rakov [64] have further suggested that the total linewidth (Γ) as a function of temperature (T) as,

$$\Gamma \cong \Gamma_{vib} + C \exp(-E_a/k_B T) \qquad 1.19$$

Here, vibrational part (Γ_{vib}) is assumed to be temperature independent and C is a constant. Thus, the linewidth variations with temperature measures the activation energy.

Again, if one can estimate the contribution of vibrational relaxations from the isotropic Raman lineshapes using eqn 1.15, it is, in principle, possible to get the information about the reorientational relaxations. Of course, in general, it is not so easy [4,48,52]. Utmost important

limitation is the finite resolution of the detecting system. The maximum time limitation is given by,

$$T_{max} = (2\pi \times \text{resolution in Hz})^{-1} \qquad\qquad 1.20$$

The double monochromator used in the present investigation has a spectral resolution of 0.15 cm^{-1} ($\cong$ 35 psec.). Thus it is not possible to study a process which occur at slower time scales.

1.6 PHASE TRANSITIONS

Generally, the detection of a phase transition means a search for the specific physical quantity which differs by several orders of magnitude in both the phases. In well known liquid to vapour transition, density difference is the relevant parameter. The other examples of the order parameter are the magnetization in ferro to paramagnetic transition, the spontaneous polarization in ferroelectric transition and the energy gap in superconductivity *etc*. The transitions which are at present interesting to us are related to the changes in crystal symmetries. When a crystal changes its structure, it will have definite symmetry at all temperatures. A transition of this kind could occur with a sudden rearrangement of constituent atoms resulting in a first order transition or by an arbitrarily small displacement of atoms from their equilibrium configuration resulting in a second order transition. The two states in the

former case are in equilibrium but there is no predictable symmetry relation between them. However, a definite relationship exists between the two phases in latter case [9,30].

Order Parameter

The *quantity* which characterizes the two phases is known as the *order parameter*. The order parameter (η) measures numerically the amount and kind of ordering which is built up in the neighbourhood of the critical point. The properties of η are summarized as follows [65,66].

(a) It may vanish above the critical point but it must be non-zero in the region just below T_c.

(b) Below the transition it is not fully determined by the external conditions, but may take on two or more different values under physically identical conditions.

On the basis of order parameter behaviour, transitions are broadly classified as discontinuous (first order) and continuous (second order) type. It is customary to represent the critical temperature that represents the thermodynamical stability limit of a particular phase by T_o. In the case of second order transition $T_c = T_o$. However, for the first order transition, $T_o > T_c$ and $(T_o - T_c)$ represents the temperature range of thermal hysteresis.

Exponents and Universality

As we approach a second order transition either from above or below T_c, the physical properties such as the order parameter (η), susceptibility (χ) and specific heat (C) *etc* of the system vary in a smooth fashion. Therefore, near T_c these parameters can be expanded in the power series of reduced temperature t ($t = ((T-T_c)/T_c)$. As we go closer and closer to T_c, the properties of these parameters are dominated by the leading term in the power series. Thus the exponent of t for this leading term acquires a particular significance and is referred as the *critical exponent*. Such as,

$$C \propto |t|^{-\alpha} \; ; \; \eta \propto (-t)^{\beta} \; ; \; \chi \propto |t|^{-\gamma} \; ; \; \xi \propto |t|^{-\nu} \qquad 1.21$$

Here α, β, γ and ν are known as critical exponents. Thus by knowing these exponents one can measure or calculate the physical properties of the system as a function of t. The critical regime may exceed by about 20 K for a structural transition. However, this could be as less as 0.01 K for a magnetic transition.

Interest in critical exponents is due to the fact that they show a great deal of similarities in different systems. This independence of the critical exponents on the nature of the system is referred as *universality*. In its simplest terms, the

universality hypothesis is the statement that all critical problems may be divided into classes differentiated by [8,67],

    (a) dimensionality of the system,

    (b) symmetry group of the order parameter and

    (c) perhaps any criteria.

Within each class, the critical properties are supposed to be identical or at worst to be a continuous function of a very few parameters.

1.6.1 Classification of Structural Phase Transitions

The structural phase transitions are broadly divided into three categories following Burger [68],

```
                        S  P  T
                           |
     ┌─────────────────────┼─────────────────────┐
Reconstructive         Distortive            Martensitic
                           |
     ┌─────────────────────┤
Displacive             Order-disorder
                           |
     ┌─────────────────────┼─────────────────────┐
Positional             Orientational              Spin
```
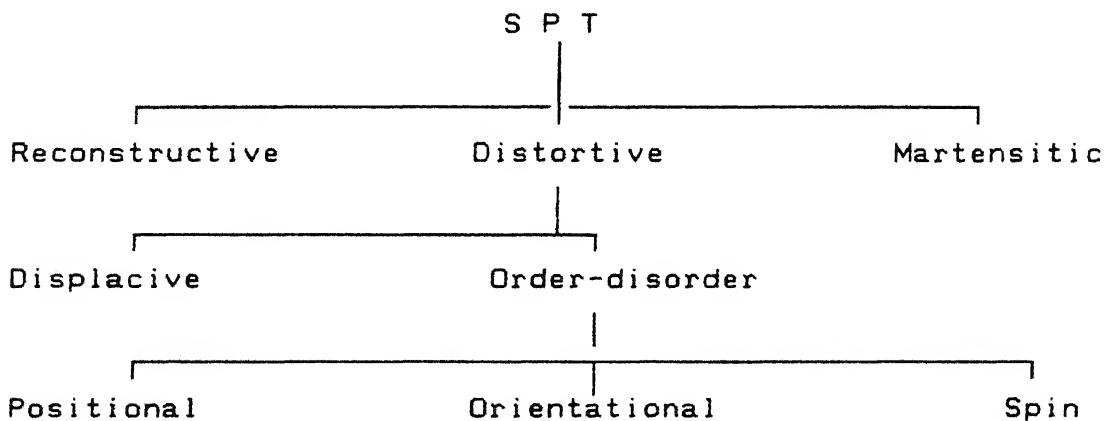
In the reconstructive type SPTs the atoms form new linkages between them by destroying the existing linkages *eg.* crystalline to amorphous silica. Martensitic transitions which occur mainly in metals are not of much importance in the present study. In distortive type transitions crystal changes its symmetry due to

small distortions in the lattice without changing the basic linkages. This type is very common and is further sub-divided into two classes *viz.*, *displacive* and *order-disorder* type.

(a) as a result of small *displacements* in the lattice positions of constituent atoms or molecules and

(b) as a result of *ordering* of atoms or molecular groups in the crystal.

Transitions which rigidly follow these two categories are very rare and in practice, a combination of the two is observed in most of the structural transformations. Typical examples for these two classes are found, respectively, in $BaTiO_3$ and $NaNO_2$ crystals.

The displacive and order-disorder transitions can be viewed as a limiting case of the single particle potential given by [69-71],

$$V(Q_i) = AQ_i^2 + BQ_i^4 \qquad \text{with } A < 0 \text{ and } B > 0 \qquad 1.22$$

and this has minima at

$$Q_i = \pm \left(|A|/2B \right)^{1/2} \qquad 1.23$$

which are separated by the energy barrier given by, $\Delta E = A^2/4B$. The difference between the displacive and order-disorder transitions can be characterized through the introduction of the dimensionless parameter $g = (\Delta E/k_B T_C)$ where, k_B is the Boltzmann

constant. The displacive and order-disorder limits are associated with regimes $g \ll 1$ and $g > 1$, respectively. On the basis of transition entropy, the displacive and order-disorder can be characterized and it is small ($\ll k_B \ln 2$) and large ($\geq k_B \ln 2$) for these two types.

In a positionally disordered crystal, the lattice sites are more in number than required by the constituent atoms or molecules. Examples of this type are found in binary alloys and crystals like Li_2SO_4 etc. The *orientational disorder* which is commonly observed in crystals like NH_4Cl and $NaNO_2$ arises because of the fact that the molecular groups can exist in more than one distinguishable orientation in the crystal.

1.7 THEORIES OF PHASE TRANSITIONS

1.7.1 Landau Approach

An outline of the basic formulation of the theory is as follows [10,65,69, 72-75]. Let the density function which gives the probability distribution of the atoms among the sites in a crystal be $\rho(x,y,z)$, which is invariant under the space group of the crystal. If the crystal changes its structure continuously from high (G_0) to low (G) symmetry space group resulting in a new distribution, $\rho(r) = \rho_0(r) + \Delta\rho(r)$, then G should be a sub-group of G_0. It is also possible to have a structural change which is first order in nature, but could be considered as a second order from a symmetry point of view, *e.g.*, $BaTiO_3$.

Expanding $\Delta\rho$ in terms of φ_1, (the basis vector) which are invariant under G_0 as,

$$\Delta\rho = \sum \eta_i^n \, \varphi_i^n \qquad\qquad 1.24$$

where n represents the order of the group. A second order phase transition generally corresponds to a change in single irreducible representation and hence the n dependence is omitted from the above equation.

The thermodynamical potential of the crystal $\phi(P,T,\eta)$ is a function of pressure, temperature and the coefficients η_i. For a second order transition, any one of the coefficients η_i should be non-zero in less symmetric phase and should continuously decrease and vanish at the transition point. Expanding the potential energy ϕ in terms of the Taylor series near the transition point,

$$\phi(P,T,\eta) = \phi_0 + A\,\eta^2 + B\,\eta^4 + \ldots \qquad\qquad 1.25$$

Assuming $A = a(T-T_c)$; $B>0$ and applying the stability conditions w.r.t. η we get,

$$\frac{\partial\phi}{\partial\eta} = 0 = 2A\eta + 4B\eta^3$$

$$\Rightarrow \eta = 0 \qquad \text{for } T>T_c$$

$$\eta^2 = -\frac{A}{2B} = \frac{a(T_c-T)}{2B} \qquad \text{for } T<T_c \qquad 1.26$$

So, in less symmetric phase (where $\eta \neq 0$) the coefficient η changes its value like $(T_c - T)^{1/2}$ and vanishes at $T = T_c$. Landau theory predicts the order parameter exponent (β) as 0.5. However, in practice the observed behaviour of the order parameters significantly vary from this and hence other theoretical models are needed [7,8].

1.7.2 Soft Mode Approach

This is based on lattice dynamics first proposed independently by Cochran and Anderson in 1959. Experimentally a soft mode like behaviour was observed by Nedungadi and Raman in 1940. In simple terms, soft mode is a collective excitation which may be either propagative or diffusive whose frequency decreases substantially as the transition temperature T_o is reached from above or below. This concept of lattice instability against a particular lattice vibration has extensively been pursued to study the structural phase transitions.

The concept of soft mode can be best understood in terms of the Landau theory for one dimensional harmonic oscillator. In this frame, the second derivative of energy (ϕ) with respect to displacement (x) is given by,

$$\frac{\partial^2 \phi}{\partial x^2} = m\omega^2 \qquad\qquad 1.27$$

where ω is the frequency of the mode. The analogous expression from the Landau theory is $(\partial^2 \phi / \partial \eta^2) = 2A$, so

$$\omega^2 \propto A \propto a \ (T-T_o) \qquad\qquad 1.28$$

Thus, a soft mode in Landau frame is active in low temperature phase and varies like a order parameter.

Conceptually the soft modes were explained in a great detail by considering the anharmonicity which predicts the behaviour similar to eqn 1.28 [75].

Initially the soft mode concept was extensively used for displacive transitions and later extended to order-disorder type. A soft mode in the order-disorder transitions can be explained by a pseudo-spin wave [75]. The soft modes in the displacive transitions are resonant in nature though they are highly damped. However, in the order-disorder transitions, the soft modes are relaxational in nature [76-80].

1.7.3 Hard Mode Spectroscopy

The soft mode approach is undoubtedly the most attractive way of explaining the changes in the crystal structure. However, other modes called *hard* or *rigid* modes are also equally important and useful for such information. Normally these modes are not expected to show variations similar to those of soft modes. However, in certain conditions they show some changes similar to the soft modes. The thermal evolution of such modes carry valuable information about the transition mechanism. Certain new modes could appear and the degeneracy could be lifted by the

change in crystal symmetry. Qualitatively, all the changes in mode strengths and frequencies are somehow related to the order parameter. Quantitatively, it is not easy to understand the changes [9,10,12]. A careful study of these parameters in some favorable cases, however, could be explained quantitatively by taking the help of some other studies like polarization (in ferroelectric transition). A brief description of various models which deal with the changes occurring in hard modes near the transition are given below.

Activity of Silent Modes

Disappearance of forbidden modes at the transition temperature is the most striking feature and can definitely be attributed to structural change [81]. The strength variations of such modes *viz.*, bands which are active in ordered state only are explained via order parameter coupling [12,82]. In fact, the intensity of such modes is proportional to the square of the order parameter (η) in the ordered state. Often, it is observed that these modes which should be inactive under $K = 0$ selection rules in the disordered state, become active. Activity of such modes is explainable by $K \neq 0$ selection rules which requires a better knowledge of the density of states. Close to the transition temperature the single phonon strength of such a mode is dependent on the correlation length (ξ) and is given by the expression [82],

$$I(\omega) \propto \frac{n(\omega)+1}{\omega} \sum \rho_j(\omega) \left\{ a_j + b_j \left[1-(K_o\xi)^{-1} \tan^{-1}(K_o\xi) \right] \right\} \qquad 1.29$$

where $n(\omega)$ is the Bose-Einstien factor, K_o is the radius of the small spherical region around K, from which contributions to the Raman intensity at energy $\hbar\omega$ can be expected. ξ is the correlation length which depends on the reduced temperature t via eqn 1.21. Using this model the critical intensity variation of 190 cm^{-1} mode in KCN in 30-150 K range was explained. The critical exponents β and ν for the order-disorder transition $(T_c=83$ K) were calculated to be 0.33 and 0.68, respectively [82].

Recently, Bruce *et al* [83] worked out a theory which explains the precursor over the critical variations in the Raman intensity of the hard modes. These modes are active only in the ordered phase $(<T_c)$ and inactive in disordered phase. Soft modes themselves come under this category. They have considered the modes which are not directly involved in the transition, but their activity is induced. The intensity of such hard modes will have contribution from three components as,

$$I = I^{LR} + I^{CP} + I^{PH} \qquad 1.30$$

where LR and CP represent the long range and central peak contributions to the first order Raman scattering. I^{PH} is the contribution coming from the second order Raman scattering arising from the process involving one hard mode and one soft

phonon. The long range interaction term represents the intensity variations induced by the macroscopic ordering and is non-zero only below T_c. The intensity arising due to this term is proportional to the square of the order parameter $i.e.$, η^2. Whereas, contribution to the peak frequency and width of the bands are given by the quasi-harmonic approximation. The central peak term may give non-zero contribution above T_c. The last term which involves a soft phonon shows the variation in both frequency and lineshape in a temperature range very close to T_c. This concept has been successfully employed to explain the transitions in $Pb_3(P_{1-x}As_xO_4)_2$ system [84]. So, the intensity of a hard mode in the ordered state $(T<T_c)$ shows a significant variation with temperature via 1st and 3rd terms of eqn 1.30.

Soft Hard Mode Coupling

Soft modes show vanishing frequency near the transition temperature. The frequency of such a mode varies like $\omega^2 \cong (T_c-T)$ and the linewidth (Γ) varies like,

$$\Gamma = A + B (T/(T_c-T)) \qquad 1.31$$

where A, B are constants [79]. Apart from the soft modes, a number of hard modes also show anomalous variations close to T_c [9]. These observations are difficult to interpret; however, in

some cases it was explained as a rigid mode interacting with a soft mode. Specially, in order-disorder type where the soft mode is of relaxational type, the linewidths of few low frequency Raman modes appear to diverge near the transition. In the presence of anharmonic interactions, the linewidth is given by [85,86],

$$\Gamma(\omega) = \frac{\pi\hbar}{16N\omega_i} \sum \frac{W_{ikl}^2}{\omega_k \omega_l} \left[(n_k + n_l + 1)\left\{\delta(\omega_i - \omega_k - \omega_l) - \delta(\omega_i + \omega_k + \omega_l)\right\} + \right.$$
$$\left. (n_k - n_l)\left\{\delta(\omega_l - \omega_l + \omega_k) - \delta(\omega_i + \omega_l - \omega_k)\right\}\right] \qquad 1.32$$

where W_{ikl} are the coefficients of cubic interaction and n_i is the Bose-Einstien factor. For a soft mode near T_c, $\hbar\omega_i \ll k_B T$ and $n_i \gg n_l$. Thus the leading term in eqn 1.32 is n_i/ω_i. Then the linewidth in the lowest approximation is proportional to $(T/(T_c - T))$ [86]. So, it is possible to see an anomaly in hard phonons if a soft phonon is coupled to it.

The peak frequency of a such phonon also shows a remarkable variation near the transition temperature via anharmonic interaction terms. As shown in § 1.4.1, the cubic part is given by,

$$H_{int} \propto A\eta Q_1 Q_2 \qquad 1.33$$

where A is constant, Q_1, Q_2 are the normal modes of hard phonon and η is the same for a soft mode. Hence, by monitoring the

frequency difference ($\Delta\omega$) with respect to frequency away from T_c, one can find the dominant contribution to it. Especially, quasi-degenerate modes could split and the splitting near T_c can be attributed to a soft mode coupling in $TlGaSe_2$ and other compounds [87-89]. The splitting could be proportional to η or η^2 [12,89]. So, by monitoring such modes one can say about the linear or quadratic coupling of soft modes with the rigid modes. In such cases one can calculate the order parameter exponent and compare with other experiments [9].

1.7.4 Order-Disorder Transitions

The order-disorder transitions are distinguished from the displacive type by large entropy variations. The soft modes in this type have relaxational nature. This type of transitions show anomalies in hard mode frequencies and linewidths. It has been observed that the linewidths show drastic variations near the transitions. These changes are well understood in terms of pseudo-spin model [9,80].

Pseudo-spin Approach

In ammonium halides it was observed that some non-soft optical phonon frequencies show anomalous shifts with temperature and the linewidths diverge near the transition temperature [90]. Similar experimental observations are there for triglycine

sulfate and triglycine selenate [91]. The origin of such variations have been explained by Matsushita [92]. Basic approach of this model incorporates the pseudo-spin coupled term in the Hamiltonian of the crystal. The temperature evolution of the peak frequency under the pseudo-spin formulation is governed by the macroscopic ordering of these spins. The linewidths of the modes under this theory are expected to show sharp increase near the transition. This model well explains the observed variations in NH_4X (X=Cl,Br) and could extend to similar systems [93].

Andrade and Porto Approach

From § 1.5 it is clear that phonon linewidths are affected by vibrational and rotational motions. Experimental evidence can be obtained from NMR, NQR and vibrational spectroscopic techniques. In the disordered phase, the molecular groups in the unit cell can exist in different orientations. As $T \rightarrow T_c$ (the transition temperature), the molecular groups freeze into one orientation. In the intermediate temperatures, these involve in self diffusion which is characterized by a correlation time (τ_c). The theory which was proposed by Andrade and Porto [94], considers the molecules as *Brownian* particles undergoing random jumps between the possible orientations. A typical example is $NaNO_2$ in which the nitrogen atom of NO_2^- ion points either to left or right of the crystallographic plane.

Thus, this theory is applicable whenever a *Brownian sub-lattice* is intermixed with the ordered lattice.

The correlation time (τ_c) of the self-diffusion process gives the inverse probability per unit time for a particle to jump from one equivalent position to another in the lattice. This is connected to the activation energy (ΔE) by the equation,

$$\tau_c = \tau_o \exp(\Delta E/k_B T) \qquad 1.34$$

where τ_o is a constant proportional to h/k_B. The linewidth of the disorder affected phonons like librations are given by,

$$\Gamma = C \frac{\tau_c}{1+\omega^2\tau_c^2} \qquad 1.35$$

where C is a constant and characterizes the intensity of *Brownian Force*. Considering the contributions from the anharmonicity (upto quartic) terms also, the linewidth (Γ) vary with temperature as [9,94],

$$\Gamma = AT + BT^2 + C \frac{\tau_c}{1+\omega^2\tau_c^2} \qquad 1.36$$

So, by measuring the linewidth variations as a function of T, one can calculate the activation energy ΔE, which is an elegant way of cross checking NMR results [95].

1.8 PREVIOUS STUDIES IN $(C_nH_{2n+1}NH_3)_2MCl_4$ CRYSTALS

Crystals with the general formula $(C_nH_{2n+1}NH_3)_2MCl_4$ with n = 1,2,3 and M = Mn, Fe, Cd etc have been extensively investigated in the past with regard to the phase transitions and various transition mechanisms have been proposed [96-100]. The successive transitions occurring in 500-77 K range in the family of these crystals have attracted the attention of solid state researchers (see Table 1.2). On the other hand, these crystals which form a two-dimensional lattice, show magnetic ordering at much lower temperatures. This aspect of the magnetic transition has received special attention [101]. The crystals of this family consists of a corner-shared metal chloride octahedra (MCl_6) while the organic chains occupy the gaps created by it. The crystal structure of this family in its proto-type phase is depicted in Fig 1.1. Adjacent layers are coupled by the van der Waals interactions between the carbon atom ends of the alkylammonium ion. Within the layer, MCl_6 and alkylammonium ions are attached via hydrogen bonding between the protons of NH_3 group in the organic chain and the chlorine atom. This weak interaction makes the crystallization difficult. The crystals can be cleaved very easily along the **XY**-plane. Mostly the transitions in these crystals are due to the reorientational motion of the alkylammonium ions. However, in long chain compounds (n>3), the conformational changes and/or partial melting of the alkylammonium ions occurs during the transition

[97]. In the following paragraphs a brief summary of the previous work in the family of $(C_nH_{2n+1}NH_3)_2MCl_4$ with M = Cd (abbreviated hereafter as $C_n CdCl$) for n = 1,2,3 is given.

1.8.1 Methylammonium Series

The methylammonium crystals with M = Cd, Mn, Fe and Cu of the family, $C_n CdCl$ are iso-structural and show similar type of phase transitions. The crystal structure of recently synthesized $C_1 MCl$ compounds with M = Zn and Hg is different at room temperature [102,103]. However, the other compounds (n = 2,3) with M = Zn and Hg are iso-structural with the family. $C_1 MCl$ crystals belong to the tetragonal with space group (D_{4h}^{17}) in its proto-type phase (K_2NiF_4 - lattice type) and undergo the following structural transitions on decreasing the temperature.

$$D_{4h}^{17} \rightarrow D_{2h}^{18} \rightarrow D_{4h}^{16} \rightarrow C_{2h}^5$$

The transition sequence particularly in M = Mn, Cd has been studied by several experimental techniques in the past leading to a statistical model considering different orientations of the methylammonium ions in the lattice that are responsible for the transitions [104-106]. The model explains the first two transitions i.e., $D_{4h}^{17} \rightarrow D_{2h}^{18} \rightarrow D_{4h}^{16}$ which are due to the partial orientational ordering of $CH_3NH_3^+$ ions. However, in order to explain the latter i.e., $D_{4h}^{16} \rightarrow C_{2h}^5$ transition, a non-linear

coupling of these ions with MCl_6 octahedron has been taken into account. Occupation of different possible orientations for the C-N bond is shown schematically in Fig 1.2. In the proto-type phase, all possible orientations are populated equally. However, in lower temperature phase they preferably occupy a particular orientation. In C_{2h}^5 low temperature monoclinic (MLT) phase, C-N bonds are in ordered state. Very significant variation in the hydrogen bond scheme on time averaged basis has been observed in MLT phase:

(a) The *orthorhombic* hydrogen bonding configuration is observed in high temperature phases. In this scheme NH_3^+ ends form two H-bonds with equatorial and one with axial chlorine atoms.

(b) The *monoclinic* H-bonding scheme is opposite *i.e.*, there are two H-bonds with axial and another with equatorial chlorine atom.

This variation produces a tilt of about 20° in the octahedra and the projections of the structure is shown in Fig 1.3. The first two transitions are mainly due to the interactions among $CH_3NH_3^+$ groups. Surprisingly, very low entropy changes are observed during these transitions [107]. However, a large entropy change (10.8 $JK^{-1}mol^{-1}$) during the $D_{4h}^{16} \rightarrow C_{2h}^5$ transition has been attributed to the transition to an order-disorder type. Subsequent spectroscopic studies supported this conclusion. In Chapter III a systematic temperature dependent study of a few internal modes of the methylammonium group has been used to probe the transition.

1.8.2 Ethylammonium Series

Ethylammonium crystals of the series are less studied in the past regarding the phase transitions. In this series also M = Cd and Mn compounds are iso-structural and undergo similar phase changes. Crystallographic and other studies propose the following sequence,

$$D_{4h}^{17} \rightarrow D_{2h}^{18} \rightarrow D_{2h}^{15} \rightarrow C_{2h}^{5}$$

$D_{4h}^{17} \rightarrow D_{2h}^{18}$ transition is second and other two are first order in nature. In M = Cd crystal, the $D_{2h}^{18} \rightarrow D_{2h}^{15}$ transition occurs at 216 K and is order-disorder type as evident from a large entropy change. Because of this nature the transition has become more important. It has been observed that a few FIR modes show strong broadening near the transition and has been explained in terms of pseudo-spin coupling [108]. Such observations in the internal mode region do not exist in literature though x-ray studies indicate a large variation in C-C and C-N bond lengths [109]. In Chapter IV of the thesis, this compound along with its parent compound ethylammonium chloride has been probed for the phase transitions.

1.8.3 Propylammonium Series

The phase transition sequence in C_3CdCl crystals is much different from the other members of the family [100]. It

uniquely possesses an incommensurate phase between 183-158 K [109]. Unfortunately, the Raman spectroscopic technique fails to provide any convincing evidence [109]. Apart from this it also undergoes an order-disorder transition at 158 K [110]. The complete known transition sequence for this is as follows.

$$D_{2h}^{18} \longrightarrow (INC) \ D_{2h}^{18} \longrightarrow D_{2h}^{15} \longrightarrow (?) \ C_{2h}^{5}$$
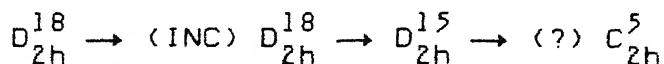
Espically, the $D_{2h}^{18} \longrightarrow D_{2h}^{15}$ transition is known to be due to the ordering of propylammonium ions. However, the entropy change for the transition is less. A detailed temperature dependent study has been carried out in chapter V of the thesis to correlate the spectral variations with other systems.

REFERENCES

1. IG Kaplan "Theory of Molecular Interactions" Elesevier, Amsterdam (1986).

2. AJ Hopfinger "Intermolecular Interactions and Biomolecular Organization" John Wiley, New York (1977).

3. JD Graybeal "Molecular Spectroscopy" McGraw Hill (1988).

4. J Yarwood and R Arndt in "Molecular Association" Ed R Foster, Academic Press **2**, (1979).

5. "Vibrational Intensities in Infrared and Raman Spectroscopy" Ed WB Person and G Zerbi, Elesevier, Amsterdam (1982).

6. R Brout "Phase Transitions" WA Benjamin Inc, New York (1965).

7. HE Stanley "Introduction to Phase Transitions and Critical Phenomena, Clarendon Press, Oxford (1971).

8. SK Ma "Modern Theory of Critical Phenomena" WA Benjamin, New York (1976).

9. "Vibrational Spectroscopy of Phase Transitions" Ed Z Iqbal and FJ Owens, Academic Press (1984).

10. JF Scott, Rev Mod Phys., **46**, 83 (1974).

11. KA Muller and E Pytte, IBM J Res and dev., **25**, 811 (1981).

12. J Petzelt and V Dvorak, J Phy., **9C**, 1571 1587 (1976).

13. LD Landau and EM Lifshitz "Statistical Physics" Pergamon Press 3rd Edn (1980).

14. "The Raman Effect" Ed A Anderson, R Savoie & GR Wilkinson

15. PW Atkins, "Physical Chemistry" WH Freeman Co., San Francisco (1978).

16. JC Decius and RM Hexter "Molecular Vibrations in Crystals" McGraw Hill (1977).

17. PMA Sherwood "Vibrational Spectroscopy of Solids" Cambridge at the University Press (1972).

18. AA Maradudin and and SH Vosko, Rev Mod Phys., **40**, 1 (1968).

19. R Durman, VA Jayasooriya and SFA Kettle, J Chem Phys., **83**, 5501 (1985).

20. G Turrell "Infrared and Raman Spectra of Crystals" Academic Press (1972).

21. JR Ferraro and JS Ziomek "Introductory Group Theory and its Applications to Molecular Structures" 2nd Edn Plenum Press (1975).

22. S Bhagavantam and K Venkatarayudu, Proc Acad Sci., **9A**, 224 (1939).

23. S Bhagavantam and K Venkatarayudu "Theory of Groups and its Application to Physical Problems" Academic Press, New York (1969).

24. RS Halford, J Chem Phys., **14**, 8 (1946).

25. H Winston and RS Halford, J Chem Phys., **17**, 607 (1949).

26. G Ramana Rao and G Zerbi, App Spectro., **38**, 795 (1984).

27. DM Adams and DC Newton, J Chem Soc A, 2822 (1970).

28. G Herzberg "Infrared and Raman Spectra of Polyatomic Molecules", Van Nostrand, New York (1945).

29. LA Woodward "Introduction to the Theory of Molecular Vibrations and Vibrational Spectroscopy" Clrendon Press, Oxford (1972).

30. W Hayes and R Loudon "Scattering of Light by Crystals" John Wiley and Sons, New York (1978).

31. AK Sood, J Indian Inst Sci., **68**, 461 (1988).

32. JL Birman in "Encyclopedia of Phys" Vol **25/2b**, Ed L Genzel, Springer-Verlag, Berlin (1974).

33. S Califano, V Schettino and N Neto "Lattice Dynamics of Molecular Crystals" Lecture Notes in Chemistry, Springer-Verlag, Berlin, **26**, (1981).

34. RA Cowley, Adv Phys., **12**, 421 (1963).

35. RA Cowley, Rep Progr Phys., **31**, 123 (1968).

36. RC Herman and KE Shuler, J Chem Phys., **22**, 481 (1954).

37. F Foldes and C Sandorfy, J Mol Spectrosc., **20**, 262 (1966).

38. GS Raghuvanshi, PhD dissertation, Dept of Physics, IIT, Kanpur (1984).

39. EJ Heller, EB Stechel and MJ Davis, J Chem Phys., **73**, 4720 (1980).

40. G Dellepiane, S Abbate, P Bosi and G Zerbi, J Chem Phys., **57**, 55 (1981).

41. "The Hydrogen Bond" Eds P Schuster and G Zundel, North Holland, Amsterdam (1976).

42. J Emsley, Chem Soc Rev., **9**, 91 (1980) and references therein.

43. S Bratos, J Chem Phys., **63**, 3499 (1975).

44. AS Pine and BJ Howard, J Chem Phys., **84**, 590 (1986).

45. M Asselin and C Sandorfy, J Mol Struct., **8**, 145 (1971).

46. E Grech, Z Malarski and L Sobczyk, J Mol Struct., **129**, 35 (1985).

47. AK Sood, PhD dissertation, Dept of Physics, IISc, Bangalore (1981).

48. DW Oxtoby in "Adv. in Chemical Physics" Ed I Prigogine and SA Rice, John Wiley, New York **40** (1979).

49. AL Verma in "Vibrational Spectra and Structures" Ed HD Bist, JR Durig and JF Sullivan, Elsevier, **17A**, 71 (1989).

50. R Ouillon, Mol Phys., **44**, 381 (1981) and references therein.

51. R Ouillon and C Breuillard, Mol Phys., **44**, 363 (1981).

52. RA Cowley, in "The Raman Effect" Ed A Anderson **Vol 1**, Marcel Dekker, New York (1973).

53. RG Gordon, Adv Mag Res., **3**, 1 (1968).

54. RG Gordon, J Chem Phys., **43**, 1307 (1965).

55. L Laubereau and W Kaiser, Rev Mod Phys., **50**, 607 (1978).

56. F Legay in "Chemical and Biochemical App of Lasers" Ed CB Moore, **Vol 3** (1979).

57. DJ Diestler in "Radiationless Processes in Mol and Condensed Phases", Ed FK Fong, Topics in Applied Phys, **Vol 15**, Springer-Verlag, Berlin (1976).

58. S Bratos, J Rios and Y Guissani, J Chem Phys., **52**, 439 (1970).

59. S Bratos and E Marechal, Phy Rev., **A4**, 1078 (1971).

60. LA Nafie and WL Peticolas, J Chem Phys., **57**, 3145 (1972).

61. M Maroncelli, HL Strauss and RG Snyder, J Chem Phys., **82**, 2811 (1985).

62. D Salmon, VL Shannon and HL Strauss, J Chem Phys., **90**, 773 (1989).

63. FJ Bartoli and TA Litovitz, J Chem Phys **56**., 404, 413 (1972).

64. AV Rakov, Opt Spectrosc., **7**, 128 (1959).

65. RM White and TH Geballe, "Long Range Order in Solids", Solid St Phy **Supp 15**, Academic Press, New York, (1979).

66. LP Kadanoff, W Gotze, D Hamblen, R Hecht, EAS Lewis, VV Palcialuskas, M Rayl, J Swift, D Aspnes and J Kane, Rev Mod Phys., **39**, 395 (1975).

67. LP Kadanoff in "Phase transitions and critical phenomena", Ed C Domb and M S Green, Academic Press (1976).

68. "Structural Phase Transitions" Ed KA Muller and H Thomas, Springer-Verlag, Berlin (1981).

69. RA Cowley in "structural Phase Transitions" Ed AD Bruce and RA Cowley, Taylor and Francis Ltd, London (1981).

70. A Dolle and T Bluhm, Prog in NMR Spectrosc., **21**, 175 (1989).

71. RL Armstrong, Prog in NMR Spectrosc., **21**, 151 (1989).

72. JC Toledano and P Toledano, "The Landau Theory of Phase Transitions" World Scientific, Singapore (1987).

73. J Petersson, Ferroelectrics, **13**, 565 (1976).

74. M Dumont and R Dagonnier, Ferroelectrics, **13**, 559 (1976).

75. R Blinc and B Zeks, "Soft Modes in Ferroelectrics and Antiferroelectrics", North Holland,Amsterdam (1974).

76. DA Bruce and W Stirling, J Phy., **16C**, 841 (1983).

77. F Gervais, Ferroelectrics, **13**, 555 (1976).

78. G Burns and BA Scott, Phy Rev Lett., **25**, 167 (1970); Phys Rev., **7B**, 3088 (1973).

79. AP Levanyuk and NV Schedrina, Sov Phy Solid St., **16**, 923 (1974).

80. TJ Hosea, DJ Lockwood and W Taylor, J Phy., **12C**, 387 (1979).

81. T Geisel and J Keller, J Chem Phys., **62**, 3777 (1975).

82. W Dultz, J Chem Phys., **65**, 2812 (1976).

83. AD Bruce, W Taylor and AF Murray, J Phy., **13C**, 483 (1980).

84. E Salje, V Devarajan, U Bismayer and DMC Guimaraes, J Phy., **16C**, 5233 (1983).

85. JHM Stoelinga and P Wyder, J Chem Phys., **64**, 4612 (1976).

86. J Holvast, SHM Stoelinga and P Wyder, Ferroelectrics, **13**, 543 (1976).

87. Sh Nurov, VM Burlakov, EA Vinogardov, NM Gasanly and BM Dzhavakov, Phys Stat Sol., **137b**, 21 (1986).

88. VM Burlakov and MR Yakheev, Phys Stat Sol., **151b**, 337 (1989).

89. VM Burlakov, AP Ryabov, MP Yakheev, EA Vinogradov, NN Melnik and NM Gasanly, Phys Stat Sol., **153b**, 727 (1989).

90. AIM Rae, J Phy., **15C**, 1883 (1982).

91. V Winterfeldt, G Schaack and A Klopperpieper, Ferroelectrics, **15**, 21 (1977).

92. M Matsushita, J Chem Phys., **65**, 23 (1976).

93. I Laulicht, J Phys Chem Solids, **39**, 901 (1978).

94. Pda R Andrade and SPS Porto, Solid St Commu., **13**, 1249 (1973).

95. FJ Owens, Chem Phy Lett., **64**, 116 (1979) and PTT Wong and JA Ripmeester, Chem Phy Lett., **72**, 122 (1980).

96. H Arend and H Granicher, Ferroelectrics, **13**, 537 (1976).

97. R Kind, S Plesko, H Arend, R Blinc, B Zeks, J Seliger, B Lozar, J Slak, A Levstik, C Filipic, V Zagar, G Lahajnar, F Milia and G Chapuis, J Chem Phys., **71**, 2118 (1979).

98. R Kind, Ber bunsenges Phy Chem., **87**, 248 (1983).

99. R Kind, Ferroelectrics, **24**, 81 (1980).

100. M Couzi, "Vibrational Spectra and Structures" Ed HD Bist, JR Durig and JF Sullivan, Elsevier, **17A**, 49 (1989).

101. LJde Jongh and AR Miedema, Adv Phy., **23**, 1 (1974).

102. A Daoud, J Appl Cryst., **10**, 133 (1977).

103. A Ben Salah, JW Bats, R Kalus, H Fuess and A Daoud, Z Anorg Allg Chem., **493**, 178 (1982).

104. R Blinc, B Zeks and R Kind, Phy Rev., **17B**, 3409 (1977).

105. DKh Blat and VI Zinenko, Sov Phy Solid St., **21**, 588 (1979).

106. R Geick and K Strobel, J Phys., **10C**, 4221 (1977).

107. A Rahman, PR Clayton and LAK Staveley, J Chem Thermody., **13**, 735 (1981).

108. M Peyarrd and M Remoissenet, J Chem Phys., **71**, 2732 (1979).

109. R Mokhlisse, M Couzi, NB Chanh, Y Haget, G Hallw and A Meresse, J Phys Chem Solids, **46**, 187 (1985).

110. MA White, VM Granville, NJ Davies and LAK Staveley, J Phys Chem Solids, **42**, 951 (1981).

TABLE 1.1 Classification of modes of $CH_3NH_3^+$ ion under C_{3v} symmetry.

C_{3v}	E	$2C_3$	$3\sigma_v$		n(T)	n(R)	n(V)	Activity[+] IR	R
A_1	1	1	1		1	0	5	A	A
A_2	1	1	-1		0	1	1	IA	IA
E	2	-1	0		1	1	6	A	A
ϕ	0	120	0						
ω_R	8	2	4						
$\chi(T)$	3	0	1						
$\chi(R)$	3	0	-1						
$\chi(V)$	18	0	4						
χ_α	6	0	2						

ϕ Angle of rotation,

ω_R Number of atoms remaining invarient under the operation

$\chi(T)$ Character for translational modes

$\chi(T) = \pm 1 + 2\cos\phi$ (+) for proper and (-) for improper

$\chi(R)$ Character for rotational modes

$\chi(R) = \pm 2\cos\phi + 1$ (+) for proper and (-) for improper

Table 1.1 (contd.)

$\chi(V)$ Character for vibrational modes

$$\chi(V) = (\omega_R - 2)(1 + 2\cos\phi) \qquad \text{for proper rotation}$$

$$= \omega_R(-1 + 2\cos\phi) \qquad \text{for improper rotation}$$

χ_α Character for polarizability tensor

$$\chi_\alpha = 2 \pm 2\cos\phi + 2\cos2\phi$$

(+) for proper and (-) for improper

Number of fundamentals of species i, $N_i = \dfrac{1}{N_G} \sum n_e \, \chi(V) \, \chi_i(R)$

The modes of species i are Raman active if $N_i^R = \dfrac{1}{N_G} \sum n_e \, \chi_\alpha \, \chi_i(R)$

The modes of species i are IR active if $N_i^{IR} = \dfrac{1}{N_G} \sum n_e \, \chi(T) \, \chi_i(R)$

N_G – Number of elements of the group (=6)

N_e – Number of elements in each class (e.g., for C_3, $N_e = 2$)

$\chi_i(R)$ – Character for species i in each class

$$N_{A_1} = \frac{1}{6}[1\times1\times18+2\times1\times0+3\times1\times4] = 5$$

$$N_{A_1}^{IR} = \frac{1}{6}[1\times1\times3+2\times1\times0+3\times1\times1] = 1 \neq 0$$

$$N_{A_1}^R = \frac{1}{6}[1\times1\times6+2\times1\times0+3\times1\times2] = 2 \neq 0$$

---

†A – active   IA – inactive

TABLE 1.2 Structural phase transitions in short chain compounds of the family $(C_nH_{2n+1}NH_3)_2MCl_4$.

Crystal	Transition temperature (K)	Structure	Transition entropy $JK^{-1}Mol^{-1}$
$(CH_3NH_3)_2CdCl_4$[†]	424	$D_{4h}^{17} \rightarrow D_{2h}^{18}$	0.17
	283	$D_{2h}^{18} \rightarrow D_{4h}^{16}$	0.24
	163	$D_{4h}^{16} \rightarrow C_{2h}^{5}$	10.80
$(CH_3NH_3)_2ZnCl_4$[‡]	483	$?? \rightarrow ??$	18.10
	426	$?? \rightarrow C_{2h}^{5}$	0.68
$(CH_3NH_3)_2HgCl_4$[*]	432	$?? \rightarrow ??$	?
	335	$?? \rightarrow C_{2h}^{5}$	?
$(C_2H_5NH_3)_2CdCl_4$[†]	485	$D_{4h}^{17} \rightarrow D_{2h}^{18}$	0.20
	216	$D_{2h}^{18} \rightarrow D_{2h}^{15}$	9.70
	113	$D_{2h}^{15} \rightarrow C_{2h}^{5}$	?
$(C_3H_7NH_3)_2CdCl_4$[†]	183	$D_{2h}^{18} \rightarrow INC$	6.16
	158	$INC \rightarrow D_{2h}^{15}$	3.85
	113	$D_{2h}^{15} \rightarrow C_{2h}^{5}$	13.98

[†] Data compiled from Refs 96 to 100 and the literature cited therein.

[‡] Taken from JM Perez-Mato et al, Phys Stat Sol., **68a**, 29 (1981).

[*] Taken from PSR Prasad et al, Chem Phys Lett., **142**, 341 (1987).
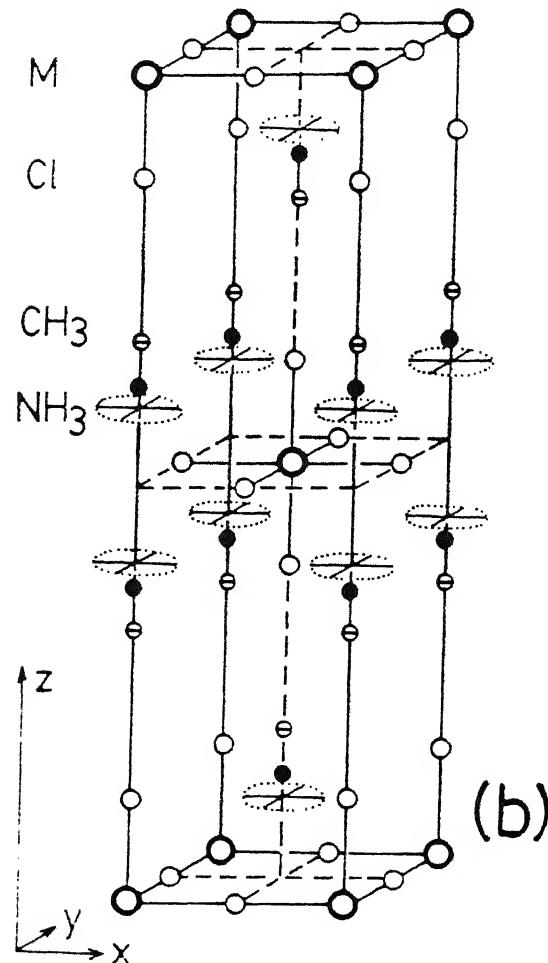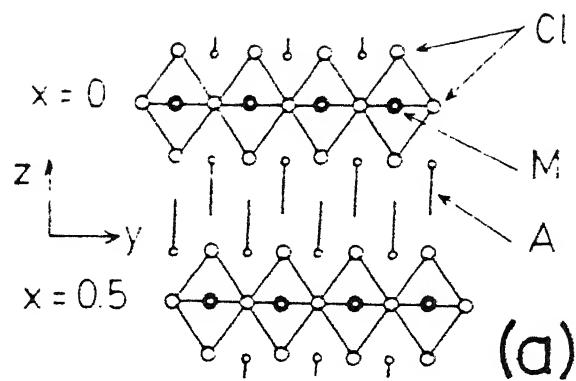
Fig 1.1 (a) The **XY** projection of $(C_nH_{2n+1}NH_3)_2CdCl_4$ type crystals.

(b) Crystallographic arrangement of $(C_nH_{2n+1}NH_3)_2CdCl_4$

type crystals in their proto-type phase.
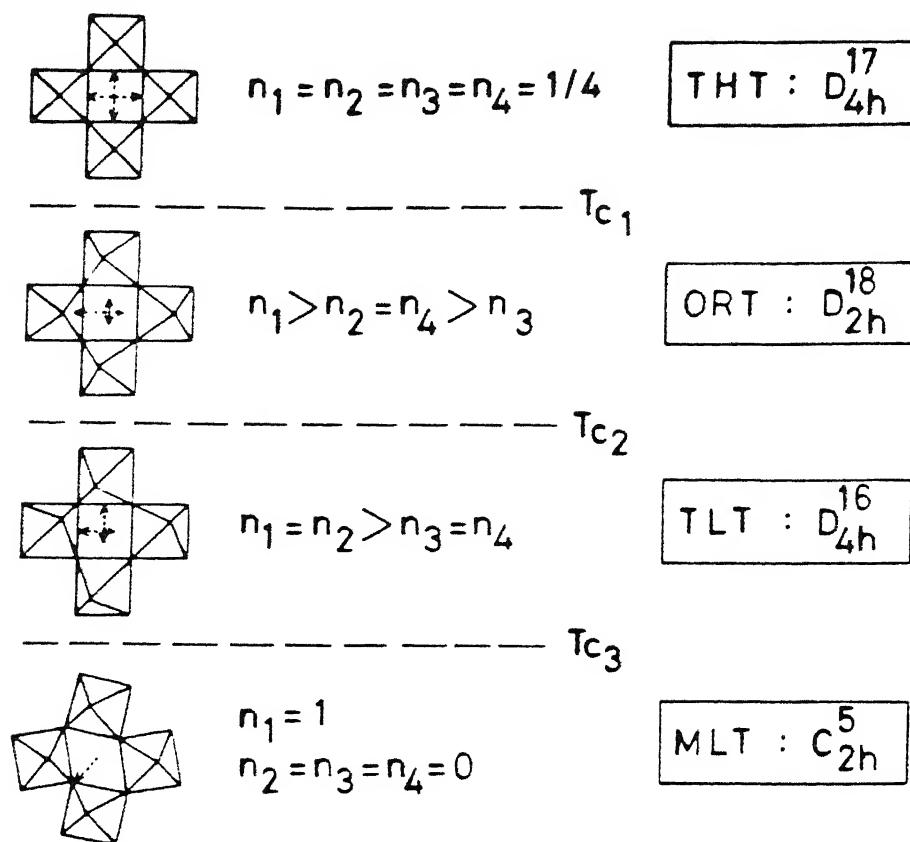
Fig 1.2 Schematic representation of the reorientational disorder of $CH_3NH_3^+$ groups in $(CH_3NH_3)_2CdCl_4$ crystals.

(a)   (b)
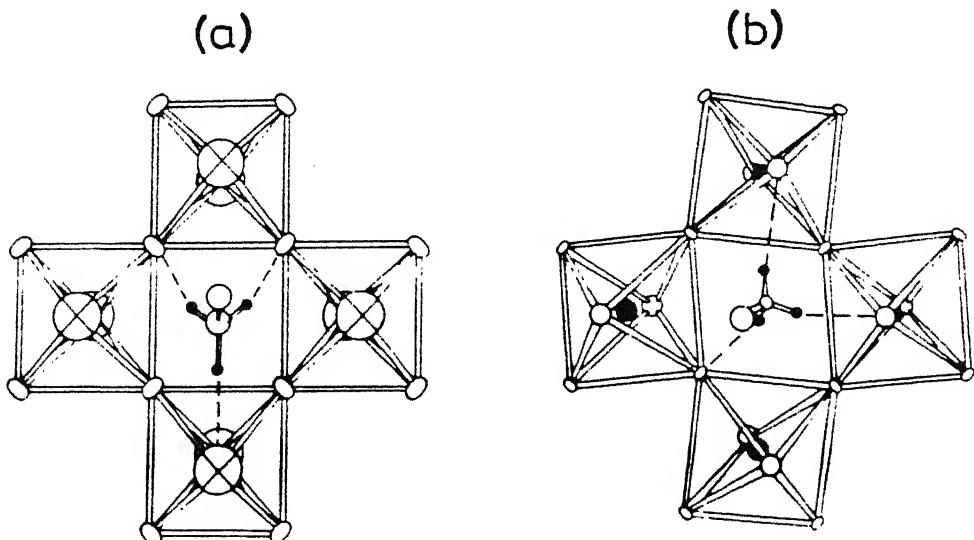
Fig 1.3 Projection of $(CH_3NH_3)_2CdCl_4$ layer along Z axis in (a) orthorhombic and (b) monoclinic hydrogen bonding schemes.

CHAPTER II

EXPERIMENTAL

2.1. SAMPLE PREPARATION

The compounds $(RNH_3)_2MCl_4$ where R = CH_3, C_2H_5 and C_3H_7, M = Cd, Zn and Hg were prepared by adding the alkylammonium chloride and the metal chlorides in stoichiometric ratio [1,2].

$$2RNH_3Cl + MCl_2 \longrightarrow (RNH_3)_2MCl_4$$
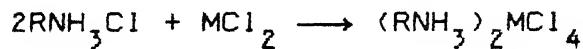
High purity starting materials have been obtained from K.K.Labs, Aldrich and BDH Chemicals. The solvents used to prepare all the metal chlorides (except for Hg compounds) is triply distilled water, the same for the mercury compounds is a equiproportionate mixture of acetone and methanol. Saturated solutions of the constituent salts have been prepared using the corresponding solvents. The two solutions have been mixed. Few drops of HCl is added to the solution in order to prepare a clear solution.

The solution obtained by this procedure has been kept in dry silica gel desiccator. After which, rectangular plates have been obtained and separated out from the solution. To

purify the compound further, these crystals are again dissolved in solvent and allowed to evaporate under low humidity conditions inside an air-conditioned room. Long-neck, flat bottom beakers have been used to obtain slower evaporation rates. In last stage, *i.e.*, at the third time a tiny crystal is used as a seed to grow a larger crystal. Thickness of M = Cd crystals are normally about 0.5 mm. All the precautions to grow thicker crystals like keeping them at constant temperature have failed. The crystals of appropriate dimensions are extracted from the mother liquor and used without preserving for a long time.

2.2. RAMAN SPECTROMETER SET-UP

The laser Raman spectrometer consisted of a source (165 Ar^+ laser from Spectra Physics), a double monochromator (1403 Spex) and a photomultiplier (RCA C-31034 GaAs) detector as shown in block diagram (Fig 2.1). The photomultiplier output is fed to a digital photon counter to process the signal, and is recorded on a X-Y recorder. The detailed optical diagram is shown in Fig 2.2. In the following paragraph, a brief description of main components of the experimental set-up, the experimental difficulties and its preventive measures have been described.

2.2.1. Source

One of the two strong lines of the Ar$^+$ laser $i.e.$, 514.5 nm line with the power 100-250 mW, has mainly been used to record the Raman spectra. A very frequent reduction in the laser power is caused by the dirty optics. Periodic cleaning has been done to keep the laser in good working condition. When the laser system is operated under current control mode the current across the tube is stabilized to ± 3% and output power is stable within ± 1%. Technical and operational details are given in manual [3].

The laser system was cooled by HX-500 Nes-Lab chiller. The chilled deionized water is circulated around the pass bank of 265 excitor and the plasma tube to take off the dessipated heat. The optimum flow rate is 8.4 lit min^{-1} at 2.11 kg cm^{-2} pressure. Inadequate flow is indicated by an LED on the front panel of the excitor. This is generally caused by the dirty filters near the exit of HX-500 chiller and the pressure switch of the 265 excitor. Periodic cleaning of these filters has been done without disturbing the flow rate.

A problem generally caused by the increase in the conductivity of circulating water has been taken care off. A simple test to ensure the high resistivity of water in the closed loop system is to measure the resistance between the magnetic housing in the laser head and the pass bank transistor cold plate in the 265 excitor. If the resistance is less than 100 kΩ, water has to be changed. Normally, water of resistance

500 kΩ has been maintained always in our system. The tube should occasionally be operated at the maximum current (38 Amps) for a short period only to get rid off the contaminated gaseous particles.

2.2.2. Ramalog System

The main parts of the spectrometer are a laser mate UVISIR illuminator and a double monochromator [4]. The laser beam first passes through the laser mate where grating G_1 will eliminate the unwanted spurious plasma lines. The laser beam now enters into the illuminator, where a flat aluminium coated mirror M_5 reflects it on to a fused silica condensing lens L_1. A beam of about 10 μm diameter spot is focused on to the sample S. Precise alignment of the sample is achieved by mounting the low (high) temperature cells on home made micro-meter controlled three way platform. The scattered light is collected by an elliptical mirror M_8 (s/1.4). A flat mirror M_9 reflects this radiation at 90° and focuses on to the entrance slit S_3 of the double monochromator.

As shown in the optical diagram, the monochromator consists of two holographic gratings (G_1, G_2 with 1800 line mm^{-1}) which act as dispersive elements whose motion is coupled and controlled by a servo motor. The collimated radiation from M_{10} is diffracted by G_2 and is focused on to S_5 by M_{11}. The mirror M_{12} again focuses light on to S_6. Together, the

intermediate slits and the mirrors act as spatial filters and cut down the stray light to the maximum extent. Now, the light falls on second grating G_3 and doubles the dispersion which in turn doubles the intensity for a given band pass. The mirror M_{14} guides this on to a photo cathode through the exit slit S_7.

The detector is a GaAs RCA C-31034 photomultiplier tube which operates best at 243 K. This temperature is achieved by the thermoelectric cooling. The useful characteristics of the photo multiplier tube are shown in Fig 2.3. For the best results, PMT was used in the plateau regions shown in Fig 2.3.

Frequent alignment of the monochromator is not required. But whenever the mismatch of stokes and anti-stokes line is observed, the alignment is performed. The mercury lines are scanned first. If the error is within 5 cm^{-1}, routine calibration will do. This has been done in the following manner. The counter has been set exactly at the known peak of Hg line. The slit S_7 is kept at 25 μm so as to allow minimum light to fall on PMT. Now, the mirrors M_{10} and M_{14} are adjusted through side exit cone (one at a time) so as to get maximum PMT counts.

2.2.3. Sample Handling

The Raman spectra were recorded for both single crystals and polycrystalline samples. The crystals were cut and finely polished before use. In order to study the polarization

dependence, the crystal was fixed on a plate and mounted on a goniometer head. The analyzer was placed before the elliptical mirror (M_8). The polarization scrambler was placed before the entrance slit (S_3). The rotation of the polarization of laser beam is achieved by placing 90° polarization rotator in front of the lasermate. The usual Porto notation [6] is used to indicate the polarization geometry. In this notation [**Z**(**XY**)**X**]; **Z** and **X** outside the parenthesis represent the incident and the scattered beam directions. The symbols **X** and **Y** inside the parenthesis denote the polarization characters of incident and scattered light respectively. The fine powdered sample was filled in sealed capillary or pyrex glass tube to record the spectra at various temperatures.

2.2.4. Variable Temperature Cells

Various temperature cells have been fabricated according to our convenience. Higher temperatures (upto 523 K) have been achieved by heating the sample holder in controlled way by using a combination of three 25 W heaters as shown in Fig 2.4. More details were given given elsewhere [7]. The temperature is measured by copper-constantan thermocouple kept close to the sample. The accuracy is better than ± 1 K.

The flow type cryostat has been designed for the first time in our lab using which we can vary the temperature in 77-300 K range. The detailed diagram is shown in Fig 2.5. The basic idea is that the cold N_2 gas is circulated through a

copper tube around the cold finger. A copper rod with appropriately modified end has been used as a cold finger. Two perpendicularly oriented windows of 1" and 1.5" dia are used to send the laser light and to collect the scattered radiation. Temperature is controlled with the accuracy of $\pm$ 2 K, by monitoring the flow of N_2 vapour using a needle valve.

2.3. INFRARED SPECTROMETER

The infrared spectra have been recorded on dry air purged Perkin-Elmer 580 spectrometer [8], the block diagram of which is shown in Fig 2.6. It depicts the double beam spectrometer which records the ratio of transmission of the sample and reference beams in 4000-180 cm^{-1} frequency range. The frequency scan motor drives both recorder and monochromator in synchronization. In addition, there is an automatic wavenumber correction system to give high frequency accuracy, irrespective of scan speed. The detailed optical diagram of the system is shown in Fig.2.7.

The infrared radiation from the hot ceramic source at about 1200° C, is divided into sample and reference beams by the action of a chopper mirror M_5. The transmitted and the reference beams recombine after the sample compartment by the action of second chopper mirror M_{10}. The recombined beam passes through a set of torroidal mirrors M_{11} - M_{13}, which reject the unwanted radiation from pre-optics. The mirrors M_{14} and M_{15}

reflects the beam on to the entrance slit Sl_3 in 4000 to 330 cm^{-1}. Below 330 cm^{-1} these M_{14} and M_{15} mirrors rotate in their plane synchronously. The grating surface of which reflects the low frequency radiation on to Sl_3, rejecting all higher wavelengths. Hence in the low frequency range, it acts as an additional filter.

The monochromator consists of four gratings operating in 4000-1980, 1980-630, 630-330, 330-180 cm^{-1} range. These gratings have 2880, 960, 250 and 90 lines cm^{-1}, respectively. These gratings are mounted on two movable tables. The gratings 1, 3 and 2, 4 form two pairs. The collimated radiation from paraboloid mirror M_{16} falls on the grating in use. The diffracted radiation is focused in the plane of the exit slit Sl_4 by M_{16}. The radiation is now allowed to fall on the detector.

The detector consists of a thermocouple placed at the focus of an on-axis ellipsoidal mirror M_{20} enclosed in an evacuated chamber. A caesium iodide lens on the thermocouple assembly reduces the dimension of the slit image falling on the target. The target of the thermocouple consists of 1.4 × 0.45 mm^2 strip of blackened gold leaf welded to two pins. The black gold leaf absorbs the radiation falling on it producing a thermoelectric voltage. This voltage is a measure of the intensity falling on the detector. This voltage is fed to the signal processing unit after proper preamplification.

2.3.1 Sample Handling

Powder Samples

The IR spectra were obtained from such samples in two ways (i) making a transparent pellet of the material after diluting it with matrix (like KBr or CsBr which is transparent in the IR range) (ii) making a fine powder of the sample and mixing it with nujol to prepare a mull. A thin layer of it is coated onto the infrared windows (like KBr or CsBr). These two techniques will provide very rough information about the phase transitions, as we get only the averaged spectra. The information about the crystal anisotropy is lost in these cases. Moreover, if the material is reactive with the matrix, pellet method is not possible. It is also possible that they form complexes.

Crystals

To avoid the above cited reasons, we have tried to record the spectra using single crystal platelets. The crystal with M = Cd grew thinner about the layer axis. Hence, it has become easy to extract a thin crystal. The thickness has been carefully reduced to typically about 20 μm, by polishing with aluminium oxide and acetone. The crystals then were observed through a Carl Zeiss Amplival-Polu polarization microscope to ensure that the surface is free from cracks which might cause major temperature gradients. The typical dimensions of the crystals

used are $3 \times 3 \times 0.02$ mm^3. The crystals were mounted on the cold finger of the Specac temperature variation cell to study the phase transitions. However, in the present study we could not study the polarization dependence because of experimental limitations. But one can do that by keeping a polarizer at M_{12} as shown in Fig 2.7.

2.3.2 Variable Temperature Cell

The commercially available Specac temperature variation cell has been used for the temperature variation study. The line diagram of which is shown in Fig 2.8. The cold-finger is enclosed in a metal jacket which is provided with two KBr windows to allow the radiation. The sample holder is fitted to the cold finger. Two heaters (5Ω each) in parallel with an effective resistance of 2.5Ω are wrapped around the sample holder. This enables the temperature to be varied in 83-523 K range. A copper constantan thermocouple was used to measure the temperature. The temperature is controlled within $\pm$ 2 K in sub-ambient and $\pm$ 1 K in above ambient temperature ranges.

Single crystals were fixed on a 1.2 mm dia copper disc with 2×2 mm^2 hole at the centre. This disc was then sandwitched between two nickel coated metal gaskets. The whole assembly was kept inside the sample cell.

2.4 INSTRUMENTAL RESOLUTION CORRECTION

It is known that the observed spectra is the convolution of true line shape with the instrumental resolution function. One may read correct peak frequencies directly but the same is not for the linewidth. A finite slitwidth produces a measurable contribution to the actual linewidths. Hence, to get the idea about the *true widths* one should have the knowledge of the instrumental resolution function.

2.4.1 Resolution Function

The vibrational normal modes can be approximately assumed to be Lorentzian line shapes given as [9,10]

$$I_L(\omega) = \left[(I_o \, \Gamma_L^2) / \{4(\omega - \omega_o)^2 + \Gamma_L^2\} \right] \qquad 2.1$$

where I_o, Γ_L and ω_o are peak intensity, full width at half maximum intensity and frequency respectively. The slit function can be approximated to a Gaussian given as [9]

$$I_G(\omega) = I_{oG} \, \exp\left[-\{\omega / (\Gamma_G / 2(\ln2)^{1/2}\}^2 \right] \qquad 2.2$$

where Γ_G is fullwidth at half maximum intensity. I_o is the peak intensity. The observed spectra normally is the convolution of these two functions given as

$$I(\omega) = \int I_L(\omega-t) \, I_G(t) \, dt \qquad\qquad 2.3$$

Substituting eqns 2.1 and 2.2 in 2.3 and making the following coordinate transformations

$$\vartheta = t/\{\Gamma_G/2(\ln2)^{1/2}\} \qquad\qquad 2.4$$

$$x = (\omega - \omega_o)/\{\Gamma_G/(2(\ln2)^{1/2}\} \qquad . \qquad 2.5$$

$$y = (\Gamma_L/\Gamma_G)(\ln2)^{1/2} \qquad\qquad 2.6$$

it transforms into *Voigt function*.

$$I(\omega) = I_o \int \frac{\exp(-\vartheta^2) \, d\vartheta}{y^2+(x-\vartheta)^2} \qquad\qquad 2.7$$

Asthana *et al* have numerically calculated eqn 2.7 for different y values upto y = 15 [9]. With the help of the table one can estimate the *true widths*.

2.4.2 Estimation of True Linewidths

The Lorentzian linewidths can be deduced from the Voigt profiles by the following manner. First we have recorded the laser line with the same slit settings with which the actual experiment is performed. The observed profile is fitted well with eqn 2.2. Now the linewidth Γ value is measured from the observed profile for our monochromator. The corresponding y values are taken for the $(\Gamma_{Raman}/\Gamma_{slit})$ from the reported data [9]. The *true linewidths* are estimated by eqn 2.6. This procedure is slightly

easier than the one adopted by Arora *et al* [10]. It has been observed that if the ratio of $\Gamma_{Raman}/\Gamma_{slit}$ is more than 3, the slit contribution to true width is marginal. So keeping this in mind the appropriate slit widths are chosen. If the Raman lines are very sharp then the y values are determined by taking the ratio of $(\Delta\omega_{1/4})_{Raman}/(\Delta\omega_{1/4})_{slit}$, where $(\Delta\omega_{1/4})$ is the full width of the profile at $(I_o/4)$. If y values do not exist for any of these ratios, *i.e.*, $\Gamma_{Raman}/\Gamma_{slit}$ or $(\Delta\omega_{1/4})_{Raman}/(\Delta\omega_{1/4})_{slit}$, then a linear interpolation is made between the relevant y values.

2.4.3 Deconvolution of overlapped bands

As already mentioned the vibrational lines are assumed to be Lorentzian shape. If the slit width is sufficiently narrow the overlapped band profile is given by a linear combination of eqn 2.1. The slit widths are set in such a way that the ratio $\Gamma_{Raman}/\Gamma_{slit}$ is always greater than 3. Then it is reasonable to assume that the resultant profile is given by,

$$I(\omega) = A + B\ (\omega-\omega_{min}) + C \sum \frac{\Gamma_i^2(obs)}{4(\omega-\omega_{oi})^2 + \Gamma_i^2(obs)} \qquad 2.8$$

where ω_{min} is the minimum Raman shift observed. To deconvolute the bands we have fitted eqn 2.8 by measuring different $I(\omega)$ values ($\cong$ 30-40) with respect to a flat background in the

frequency intervals of 1 to 0.5 cm^{-1}. Γ_i, ω_{oi} and C have been given as the parameters and the initial guess value of it is proportional to fullwidth at half maximum intensity, peaks frequency and peak intensity respectively. DEC-1090 computer was used to carry out an iterative program with the help of a non-linear least square minimization sub-routine (NAG E04-FCF) till a better fit is obtained. The fit is considered to be *good* if the errors are comparable to the measurement uncertainties. The parameter values obtained by the procedure are accurate within the measurement errors. The computer fit is well in agreement for the high temperature side but the fit is slightly poor on low temperature side, as the resultant is no more a Lorentzian but a Voigt profile.

Intensity-wise the bands are reproducible within 20% uncertainty under similar conditions. The frequency positions are accurate upto ± 2 cm^{-1} for strong/sharp bands. The same is upto ± 5 cm^{-1} for weak/broad bands.

REFERENCES

1. H Arend, W Huber, FH Mischgofsky and GKR Leeuwen, J. Crystal Growth, **43**, 213 (1978).

2. A Ben Salah, JW Bats, R Kalus, H Fuess and A Daoud, Z. Anorg Allg Chem., **493**, 178 (1982).

3. Operational Manual of Spectra Physics (165).

4. SPEX operational Manual of 1403 Monochromator.

5. Technical Report On PE 580 spectrometer.

6. B Tell, TC Daman and SPS Porto, Phy. Rev., **144**, 771 (1966).

7. Mahendra Pal, Ph.D Dissertation, Dept of physics, IIT, Kanpur, India (1984).

8. MB Patel, Ph.D Dissertation, Dept of Physics, IIT, Kanpur, India (1982).

9. BP Asthana and W Kiefer, App. Spectrosc. **36**, 250 (1982).

10. AK Arora and V Umadevi, App. Spectrosc., **36**, 424 (1982).
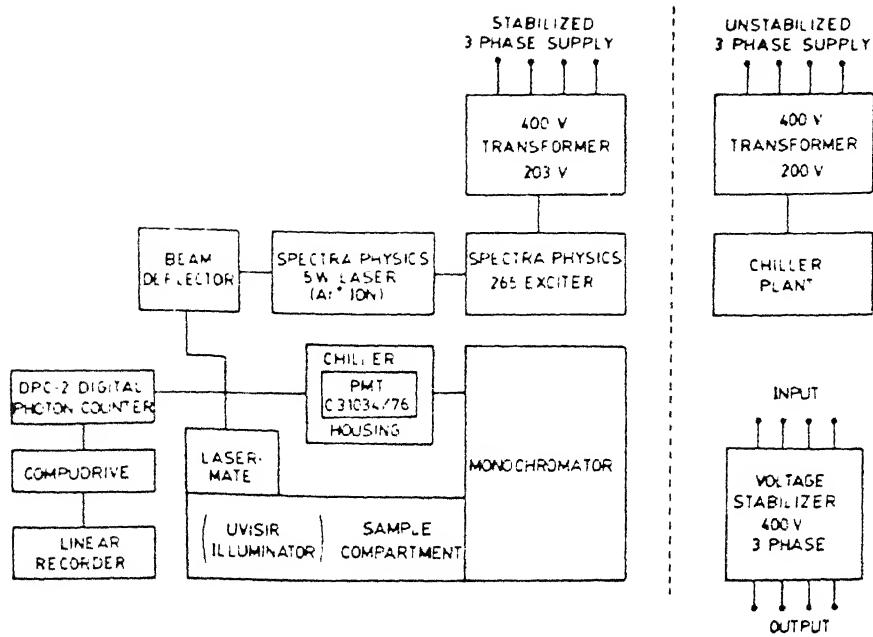
Fig 2.1 Block diagram of laser Raman spectrometer.
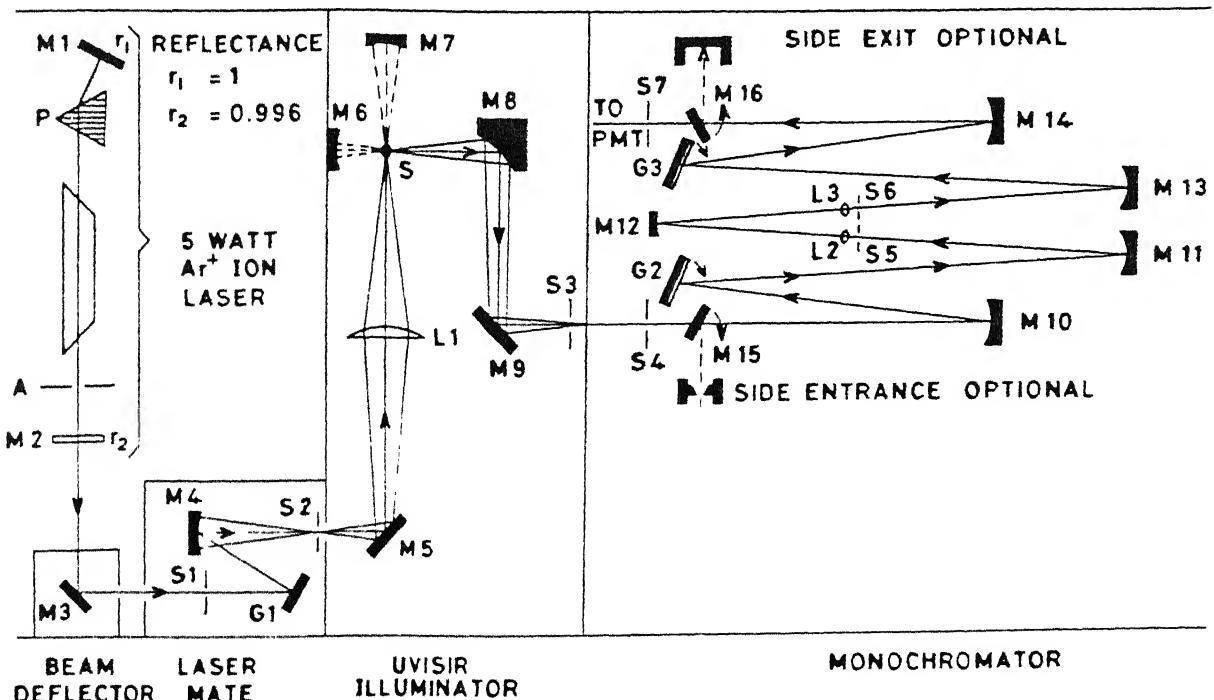
P. Prism; A: Aperture; M1-M3, M5, M9, M15, M16: Plane Mirrors; M4, M6, M7, M10-M14: Concave Mirrors; M8: Elliptical Collector Mirror; S1-S7: Slits; G1-G3: Gratings; L1: Fused Silica Condenser Lens; S: Sample; L2, L3: Optical Filter; PMT: Photomultiplier Tube.

Fig 2.2 Optical diagram of the Raman spectrometer.
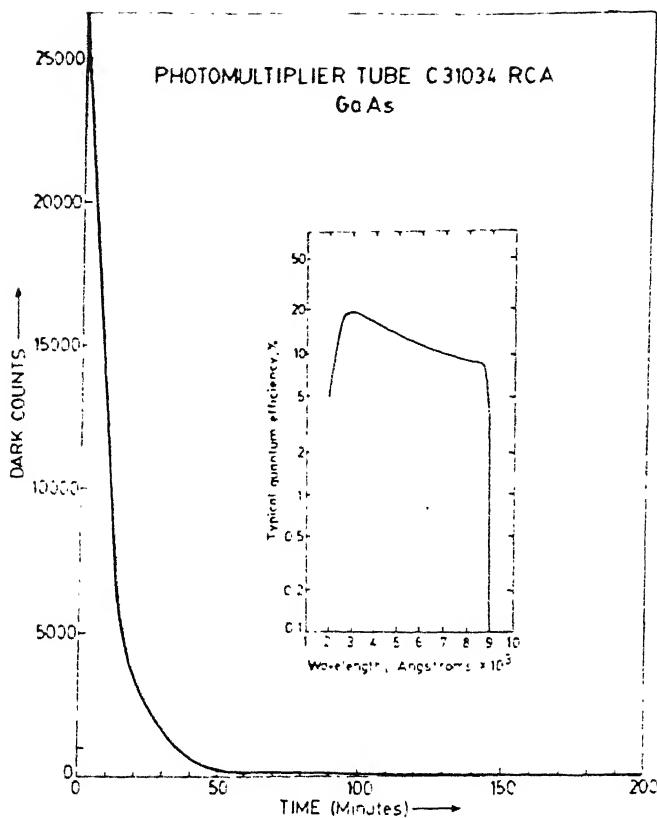
Fig 2.3 Thermoelectric cooling and quantum efficiency (inset) curves of the GaAs photomultiplier.
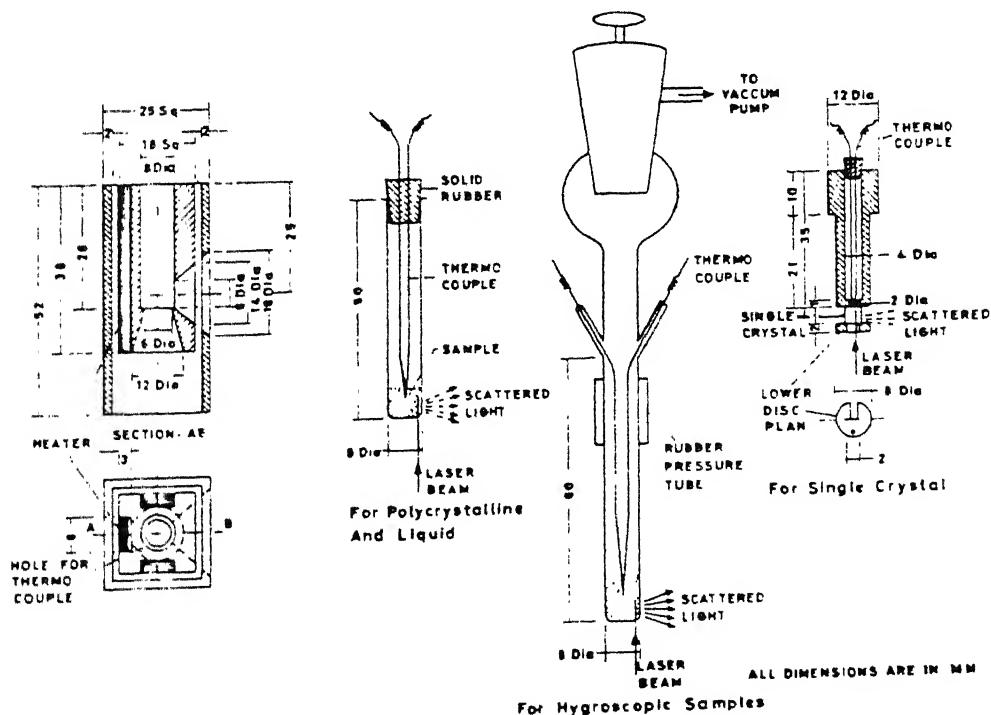
Fig 2.4 The design of the temperature cell in 300 - 523 K range used for the Raman scattering study.

N₂ N₂

9

10

1

2 → To vaccum pump

1,2 - O ring
3 - Copper rod
4 - Copper tubes
5 - Sample holder
6,7 - Glass windows
8 - Outer glass jackets
9 - Thermocouple and
     heater wires
10 - Teflon plate
11 - Sample
12 - Scattered light

3

4

8

5   12   6

11

7

Incident light

Capillary holder
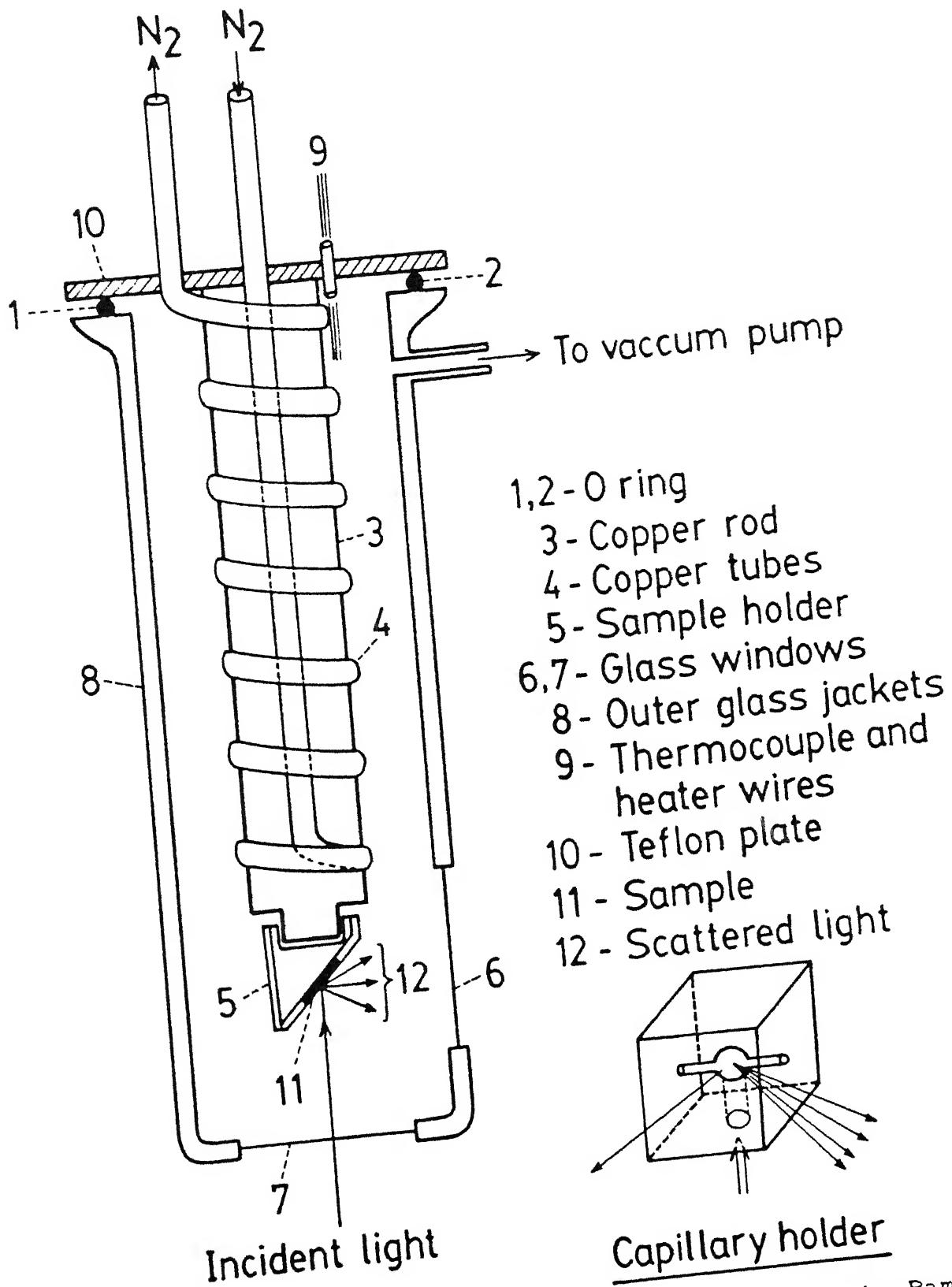
Fig 2.5 The low temperature cell diagram used to record the Raman spectra in 80 – 300 K region.
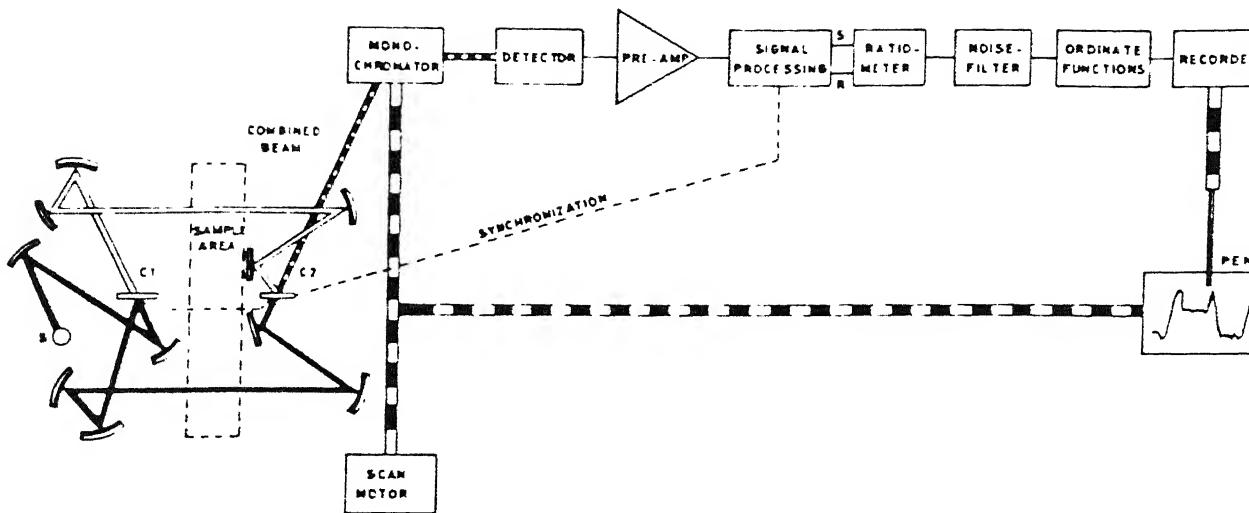
Fig 2.6 Block diagram of the Perkin - Elmer (PE 580) infrared spectrometer.
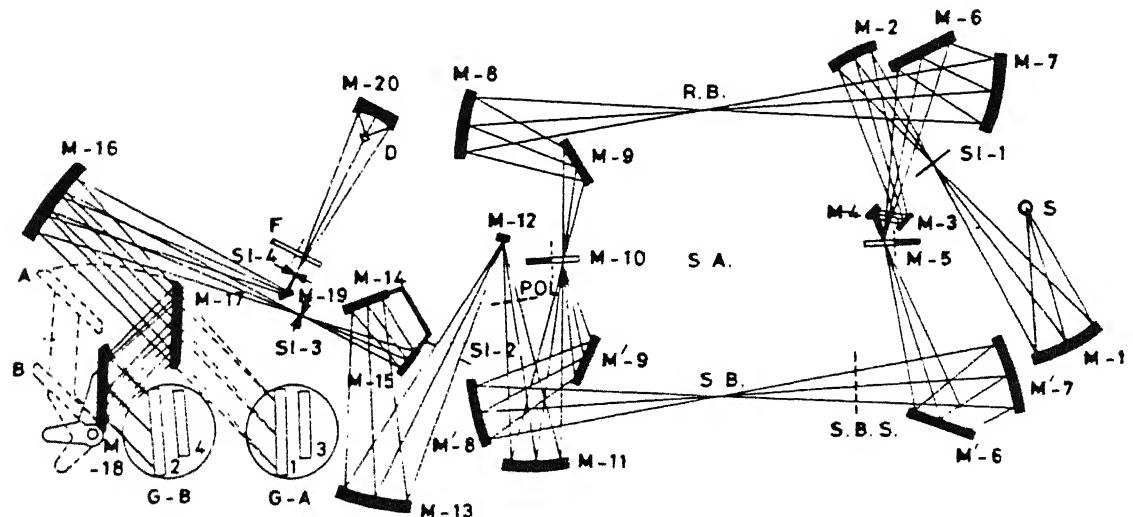
S:Source; M1,M2,M4,M7,M'7,M8,M'8,M11-M13.Toroid Mirrors;M5,M10:Chopper Mirrors;M3,M6,M'6,M9, M'9,M14,M15,M17,M19.Reflection and Scatter Grating Surface Mirrors, M16:Paraboloid Mirror;M20: Elipsoid Mirror; G-A,G-B:Grating Tables;SI-1:Baffle and Secondary Source; SI-2:Pupil Baffle;SI-3: Entrance Slit; SI-4:Exit Slit,POL:Polarizer Accessory;F:Optical Filter;D:Detector;SBS:Sample Beam Shutter; SB:Sample Beam;SA:Sample Area;RB:Reference Beam.

Fig 2.7 The optical diagram of PE580 infrared spectrometer.

MUSHROOM

TUBE

TO VACUUM PUMP

BUNG
TOP PLATE
TOP ADAPTOR

VACUUM TIGHT
JACKET

SILICONE
ELASTOMER SEAL
SCREW THREADED
OF RETAINING RING
WINDOW

CLAMP SCREW

THERMOCOUPLE

SCREW PLUG

PIN (TO LOCATE CELL

O-RING
SILICONE
SILASTOMER SEAL

REFRIGERANT
CHAMBER

POLYURETHANE
FOAM

PLATE
FOR CELL-MOUNT

IR RADIATION

SAMPLE CELL
SAMPLE HOLDER
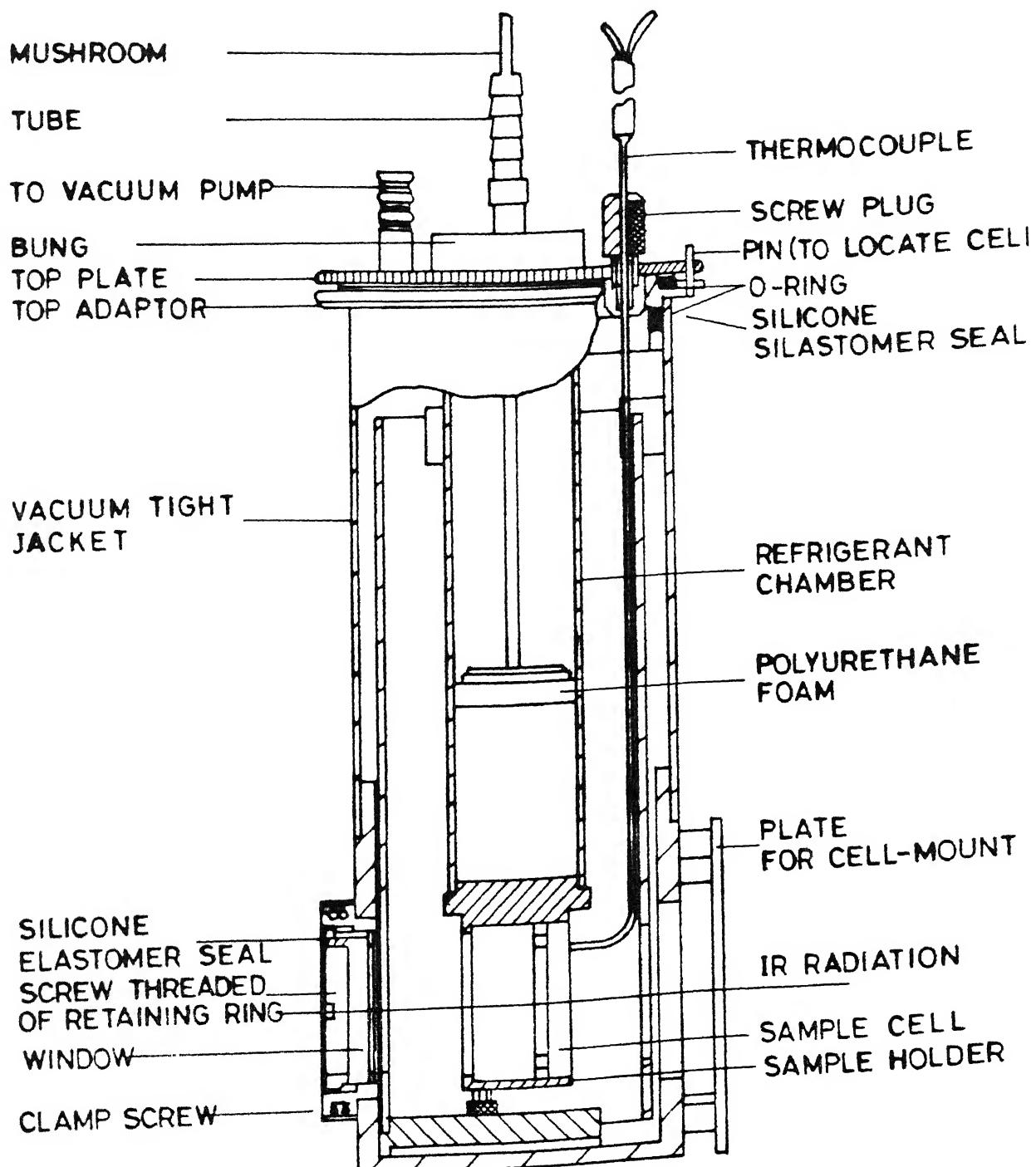
Fig 2.8 The line diagram of Specac temperature cell used to recor

the infrared spectra in 77 – 523 K range.

CHAPTER III

VIBRATIONAL SPECTROSCOPIC STUDY OF STRUCTURAL PHASE TRANSITIONS IN $(CH_3NH_3)_2MCL_4$ CRYSTALS: M = CD, ZN AND HG

ABSTRACT

The Raman and infrared (IR) spectroscopic study of the structural phase transitions (SPT) in methyl substituted ammonium metal chlorides have been presented in this chapter. The metal ions are Cadmium, Zinc and Mercury. The detailed Raman polarization study of the crystal with M = Cd in ORT phase and thermal evolution of a few thermosensitive bands in 95-300 K region are reported. The phase transition at 163 K in the compound has been corroborated by the present study.

The Raman spectroscopic study of M = Zn and Hg crystals are used to assign their vibrational spectra. Phase transitions in these compounds are studied by DTA/DSC and Raman spectroscopic techniques. Similarities in $\nu(CN)$ band have been attributed to the reorientational motion of the methylammonium ion.

3.1 INTRODUCTION

The methylammonium compounds with the formula $(CH_3NH_3)_2MCl_4$ (abbreviated hereafter as C_1MCl, M is the corresponding metal ion, M = Cd, Zn and Hg) are known to undergo several phase transition in 500-77 K range (see Table 1.2). The phase sequence in C_1CdCl have been investigated by several studies like calorimetric [1], crystallographic [2], Raman [3,4], infrared [5-7] and NMR [8,9]. However, there are no Raman and IR studies in the internal mode region. In the present study, a few thermosensitive bands in the internal mode region are monitored and the changes in spectral parameters are attributed to the dynamical reorientational motion of methylammonium ions.

C_1ZnCl and C_1HgCl are structurally different from that of C_1CdCl. They belong to monoclinic at room temperature [10,14]. The structural phase transitions (SPTs) in these crystals have not been studied in detail. Structural information in other phases are not available. However, thermal expansion and other studies [11] propose two high temperature phase transitions for M = Zn crystal. During our present investigation, two other groups have also reported SPTs through the Raman studies [12,13]. The phase transitions in M = Hg were not known previously, but the room temperature crystal structure is known [14]. From the present study, two high temperature phase transitions for the crystal were reported [15].

3.2 CRYSTAL STRUCTURE

The number of atoms (21) in the formula unit for these crystals is rather large resulting in large degrees of freedom. However, the observed spectra could be correlated by site group approach. The undistorted methylammonium ion has free molecular symmetry C_{3v}. The expected 18 vibrational modes belong to $5A_1 + A_2 + 6E$ irreducible representations (see Table 1.1). The A_1 and E modes are both IR and Raman active, whereas A_2 mode is inactive in both. The other translatory and rotatory modes belong to $A_1 + E$ and $A_2 + E$. The previous group theoretical studies considered the methylammonium ion as a single rigid entity to carry out the analysis for C_1CdCl type crystals in tetragonal high temperature (THT) and orthorhombic room temperature (ORT) phases [16,17]. The analysis was extended on similar lines in tetragonal low temperature (TLT) and monoclinic low temperature (MLT) phases [3]. In the present case, the free ion symmetry of methylammonium ion (C_{3v}) has been used for the factor group analysis.

3.2.1 Distribution of Modes of $CH_3NH_3^+$ Group In C_1CdCl

As noted in Table 1.2, C_1CdCl undergoes a transition above the ambient temperature. Below room temperature it undergoes two transitions. The corresponding space groups and the number of molecules in the unit cell starting from the proto-type phase

are D_{4h}^{17} (Z=4); D_{2h}^{18} (Z=2); D_{4h}^{16} (Z=4) and C_{2h}^{5} (Z=2). The expected mode distribution in ORT and MLT phases is given (in Table 3.1). A brief description of the procedure is already given in § 1.2.2.

Orthorhombic Room Temperature Phase

C_1CdCl exists in orthorhombic phase between 424 and 283 K. In this phase (D_{2h}^{18}) there are two molecules in a unit cell. The number of expected internal (int) modes for $CH_3NH_3^+$ are (3×8-6)2×2 = 72. These are distributed among the irreducible representations as,

$$\Gamma_{int} = 11A_g + 7B_{1g} + 7B_{2g} + 11B_{3g} + 7A_u + 11B_{1u} + 11B_{2u} + 7B_{3u}$$

The remaining 24 would be the external modes, translational (T) and librational (R) modes.

$$\Gamma_T = 2A_g + B_{1g} + B_{2g} + 2B_{3g} + A_u + 2B_{1u} + 2B_{2u} + B_{3u}$$
$$\Gamma_R = A_g + 2B_{1g} + 2B_{2g} + B_{3g} + 2A_u + B_{1u} + B_{2u} + 2B_{3u}$$

Tetragonal Low Temperature Phase

C_1CdCl goes to tetragonal phase with the space group D_{4h}^{16} (Z=4) from its ORT phase at 283 K. The previous studies suggested a site group of C_s to the methylammonium ion [3.6]. However,

extending a similar analysis, it yields fractional numbers, which are not acceptable. So, the chosen site group C_s seems to be incorrect. The next possible site group is C_1 which gives the following distribution for Γ_{int}, Γ_T and Γ_R modes of the methylammonium ions.

$$\Gamma_{int} = 12(A_{1g}+A_{2g}+B_{1g}+B_{2g}+E_g+A_{1u}+A_{2u}+B_{1u}+B_{2u}+E_u)$$
$$\Gamma_T = 2(A_{1g}+A_{2g}+B_{1g}+B_{2g}+E_g+A_{1u}+A_{2u}+B_{1u}+B_{2u}+E_u)$$
$$\Gamma_R = 2(A_{1g}+A_{2g}+B_{1g}+B_{2g}+E_g+A_{1u}+A_{2u}+B_{1u}+B_{2u}+E_u)$$

Since there are no observable spectral variations during the transition, [3,6,7] detailed crystallographic studies are necessary to find the correct site group.

Monoclinic Low Temperature Phase

C_1CdCl undergoes a tetragonal to monoclinic transition below 163 K. The methylammonium ion occupies C_1 site while $CdCl_4^{2-}$ occupies C_i. A detailed site group analysis for $CdCl_4^{2-}$ (with free ion symmetry D_{4h}) is given in Table 3.2 so as to point out the difference with C_1ZnCl and C_1HgCl systems in which the molecular symmetry of the corresponding metal chloride group is T_d.

3.2.2 Mode Distribution for C_1ZnCl and C_1HgCl

The compounds with M = Zn and Hg differ from that of Cd as the crystals are monoclinic at room temperature. The phase

transitions in these compounds have not been studied previously in detail. The crystal structure in other phases are not known. In room temperature phase, as already pointed out, MCl_4 forms a tetrahedron [10,11,14].

At room temperature the unit cell consists of four molecules [10,14]. For simplicity, we consider methylammonium (A) and metal chloride (M) as independent groups with free ion symmetries C_{3v} and T_d respectively. Following the usual correlation method with site symmetry C_1 for both the groups we get the following distribution which also includes three acoustic modes (see Tables 3.1 and 3.2),

$$\Gamma^A_{int} = 36 \ (A_g + B_g + A_u + B_u)$$

$$\Gamma^A_R = 6 \ (A_g + B_g + A_u + B_u)$$

$$\Gamma^A_T = 6 \ (A_g + B_g + A_u + B_u)$$

$$\Gamma^M_{int} = 9 \ (A_g + B_g + A_u + B_u)$$

$$\Gamma^M_R = 3 \ (A_g + B_g + A_u + B_u)$$

$$\Gamma^M_T = 3 \ (A_g + B_g + A_u + B_u)$$

3.3 VIBRATIONAL SPECTRAL ANALYSIS IN THE ROOM TEMPERATURE PHASE

Among 18 internal modes of the methylammonium ion with the free ion symmetry C_{3v}, eight are doubly degenerate (E) and five are (A_1) modes. One (A_2) mode is inactive in both the infrared and the Raman spectra. In the Raman spectra one would expect 11 internal modes that belong to methylammonium ion. If the

interaction between the MCl_6 octahedra and organic ion is weak one would expect a little variation in the internal modes for different metal ions. Indeed, the weak linkage is evident from the band positions of methylammonium ion in M = Cd, Zn and Hg crystals noted in the Table 3.3.

3.3.1 Raman Polarization Studies of C_1CdCl

Since the number of molecules are large resulting in large degrees of freedom, a precise assignment is difficult. However, recorded Raman polarization spectra of C_1CdCl in D_{2h}^{18} phase throw some light on weak factor group effects on the methylammonium ion. The Raman polarization spectra of C_1CdCl in A_g, B_{1g}, B_{2g} and B_{3g} species for the **XX, XZ, YZ** and **YX** polarization geometries are shown in Fig 3.1, and the band positions are tabulated in Table 3.4.

External Modes of Methylammonium Ion

The Raman polarization study of C_1CdCl have been carried out previously upto 500 cm^{-1} in ORT and MLT phases and detailed assignments were proposed [4]. Present study corroborates the polarization behaviour. One would expect external modes of the crystal along with metal chloride internal modes in the range below 500 cm^{-1} (for consistency we call all the modes in this range as *external*).

The A_g modes in ORT phase are expected to be active in α_{zz}, α_{yy} and α_{xx} polarizations. The Raman modes at 65, 110, 125 cm^{-1}, observed in α_{xx} polarization (see Fig 3.1) are assigned to the external modes of the methylammonium ion [4]. The other modes in the same polarization geometry at 80, 172 and 213 cm^{-1} have been attributed to the $CdCl_6$ octahedra [4]. Since the crystals were too small and thin, it was not possible to record the spectra in YY and ZZ polarizations. Moreover, the sample got burnt for the same power (i.e., 80 mW) on exciting along X or Y axes. Hence, the spectra were recorded by exciting along Z axis. The α_{xx} (A_g) Raman spectra possess well defined bands, whereas the cross polarization spectra are very weak and broad. In the α_{xx} polarization, the low lying frequencies at 65, 110 and 125 cm^{-1} are due to the librational and translational (T_x and T_z) modes, respectively, of the organic ion. The other modes at 172 and 212 cm^{-1} are due to the bending and stretching modes of $CdCl_6$ octahedra [4]. The band positions measured in the present experiment in all four polarization geometries with a uncertainty of 2 cm^{-1} are given in Table 3.4. The B_{ig} (i = 1,2, 3) are very tentative because of crystal twinning effects [4].

Internal Modes

Following the correlation $C_{3v} \rightarrow C_s \rightarrow D_{2h}^{18}$ it is expected that ν_1 to ν_5 modes which belong to A_1 irreducible representation are not allowed in the B_{1g} and B_{2g} species. The ν_6 mode is not

allowed under A_g irreducible representation. The detailed polarization studies along with previously reported data [3,4] clearly confirm the fact that $K = 0$ selection rules are not strictly applicable in ORT phase.

Though the crystal is known to be disordered and highly twinned in nature [4], a clear directional dependence of strong ν_5 and ν_2 modes indicate that a particular domain is excited in the present study. The ν_1 symmetric stretching mode of NH_3 is found at 3098 cm^{-1} of A_g and B_{1g} spectra as a broad and weak band. The asymmetric stretching modes of NH_3 (ν_7) and CH_3 (ν_8) are observed to be weak in all the polarizations at 3160 and 3035 cm^{-1}, respectively. The CH_3 symmetric stretching (ν_2) mode is very strong in all four geometries. The asymmetric bending mode in the region 1400 - 1600 cm^{-1} are very weak in the A_g spectra and not seen in B_{ig} spectra.

3.3.2 Vibrational Spectra of C_1MCl M = Zn and Hg

The vibrational spectra of M = Zn and Hg are not available in literature. These two compounds are iso-structural at room temperature (C_{2h}^5), with a = 10.865, b = 7.627, c = 12.661 Å and β = 96.58° (for Zn) and a = 7.779, b = 12.925, c = 10.962 Å and β = 96.32° (for Hg) [10,14]. The observed infrared and Raman spectra of these compounds are shown in Fig 3.2. Insets in the figure are the far-infrared (FIR) spectra.

Modes Below 400 cm^{-1}

The vibrations due to the inorganic part along with the translational and librational modes of the organic part of the crystal would appear in this region. The strong Raman modes at 275 and 270 cm^{-1} in $C_1 ZnCl$ and $C_1 HgCl$ are assigned to the symmetric stretching (M-Cl) modes. The strong IR modes at 287 and 324 cm^{-1} (corresponding to 300 cm^{-1} in the Raman spectra of $C_1 HgCl$ crystal) are due to the M-Cl asymmetric stretching modes in Zn and Hg crystals respectively [18-20]. By comparing these spectra with those of $C_1 CdCl$ the Raman bands at 120, 90 cm^{-1} (145 and 111 cm^{-1} in FIR) in Zn, and 85 cm^{-1} (127 cm^{-1} in FIR) in Hg, could tentatively be assigned to the translations of $CHN_3 H_3^+$ ion. The librational mode of the methylammonium group is found at 57 cm^{-1} (60 cm^{-1} in FIR) in $C_1 HgCl$.

Modes Above 400 cm^{-1}

The internal modes of the methylammonium ion have been observed above 800 cm^{-1}, separated by the external modes indicating the weak interactions between the two parts of the crystal. The main difference in $C_1 ZnCl$ with the corresponding $C_1 CdCl$ and $C_1 HgCl$ is that the ν(CN) consists of a doublet. However, the solution spectra of it show a single band at 992 cm^{-1}. Observed doublet in the solid state spectra could probably be due to the correlation splitting. The other modes are consistent with the C_{3v} (free molecular) symmetry as indicated in Table 3.4. $C_1 HgCl$

spectra in the internal mode region show no such deviations. All the fundamental modes in the three systems show similar spectra indicating weak crystal field interactions.

STRUCTURAL PHASE TRANSITION

The phase transition study of $(CH_3NH_3)_2MCl_4$ M = Cd, Zn and Hg crystals have been probed by spectroscopic techniques. In these systems the transitions are mainly due to the reorientational motion of the organic ion (see § 1.8.1). The coupling between these two parts is provided by the N-H..Cl hydrogen bonding. Hence, it is expected that the Raman/infrared spectral studies will give useful information about the phase transitions which motivated the present study.

3.4 PHASE TRANSITIONS IN C_1CdCl

3.4.1 Infrared Results

As already pointed out, the C_1CdCl crystal undergoes two phase transitions at 283 (Tc_1) and 163 K (Tc_2). The infrared spectra using a platelet of C_1CdCl in ORT and MLT phases are shown in Fig 3.3. The band positions in both the phases along with the Raman bands are compared with earlier IR studies in Table 3.5. The spectrum of the intermediate (TLT) phase shows no remarkable changes. This is evidently clear from the spectra taken in our preliminary scan using mull technique. However, few bands show

drastic variations during the TLT-MLT transition. To probe the transition, a clear and systematic temperature variation study is carried out in three regions comprising the rocking (ν_{11} and ν_{12}) modes and a combinational mode involving the ν_6 (torsional) band.

The infrared spectrum in 750-1150 cm^{-1} consists of CH_3 rocking (ν_{12}) and CN stretching (ν_5) modes which show interesting changes with temperature. The typical thermal behaviour of the spectrum in this region is shown in Fig 3.4. The most dramatic changes can be noticed in the band position (Fig 3.5a) and linewidth (Fig 3.5b) around 160 K. The peak position of ν_{12} shifts by about 6 cm^{-1} accompanied by a sudden sharpening. The broad and weak band around 1040 cm^{-1} in the range, which could be a combinational mode involving ($\nu_{12}+$ lattice) also shows a similar sharpening around the same temperature. The spectral parametric measurement is not attempted for this mode because of large uncertainties associated with them.

The predominant changes in the NH_3 rocking mode (ν_{11}) with temperature are shown in the Fig 3.6. At room temperature there is only one component of ν_{11} at 1266 cm^{-1}. As the temperature is decreased to about 158 K, a slight asymmetry appears. At 160 K this can be clearly seen. Further decrease in temperature results in the upward shift in the frequency of new component while 1269 cm^{-1} component shows little variation in its peak position. The temperature variations of spectral

parameters of ν_{11} mode i.e., (a) peak position, (b) linewidth and (c) the ratio of the intensities of 1290 cm^{-1} component (I') to that of 1269 cm^{-1} component (I) are shown in Fig 3.7. All these parameters show a dramatic variation near 160 K indicating the phase change.

At the TLT-MLT transition, the ν_9 and ν_{10} modes splits into two components each 1572, 1602 cm^{-1} and 1482, 1502 cm^{-1} respectively (see Table 3.5). These observations broadly corroborate previous reports [6,7]. Eventhough almost all the prominent bands at room temperature agree with earlier observations [6,7], several split components in our platelet spectra at low temperature differ beyond experimental uncertainties. For example, one component of the ν_9 mode at 1572 cm^{-1} observed in the present study compares with a 1590-1595 cm^{-1} doublet [7]. These variations could be attributed to orientational effects. Significantly, the strengthening of the hydrogen bonding which was deduced from a change of 20 cm^{-1} in the mean frequency of the ν_9 mode at low temperature [6], is corroborated by the present study. Additional evidence for strengthening of H-bonding in the MLT phase is clearly seen from the temperature dependence of the combinational mode ($\nu_6 + \nu_9$) appearing at 1881 cm^{-1} [21,22] at room temperature as shown in Fig 3.8.

The temperature evolution of the band at 1881 cm^{-1} is shown in Fig 3.8. This single broad band gains intensity and splits into two components (1889 and 1925 cm^{-1}) at 160 K. The

spectral parametric changes of $(\nu_6 + \nu_9)$ mode with temperature are shown in Fig 3.9. As can be seen from figure, both the (a) peak frequency and (b) linewidth of the mode show dramatic variations near 160 K corroborating the phase change.

Similar changes were observed for the $(\nu_6 + \nu_{11})$ mode (1654 cm^{-1} at RT) also on approaching 160 K. The other combinational modes at 2230, 2460, 2550 and 2775 cm^{-1} also show sharpening near Tc_3. The whole spectrum becomes better resolved at low temperature (93 K). However, the CH_3 and NH_3 stretching modes overlap strongly and form a broad unresolved band near 3100 cm^{-1}. This broad structure shows a definite sharpening near 160 K. A weak band observed at 332 cm^{-1} in the MLT phase could be assigned as the ν_6 (torsional) mode [7] corresponding to the Raman value of 341 cm^{-1} (at 20K) [4].

The observed sudden and discontinuous variations in the spectral parameters near 160 K indicate a definite phase change. Absence of any measurable hysteresis indicate that the transition could be a weak first order in nature.

3.4.2 Raman Spectroscopic Study
About The High Temperature Phase

The transition at 424 K in C_1CdCl is well above the thermal decomposition temperature [2]. However, this was probed under some special experimental conditions like immersing the sample in silicon oil or grease [2]. We tried to record the spectra at

higher temperatures by applying a thick layer of silicon oil and collecting the Raman spectra by defocussing the laser light. In Fig 3.10 shows the typical Raman spectral changes in (a) some low frequency and (b) in CN stretching (ν_5) mode regions. The spectral variations in 298-383 K are very marginal and efforts to record the spectra at still higher temperatures was unsuccessful as the sample got damaged at T $\geq$ 383 K. The linewidth changes in 172, 212, 926 cm^{-1} do not show any anomalies in 298-383 K range which can be attributed to the precursors to the transition at 424 K. Attempt to probe the high temperature transition without damaging the sample proved unsuccessful in the present case. Therefore, present study restricted only to sub-ambient transitions. The same is true with C_2CdCl crystals.

About the Sub-Ambient Phases

The earlier Raman studies of the phase transition in C_1CdCl were restricted only upto 500 cm^{-1} range [3,4]. In view of the infrared results, temperature dependence study of the Raman spectra is extended upto 3300 cm^{-1}. Special attention is given to the stretching mode range (where in IR they form an unresolved broad structure). A randomly oriented single crystal was used for the temperature dependent Raman studies. The sample was irradiated by 514.5 nm Ar$^+$ laser line with about 50 mW power. A number with 'x' mark shown wherever in the figure represents recording sensitivity of that portion of the spectra. The same convention is used throughout the thesis.

The Raman spectra of C_1CdCl in ORT and MLT phases are shown in Fig 3.11. However, the intermediate TLT phase does not provide any strong spectral anomalies. Many changes were observed in the Raman spectra of the low frequency modes during TLT-MLT transition which corroborates the previous reports [3,4]. A brief description of these changes is given for the sake of completeness. The Rayleigh wing was reduced considerably around 163 K and the low frequency spectra became extremely complex with many bands appearing out of broad features. The detailed assignments of these modes have already been made [4]. Another noticeable point is that the broad torsional mode near 300 cm^{-1} (ORT) shifted about 30 cm^{-1} to higher side in MLT phase and became stronger. The ν(CdCl) mode splits into at least two components at 180 and 220 cm^{-1} near the TLT-MLT transition.

There are many attractive changes in the internal mode region near TLT-MLT transition. However, the spectra essentially remains unaffected near ORT-TLT transition. The main observed spectral variations at the TLT-MLT transition are (i) ν_5 shows a frequency shift of 5 cm^{-1} accompanied by sharpening and the linewidth is comparable to that of the external modes indicating the freezing of CN bond in the MLT phase. (ii) The CH_3 rocking mode (ν_{12}) which is weak and broad in ORT phase gains intensity and splits into two components. (iii) The deformation mode region is better resolved in the MLT phase. (iv) There is a dramatic shift in the NH_3 stretching

mode frequency similar to the ν_6 mode. The NH_3 symmetric (ν_1) and asymmetric (ν_7) modes show about 30 and 50 cm^{-1} downward frequency shift respectively. (v) The most intense line in ORT phase, the CH_3 symmetric stretching mode at 2968 cm^{-1}, splits into two components. (vi) The CH_3 asymmetric stretching mode (ν_8) shows a sharp increase in peak intensity. In general, the MLT spectrum is much sharper than that in ORT phase indicating the orientational order of the methylammonium ions.

Some of the thermosensitive Raman bands of $C_1 CdCl$ are shown as a function of temperature in Fig 3.12. The above mentioned spectral changes (v) and (vi) can be clearly noticed. The discontinuous change in the (a) intensity of ν_8 mode and (b) relative intensity ratio (I_2/I_1) of ν_2 components at the transition temperature (160 K) is shown more clearly in Fig 3.13. The plot between $-\ln(I_2/I_1)$ and $(1000/T)$ shown in the inset was used to determine the activation energy as described in the following section.

3.4.3. Discussion

The phase transition sequence in $C_1 CdCl$ has been explained by a stepwise ordering of methylammonium ions [23,24]. In the prototype phase (TLT), methylammonium ions are equally distributed among four possible orientations making it a disordered phase (see Fig 1.3). In the MLT phase these ions

occupy a particular orientation *i.e.*, they are in an ordered state. The intermediate phases [ORT and TLT] result from the partial disorder of these ions [23,24]. It has been observed previously that vibrational lines show a large change in linewidth during order-disorder transitions [25-27]. The linewidth changes in C_1CdCl during the TLT-MLT transition are discussed in the following section.

Line Broadening And Order Parameter Exponent

It is clearly seen from the IR spectra that many vibrational lines show broadening near the MLT-TLT transition. For example, it is clear that the change in the linewidth ($\Delta\Gamma$) of the ν_{11} mode (Fig 3.7b) is smaller ($\cong 4$ cm^{-1}) than that of the ν_{12} mode (Fig 3.5b) ($\cong 14$ cm^{-1}) in the small temperature interval of 4 K on either side of Tc_3. Additionally, one component (1282 cm^{-1}) of the ν_{11} mode shows a slight increase in linewidth near Tc_3 while both components show similar behaviour (*i.e.*, monotonic decrease with temperature) up to 90 K.

If this broadening in the ν_{11} and ν_{12} modes is only due to the ordering of methylammonium ions, one would expect similar linewidth changes for both. The dissimilarities in the linewidth changes suggest that the NH_3 and CH_3 ions are under the influence of different forces apart from the C-N binding force. This fact indeed supports the NMR results that eventhough the C-N bond occupies a particular orientation, CH_3 and NH_3 ions

undergo hindered reorientations [8,9]. The small linewidth change for the ν_{11} mode could be attributed to the additional disorder of NH_3 ions in the MLT phase. The origin of additional disorder can be understood in terms of the hydrogen bonding associated with the NH_3 ions. In the completely disordered (THT) state, NH_3 polar ends form one H-bond (in *orthorhombic scheme*) with equatorial chlorine atoms of the MCl_6 octahedra on a time averaged basis [8,9]. In the ordered (MLT) state, the opposite (*monoclinic*) hydrogen bonding scheme for NH_3 ions has been found i.e., two and one hydrogen bonds with axial and equatorial chlorine atoms of the MCl_6 octahedra [8,9]. The additional disorder (hence line broadening) for the NH_3 ions in the MLT phase could be attributed to the time averaged hydrogen bonding scheme.

The frequency changes in the ν_{11} and ν_{12} modes and the drastic linewidth change in the ν_{12} mode could be understood on the basis of a soft-hard mode coupling model (see § 1.7.3) [28]. According to this model, the frequency of a hard mode varies like a soft mode if it is coupled to it. The temperature dependence of such a phonon frequency [ω_{sh}: soft-hard coupled mode] is given by

$$\omega_{sh} \propto (T_c - T)^{1/2} \qquad\qquad 3.1$$

and the linewidth Γ_{sh} of this mode varies as follows [28]

$$\Gamma_{sh} \propto \{T/(T-T_c)\} \qquad\qquad 3.2$$

Assuming the general validity of this model, if ω_{sh} varies like an order parameter i.e.,

$$\omega_{sh} \propto (T_c - T)^\beta \qquad\qquad 3.3$$

where β is the order parameter exponent, then

$$\Gamma_{sh} \propto \{T/(T_c - T)\}^{2\beta} \qquad\qquad 3.4$$

From Fig 3.14a it is clear that the ln-ln plot of the peak frequency difference $(\omega - \omega_0)$ vs $(Tc_3 - T)$ is a straight line (in the range of 95 - 160 K) with a slope of 0.27 ± 0.05 and with $\omega_0 = 937.5$ cm^{-1}. A similar plot for the linewidth change (Fig 3.14b) with $\Gamma_0 = 26$ cm^{-1} is also a straight line with a slope 0.52 ± 0.05 (i.e., $2\beta = 0.52 \pm 0.05$). Additionally, the validity of eqn 3.3 is also checked from the temperature dependence of ν_{11} mode. A similar ln-ln plot with $\omega_0 = 1269$ cm^{-1} (Fig 3.14c) also gives a straight line with slope 0.25 ± 0.05. All these observations are in accordance with the soft-hard mode coupling scheme for temperatures over 65° below Tc_3. The existence of a soft mode for C_1CdCl was not found in previous FIR studies, but it has been observed that some low frequency modes do show drastic broadening [5] near Tc_3. The observed absence of hysteresis and the calculated value of the order parameter exponent (0.26 ± 0.05) is comparable to similar systems [29,30].

Hydrogen Bonding Scheme

The shorter N-Cl bonds and the monoclinic distortion of the MCl_6 octahedra about the unique axis provide evidence for an increase in the strength of hydrogen bonding [2] in the (MLT) phase. The spectroscopic manifestation of this can be found from the stretching, bending and torsional modes involving N-H bonds [31]. Here, stretching modes in IR spectra form a broad band near 3100 cm^{-1} and many overlapping bands are present in the N-H bending mode region. Hence, we have chosen the 1800 - 2000 cm^{-1} range, where one expects ν_6 (torsion) coupled modes. From the temperature dependence of the $(\nu_6+\nu_9)$ mode (Fig 3.8 and Fig 3.9) it is clear that this shows splitting near 160 K. The split components of this mode show a frequency shift towards higher values on lowering the temperature. The linewidth of this mode $(\nu_6+\nu_9)$ shows sharpening near Tc_3. From the observed frequency of the ν_9 and $(\nu_6+\nu_9)$ modes, it is concluded that hydrogen bonding is stronger in the MLT phase. Additionally, a band which could be assigned to the ν_6 mode was found near 332 cm^{-1}. Our Raman data indeed shows a diminution in the frequency of the stretching modes corroborating the strengthening of hydrogen bonding in the MLT phase. The intensity ratio of the ν_2 components shows an Arrhenius type variation near Tc_3 (see inset of Fig 3.13) and the calculated orientational barrier height (0.37 eV) from this plot is comparable with the NMR results [8].

3.5 PHASE TRANSITIONS IN C_1MCl WITH M = Zn AND Hg

The phase transitions studies are less for the systems with M = Zn and Hg. These two systems crystallize into monoclinic structure at room temperature [10,11,14] which are different from the corresponding C_1CdCl crystals. However, the ethyl- and propyl- compounds of the same family (C_1MCl) with M = Zn and Hg are isostructural with the M = Cd crystals [32,33]. To the best of our knowledge this is the first attempt to study the phase transitions in these systems using vibrational spectroscopic methods. A preliminary scan of DTA/DSC was performed to confirm the transitions.

3.5.1 Differential scanning calorimetric study of C_1ZnCl

The DSC has been performed on a Perkin-Elmer calorimeter using polycrystalline sample and is shown in Fig 3.15. The transition observed in this study at 481 K is comparable to the previous studies [11]. The transition enthalpy has been calculated as 36.46 J gr^{-1}. The transition at 426 K is not observed in this study-most probably due to small enthalpy change. However, the Raman spectroscopic study gives strong evidences for 426 K transition.

3.5.2 Raman spectroscopic results of C_1ZnCl

The Raman spectra were recorded from the randomly oriented crystals. Initially 80 mW power was used to record the spectra. But the crystal was burnt and a large increase in the *background* was observed well below the transition (375 K). Then the spectra were recorded at reduced powers of 13 and 3 mW in two different experiments in order to probe the transition at 426 K without damaging the sample.

The survey spectra at three different temperatures are shown in Fig. 3.16. The spectrum essentially remains unaffected till 402 K (a typical value). A sudden increment in the *background* intensity is observed along with the other changes in both lattice and internal modes as can be seen from the figure. Fig. 3.17 shows the temperature dependence of the (a) low frequency and (b) $\nu(CN)$ mode regions. It can be seen that the translational modes of methylammonium groups at 114 and 123 cm^{-1} gradually broaden by increasing the temperature. The $\nu(ZnCl)$ mode shows a marginal variation with temperature. The variation in the normalized intensity (with respect to RT) of the $\nu(CN)$ mode is shown in Fig 3.18.

The $\nu(CN)$ doublet at RT merges near the transition temperature. The thermal variations of the peak frequency difference and intensity ratio of $\nu(CN)$ are plotted in Fig 3.19. Inset of Fig 3.19a shows the variation of $\log(I_2/I_1)$ with $(10^3/T)$. The full lines are only a guide to eye.

3.5.3 Differential Thermal Analysis of C_1HgCl

The DTA plot of C_1HgCl (polycrystalline) is shown in Fig 3.20. Two sharp transitions at 335 and 432 K were observed.

3.5.4 Raman Spectroscopic Study of C_1HgCl

The Raman spectra were recorded from a randomly oriented crystal using a power of 80 mW. The Raman spectra of C_1HgCl at 294 and 355 K are shown in Fig 3.21. In order to get more insight into the nature of the transition near 335 K, we monitored two thermosensitive Raman bands in 290-375 K range. The low frequency spectra in both the phases consist of a broad Rayleigh wing. A broad band at 180 cm^{-1} at room temperature becomes still broader at higher temperature. The weaker modes at 60 and 126 cm^{-1} are almost merged into the Rayleigh wing. The $\nu(HgCl)$ and $\nu(CN)$ modes show interesting changes near the transition.

The Raman spectra in 200-370 cm^{-1} range is shown in Fig 3.22. The thermal evolution of (a) the linewidth and (b) peak intensity of $\nu(HgCl)$ mode is plotted in Fig 3.23. There is no appreciable shift in the peak frequency. The linewidth shows a non-linear increment along with a sharp increase in intensity around 330 K.

The thermal evolution of $\nu(CN)$ mode is depicted in Fig 3.24. The spectral parameter variations are plotted in

Fig 3.25. The (a) peak frequency shows a diminution of 6 cm^{-1} (b) the linewidth increases near 330 K (c) the reduced peak intensity (I_p) increases sharply below 332 K and becomes constant at higher temperatures. A plot of $\ln(\Gamma_L)$ vs. T^{-1} is also shown in Fig 3.25d. The (e) and (f) plots are the $\log(\omega-\omega_0)$ and $\log(I_p)$ against $\log(T_c-T)$ respectively. Here T_c (= 332 K) represents the transition temperature.

3.5.5 Discussion

Unlike in C_1CdCl, the MCl_4^{2-} forms a distorted tetrahedra in C_1ZnCl, C_1HgCl crystals. The methylammonium ions are attached to it by hydrogen bonds [10,14].

The observed marginal changes in the spectral parameters of $\nu(NH_3)$ modes in C_1ZnCl suggests that H-bonding strength is not affected much during the transition. The $\nu(CN)$ mode shows strong variation near the transition temperature. The changes in frequency difference ($\Delta\omega$) with increasing temperature of this mode are fitted to an empirical relation $\Delta\omega \propto (T_c-T)^\beta$, where β is order parameter exponent [34,35]. From the log-log graph of $\Delta\omega$ with temperature, β is calculated to be 0.28 ± 0.05. The other mode which show maximum variation with temperature is $\nu(ZnCl)$. The peak position or line width of this mode donot change much with temperature. However, the intensity decreases rapidly on approaching the transition temperature. These variations are fitted well with the relation $I \propto (T_c-T)^{2\beta}$,

resulting $2\beta = 0.58 \pm 0.05$. The above two observations give consistent β value.

The Raman spectra of $C_1 ZnCl$ in its crystalline phase gives two bands in $\nu(CN)$ region while the solution spectra gives one band. Hence, by assuming that the origin for the splitting is correlational field effect, we can calculate the energy barrier [36,37]. So, using the plot of $\ln(I_2/I_1)$ versus T^{-1} as shown in the inset of Fig 3.19b, the activation energy is calculated as 0.086 eV. This value is comparable with similar systems [8,38].

From these observations it is concluded that the transition at 426 K is due to the reorientational motion of methylammonium ions. Further, the sudden increase in background intensity corroborates the transition. The other transition at 483 K could not be studied because the background intensity increases rapidly and masks the Raman spectra.

It is clear from Fig 3.24 that $\nu(CN)$ band in $C_1 HgCl$ shows a small but measurable shift near 332 K. A systematic study of the spectral parameters of this mode (see Fig 3.25) suggests a clear phase change. The frequency $(\Delta\omega)$ variation of the mode is again consistent with the relation $\Delta\omega \propto (T_c - T)^\beta$, where $T_c = 332$ K. A log-log plot is a straight line (see Fig 3.25e) with a slope $(= \beta)$ of 0.31 ± 0.04. Further, the reduced peak intensity of $\nu(CN)$ mode $i.e.$, $I_p = \left\{ I_{op}\omega_p / (n(\omega) + 1) \right\}$, where $n(\omega)$ is the Boltzmann factor and I_{op}, ω_p are the peak intensity and frequency respectively, shows a diminution which

is proportional to η^2 (see § 1.7.3). A plot of $\log(I_p)$ vs. $\log$ (T_c-T) is shown in Fig 3.25f from which 2β value is calculated to be 0.70 ± 0.04 which is remarkably consistent. The arrows on these two plots indicate experimental uncertainties in the measured quantities. The full line indicate the best fit obtained by optimizing with York-routine [39,40]. A trial fit to the linewidtth (Γ_L) data assuming cubic and quartic anharmonicity contributions results in large variations. Hence, by assuming the reorientational contribution to Γ, the Arrhenius plot shown in Fig 3.25d gives the activation energy as 0.13 eV, which is comparable to that of C_1ZnCl. The transition is further corroborated by the discontinuous intensity and nonlinear Γ variations for $\nu(HgCl)$ mode. On the basis of the present study it is concluded that C_1HgCl undergoes a transition at 332 K and in high temperature phase methylammonium ions are in orientationally disordered state.

3.6 CONCLUSIONS

The small shift in the internal modes of the methylammonium ions in C_1MCl with M = Cd, Zn and Hg crystals suggests a weak factor group affects. The TLT-MLT transition at 160 ± 2 K in C_1CdCl is indicated by the dramatic variations in the IR and Raman spectra. The anomalies in the rocking modes near 160 K indicate the ordering of methylammonium ion below this temperature. Strengthening of the hydrogen bonding in MLT phase is shown by

the sudden frequency shift for the $(\nu_6+\nu_9)$ mode and the appearance of the ν_6 mode itself.

The temperature dependent Raman spectra of C_1ZnCl and C_1HgCl provide an additional evidence for the transitions detected by DSC/DTA. From the thermal evolution of $\nu(CN)$ mode, the activation energy is calculated to be 0.09 and 0.13 eV respectively .

REFERENCES

1. A Rahman, PR Clayton and LAK Staveley, J. Chem. Thermodynamics, **13**, 735 (1981).

2. G Chapuis, R Kind and H Arend, Phys Stat Sol., **36a**, 285 (1976). *ibid*. **31a**, 449 (1975).

3. M Couzi, A Daoud and R Perret, Phys Stat Sol., **41a**, 271 (1977).

4. R Mokhlisse, M Couzi and JC Lossegues, J. Phys., **16C**, 1367 (1983) and R Mokhlisse, M Couzi and PL Loyzance, J. Phys., **16C**, 1353 (1983).

5. JHM Stoelinga and P Wyder, J. Chem. Phys. **64**, 4612 (1976).

6. IA Oxton and O Knop, J.Mol.Struct. **37**, 59 (1977).

7. CNR Rao, S Ganguly, H Ramachandra Swamy and IA Oxton, J. Chem Soc. Faraday Trans 2. **77**, 1825 (1981).

8. R Blinc, M Burgar, B Lozar, J Seliger, V Rutar, H Arend and R Kind, J. Chem Phys., **66**, 278 (1977).

9. J Seliger, R Blinc, H Arend and R Kind, Z. Phys., **25B**, 189 (1976).

10. A Daoud, J. Appl Cryst., **10**, 133 (1977).

11. JM Perez Mato, JL Manes, J Fernandez, J Zuniga, MJ Tello, C Socias and MA Arriandiaga, Phys Stat Sol., **68a**, 29 (1981).

12. A Kulshreshtha and JP Srivastava, Int Conf on Raman Spectros., Calcutta, **abs.**, 65 (1988).

13. TKK Srinivasan, M Mylarajan and JB Srinivasa Rao, Int Conf on Raman Spectros., Calcutta, **abs.**, 103 (1988).

14. A Ben Salah, JW Bats, R Kalus, H Fuess and A Daoud, Z. Anorg Allg Chem., **493**, 178 (1982).

15. PSR Prasad, S Sathaiah and HD Bist, Chem Phys Lett., **142**, 341 (1987).

16. J Petzelt, J. Phys Chem. Solids., **36**, 1005 (1975).

17. R Geick and K Strobel, J. Phy. **10C**, 4221 (1977).

18. DFC Morris, KL Short and DN Waters, J. Inorg Nucl Chem., **25**, 975 (1963).

19. CO Quicksall and TG Spiro, Inorg Chem., **5**, 2232 (1966).

20. AW Herlinger, Spectro Lett., **8**, 787 (1975).

21. IA Oxton, J. Mol Struct., **54**, 11 (1979).

22. W Depmeier and IA Oxton, J. Mol Struct., **77**, 91 (1981).

23. R Blinc, B Zeks and R Kind, Phys Rev., **17B**, 3409 (1978).

24. DKh Blat and VI Zinenko, Sov. Phys Solid St., **21**, 588 (1979).

25. VP Dimtrier and VV Loshkarey, Sov. Phys Solid St., **29**, 699 (1987).

26. M Schlaak, M Couzi and PV Huong, Ber Bunserges Physik Chem., **80**, 881 (1976).

27. PSR Prasad and HD Bist, Proc.XI Int. Conf. on Raman Spectrosc (London). 457 (1988).

28. I Laulicht, J. Phys. Chem. Solids. **39**, 901 (1978).

29. R Kind and J Roos, Phys Rev., **13B**, 45 (1976).

30. E Karajamaki, R Laiho, T Levola, W Kleemann and FJ Schafer, Physica., **111B**, 24 (1981).

31. G Turrel, Infrared and Raman Spectra of Crystals. Academic Press (1972).

32. FJ Zuniga, MJ Tello, JM Perez Mato and MJ Perez Jubindo, J. Chem Phys., **76**, 2610 (1982).

33. A Ben Salah, A Daoud, JW Bats and H Fuess, J. Solid St Chem., **65**, 151 (1986).

34. A Le Roy, A Rahhaoui and R Guerin, J. Mol Struct., **174**, 95 (1988).

35. A Miniewicz, R Jakubas, C Ecolivet and A Girard, J. Raman Spectrosc. **20**, 381 (1989).

36. AK Sood, A Arora, S Dattagupta and G Venkataraman, J. Phy., **14C**, 5215 (1981).

37. HH Eysel and G Schumacher, Chem Phy Lett., **47**, 168 (1977).

38. PSR Prasad and HD Bist, J. Phys Chem Solids, **50**, 1033 (1989).

39. BC Reed, Am J. Phys., **57**, 642 (1989).

40. PSR Prasad and HD Bist, XII Int Conf on Raman Spectrosc., Columbia. USA, 492 (1990).

TABLE 3.1 Factor group analysis for $CH_3NH_3^+$ in $(CH_3NH_3)_2CdCl_4$ in the orthorhombic room temperature (ORT) and monoclinic low temperature (MLT) phases.

D_{2h}^{18}	A_g	B_{1g}	B_{2g}	B_{3g}	A_u	B_{1u}	B_{2u}	B_{3u}
n(int)	11	7	7	11	7	11	11	7
n(R)	1	2	2	1	2	1	1	2
n(T)	2	1	1	2	1	2	2	1

C_{2h}^5	A_g		B_g		A_u		B_u	
n(int)	18		18		18		18	
n(R)	3		3		3		3	
n(T)	3		3		3		3	

int = internal, R = librational and T = translatory

TABLE 3.2 Site group analysis for MCl_4^{-2} under free ion

symmetries D_{4h} and T_d.

a) MCl_4^{2-} with D_{4h} free ion symmetry.

FREE ION			SITE	FACTOR			
I	T	R	D_{4h}	C_i	C_{2h}^5	R	T	I
1	0	0	A_{1g}		A_g	3	0	3
0	0	1	A_{2g}					
1	0	0	B_{1g}	A_g				
1	0	0	B_{2g}					
0	0	1	E_g		B_g	3	0	3
0	0	0	A_{1u}		A_u	0	3	6
1	1	0	A_{2u}					
1	0	0	B_{1u}	A_u				
0	0	0	B_{2u}					
2	1	0	E_u		B_u	0	3	6

b) MCl_4^{-2} with T_d free ion symmetry

I	T	R	T_d	C_1	C_{2h}^5	R	T	I
1	0	0	A_1		A_g	3	3	9
0	0	0	A_2		B_g	3	3	9
1	0	0	E	A				
0	0	1	F_1		A_u	3	3	9
2	1	0	F_2		B_u	3	3	9

TABLE 3.3 Infrared and Raman frequences of $(CH_3NH_3)_2MCl_4$ (M = Cd, Zn, Hg) crystals at 300 K.

M = Cd		M = Zn		M = Hg		
IR	Raman	IR	Raman	IR	Raman	Assignment
a	3105	a	3122	a	3121	ν_1 (A$_1$) NH$_3$ sym. stretch
a	2968	a	2977	a	2978	ν_2 (A$_1$) CH$_3$ sym. stretch
1489	1496	1524	1480	1536	1491	ν_3 (A$_1$) NH$_3$ sym. deform
1419	1420	1429	1422	1429	1433	ν_4 (A$_1$) CH$_3$ sym. deform
992	990	1001	984	1006	983	ν_5 (A$_1$) CN stretch
--	--	--	992	--	--	
a	3175	a	3194	a	3200	ν_7 (E) NH$_3$ asy. stretch
a	3028	a	3038	a	3049	ν_8 (E) CH$_3$ asy. stretch
1584	1594	1576	1579	1586	1587	ν_9 (E) NH$_3$ asy. deform
--	1574	--	--	--	--	
1464	1462	1464	1467	1484	1460	ν_{10} (E) CH$_3$ asy. deform
1266	--	1261	--	1259	--	ν_{11} (E) NH$_3$ rock
934	932	956	932	931	926	ν_{12} (E) CH$_3$ rock
--	--	--	--	961	--	

TABLE 3.4 Band positions in the different polarizations at room temperature of $(CH_3NH_3)_2CdCl_4$ crystal.

$Z(XX)Y$ A_g	$Z(XZ)Y$ B_{1g}	$Z(YZ)Y$ B_{2g}	$Z(YX)Z$ B_{3g}	Assignment[†]
3098	3098	--	--	ν_1
2969	2970	2969	2971	ν_2
1484	--	--	--	ν_3
1415	--	--	--	ν_4
990	992	989	990	ν_5
3160	3175	3171	--	ν_7
3035	3034	--	3031	ν_8
1574	--	--	--	ν_9
1415	--	--	--	ν_{10}
936	936	931	936	ν_{12}
212	207	206	208	$\nu(CdCl)$
172	166	166	170	$\delta(ClCdCl)$
125	122	126	122	T
111	108	108	110	T
65	--	--	--	R

[†] $A = CH_3NH_3^+$, R = librational and T = translatory

TABLE 3.5 The IR and Raman band positions of $(CH_3NH_3)_2CdCl_4$ in the orthorhombic room temperature (ORT) and monoclinic low temperature phases.

Present Study[†]		From Ref:7		Raman freq.		Assignment & Approximate
293K	91K	298K	120K	ORT	MLT	Description[‡].
a	a	3040 m	3040 s	3105	3070	$\nu_1(A_1)$:NH3 Sym.Stretch.
a	a	2900 sh	2900 sh	2968	2968	$\nu_2(A_1)$:CH3 Sym.Stretch.
					2954	
1489 s	1462 m	1500 s	1500 s	1496	1496	$\nu_3(A_1)$:NH3 Sym.Defor.
		1488 m	1490 m			
1419 sh	1422 s	1420 s	1422 s	1420	--	$\nu_4(A_1)$:CH3 Sym.Defor.
992 sh	1002 m	994 m	1000 m	990	995	$\nu_5(A_1)$:CN Stretch.
--	332 w	--	380 w	--	330	$\nu_6(A_2)$: Torsional.
a	a	--	3120 s	3175	3112	$\nu_7(E)$:NH3 Asy.Stretch.
			3080 m			
a	2960 sh	2955 m	2955 m	3028	3042	$\nu_8(E)$:CH3 Asy.Stretch.
1584 s	1602 s	1585 s	1605 m	1594	1609	$\nu_9(E)$:NH3 Asy.Defor.
			1585 s		1593	
	1572 sh		1590 sh	1574	1578	
1464 s	1502 s	1460 w	1475 m	1462	1466	$\nu_{10}(E)$:CH3 Asy.Defor.
			1465 m		1450	
	1482 s		1460 m			
1266 s	1290 s	1263 s	1288 m	--	--	$\nu_{11}(E)$:NH3 Rock.
	1269 s		1265 s			
934 s	941 s	935 s	947 s	932	943	$\nu_{12}(E)$:CH3 Rock.
			937 s		934	
1881 m	1932 m	--	1925			$\nu_6+\nu_9$
	1900 w		--			
--	--	--	1897			$\nu_6+\nu_{10}$
	--		1880			
1654 sh	1737 m	--	1725			$\nu_6+\nu_{11}$

[†] a: Indicates part of the broad band at 3100 cm^{-1}.

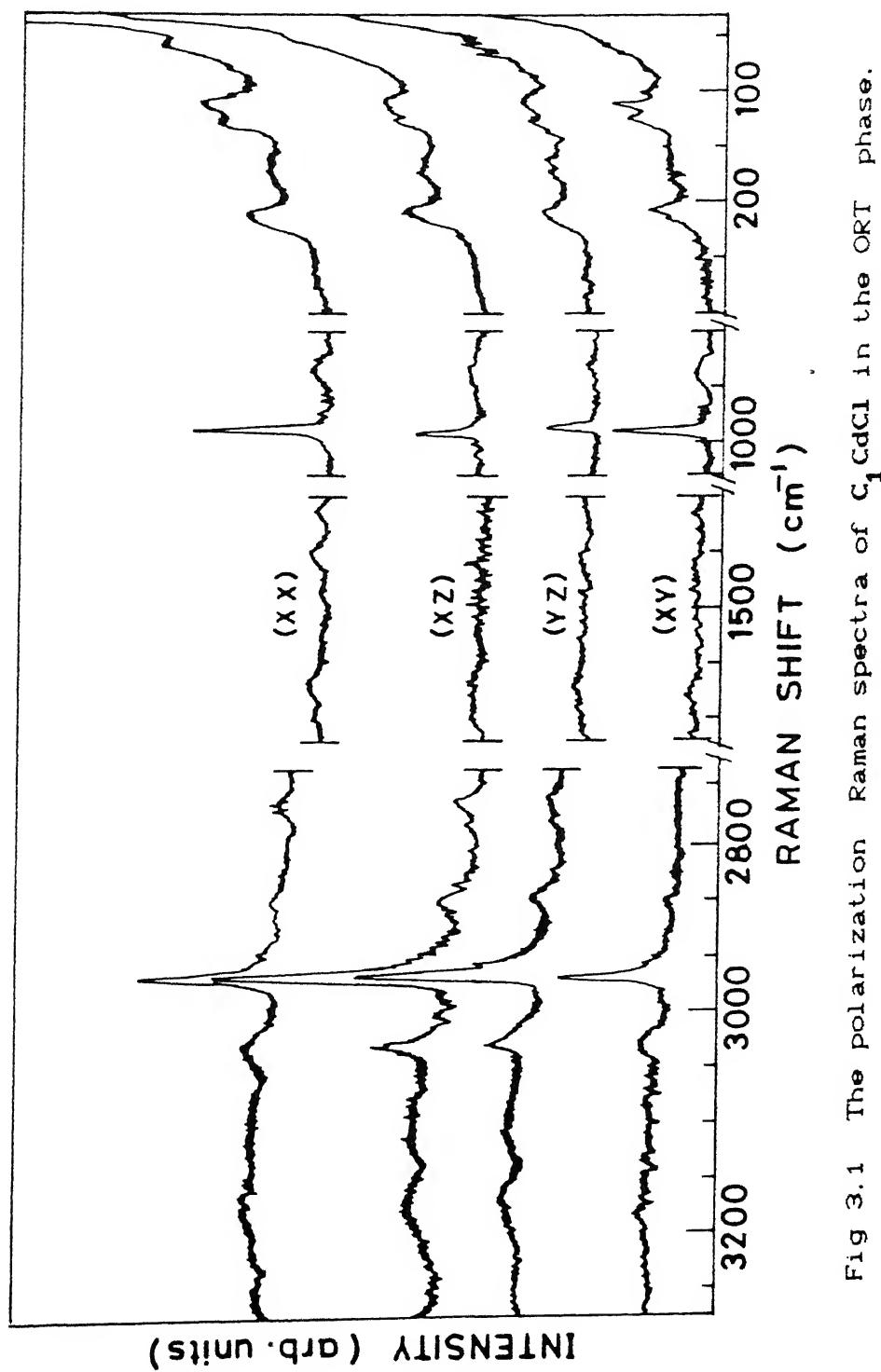[‡] s = strong, m = medium, w = weak and sh = shoulder type peaks respectively.

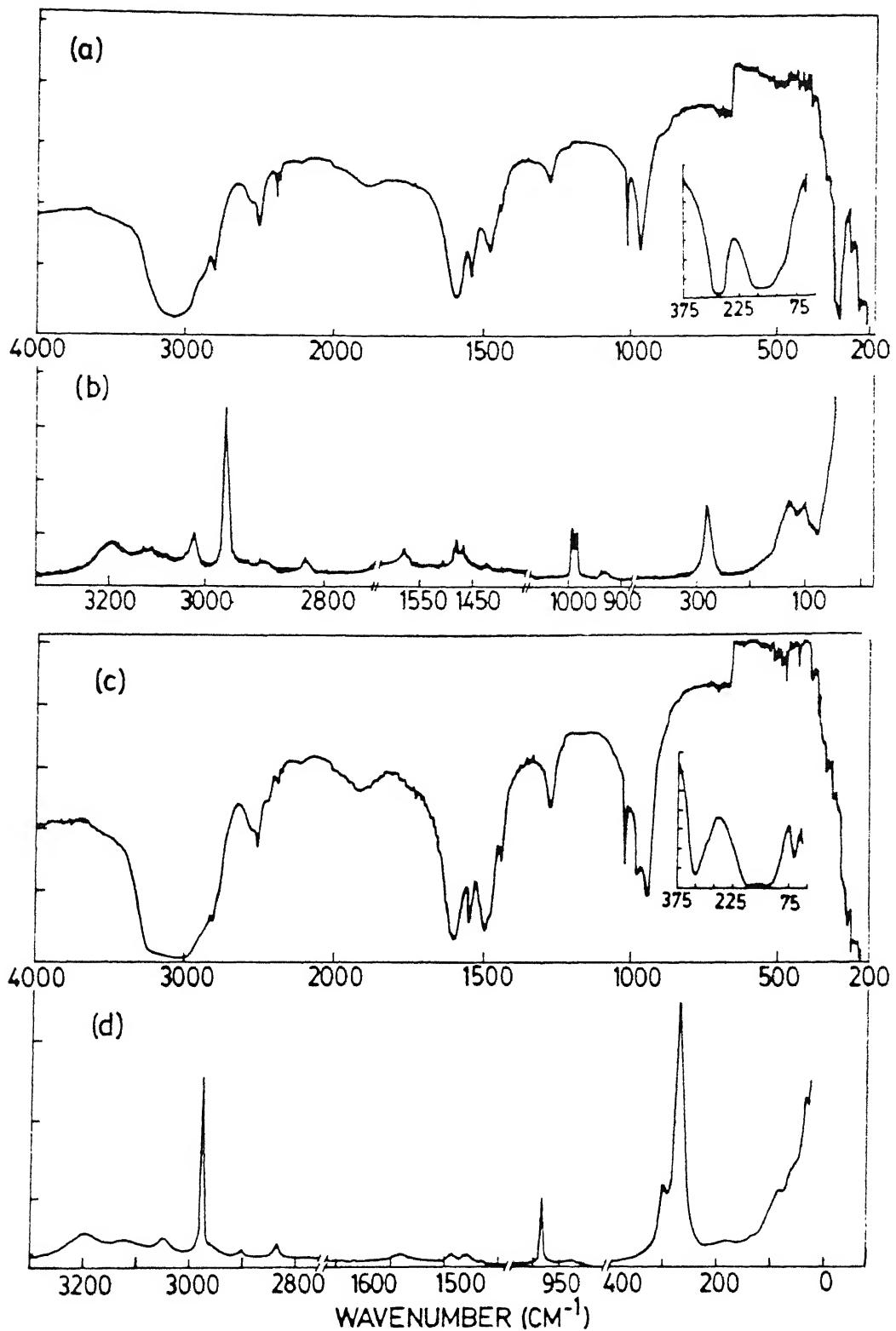Fig 3.1 The polarization Raman spectra of C_1CdCl in the ORT phase.

Fig 3.2 Infrared (a & c) and Raman (b & d) spectra of C_1MCl with
M = Zn and Hg crystals at ambient temperature. FIR
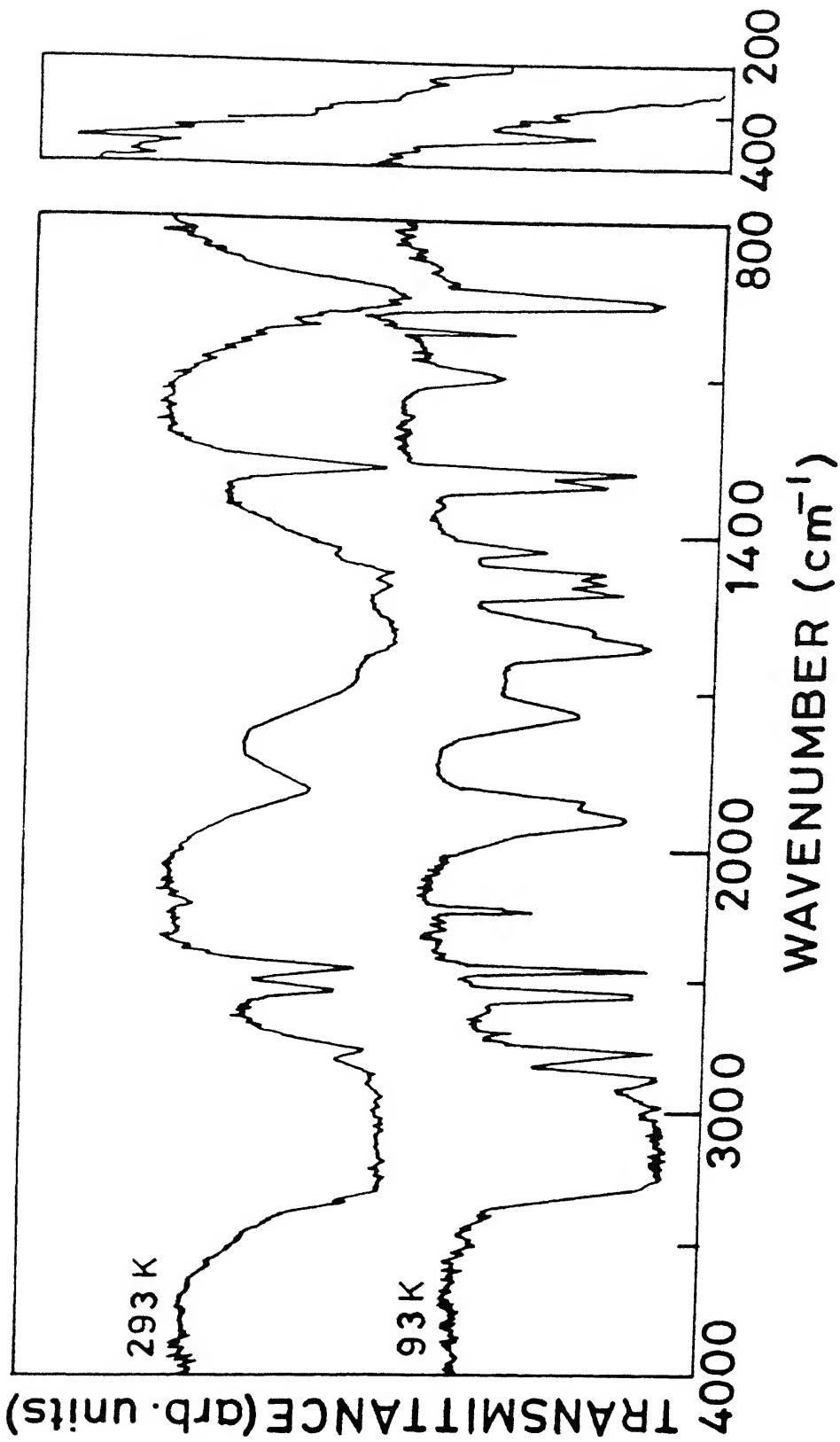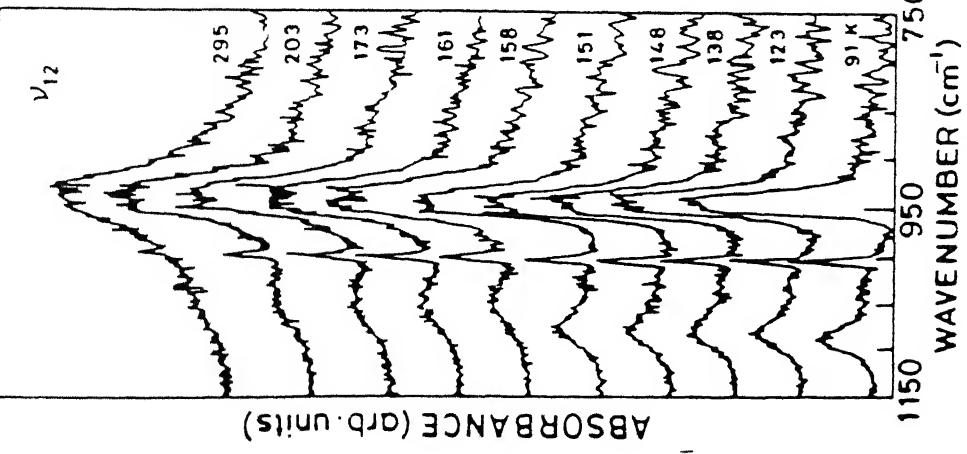spectra of the same are shown as insets in a & c.

Fig 3.3 Infrared spectra of C_1CdCl in the ORT and MLT phases.

Fig 3.5 Temperature dependence of (a) frequency and (b) linewidth for ν_{12} band of C_1CdCl.

3.4 Typical infrared spectral evolution of ν_{12} mode in 91 – 295 K range.

Fig 3.7 (a) Frequency (b) linewidth and (c) relative peak intensity of ν_{11} of C_1CdCl in 90 - 298 K range.
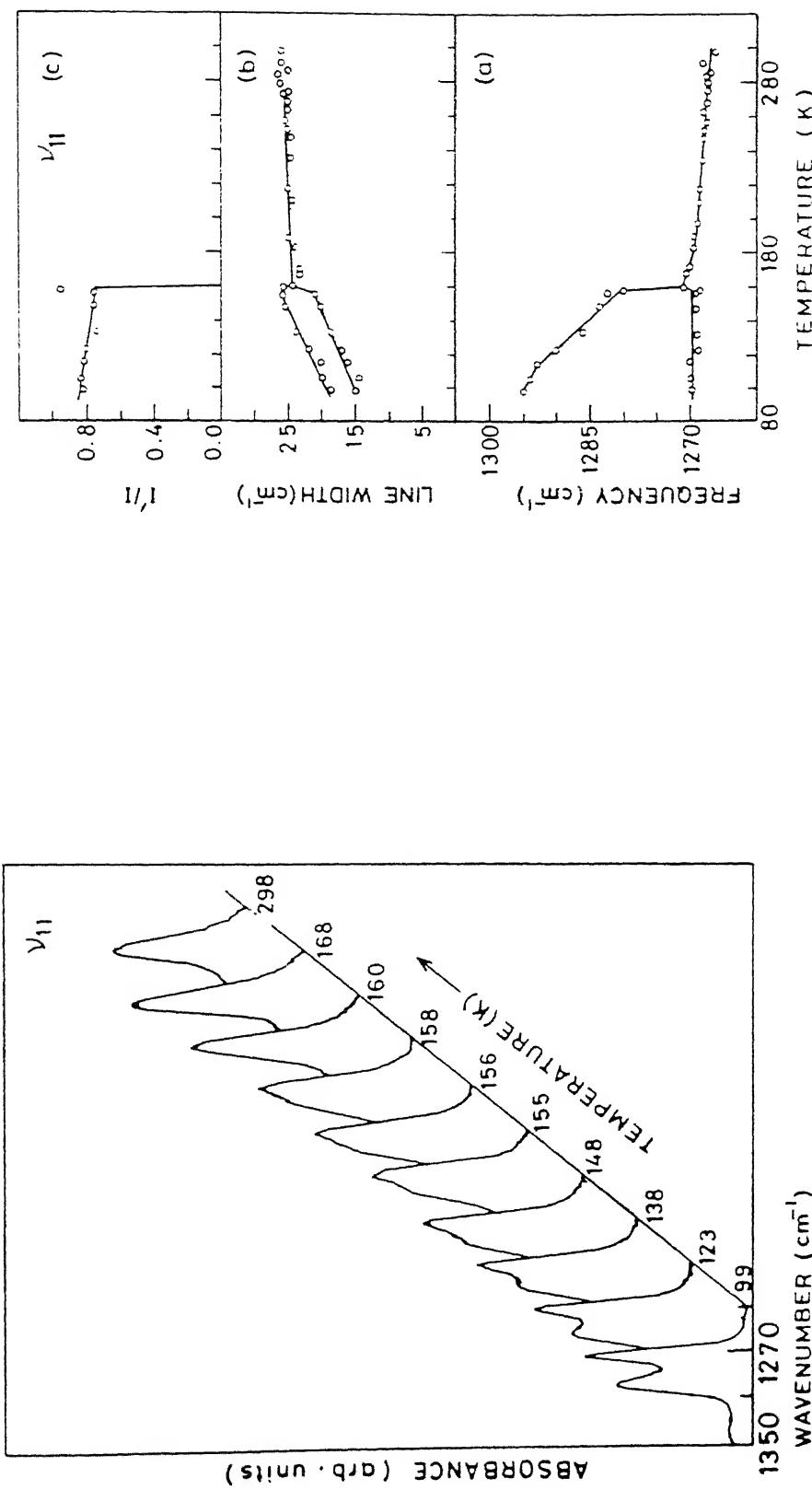
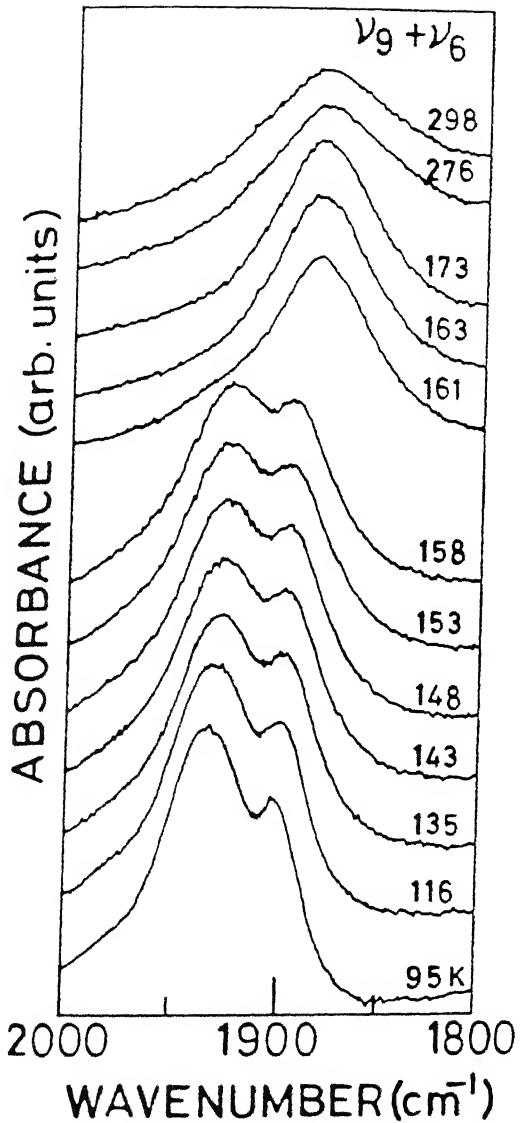Fig 3.6 Spectral thermograph of C_1CdCl in ν_{11} mode region.

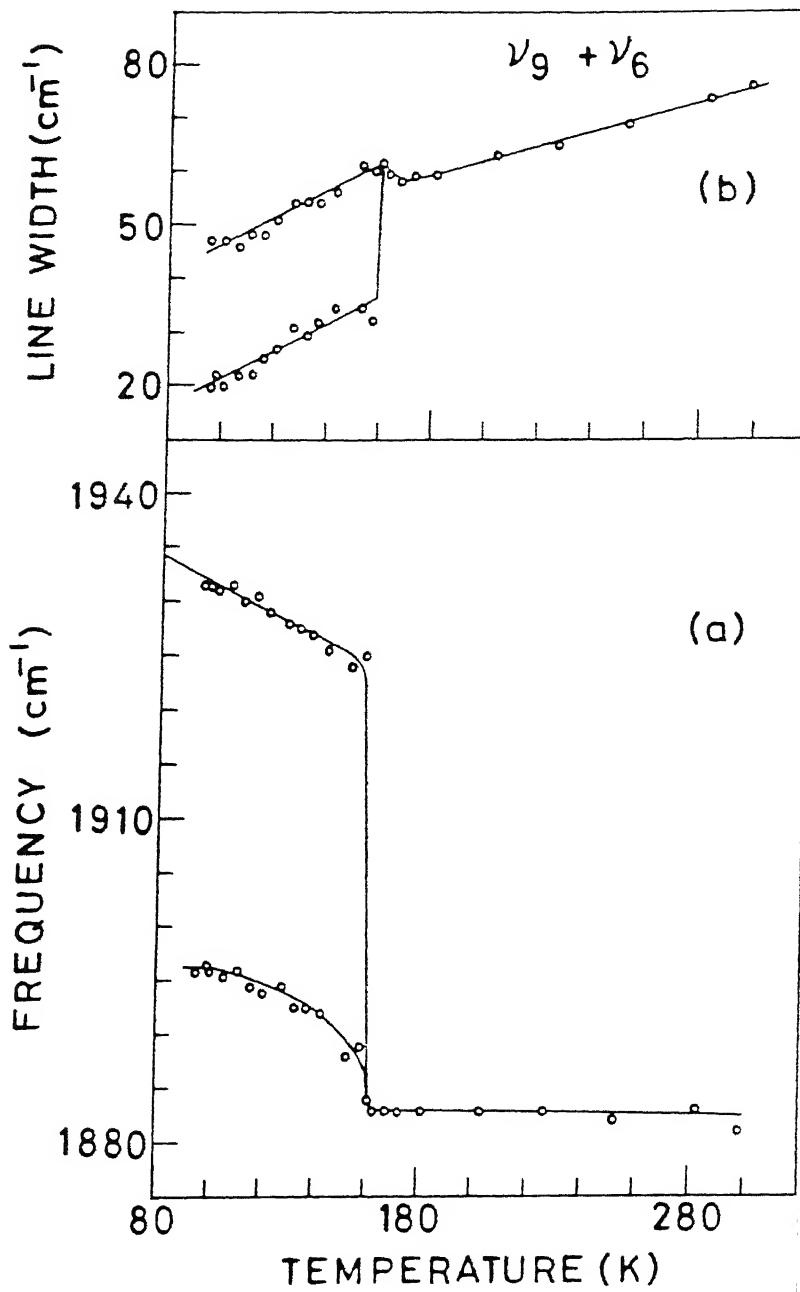Fig 3.8 Several representative curves of C_1CdCl in 1800-2000 cm^{-1} region.

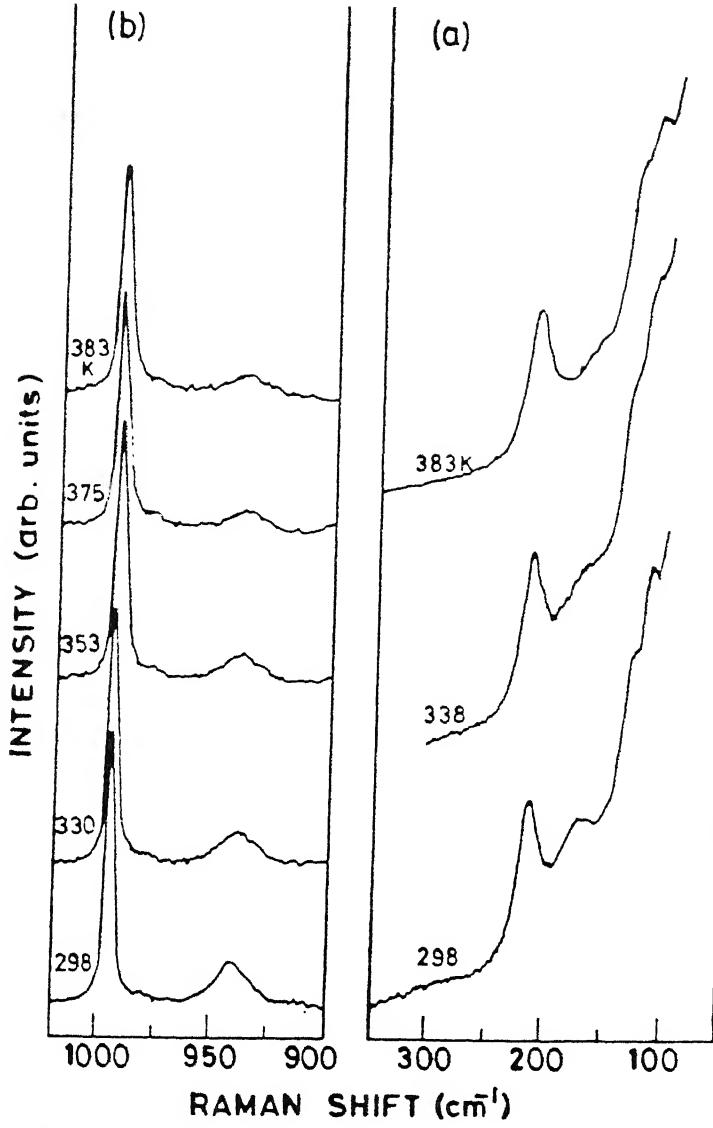Fig 3.9 Thermal variations of (a) peak frequency (b) linewidth of the $(\nu_6+\nu_9)$ band.

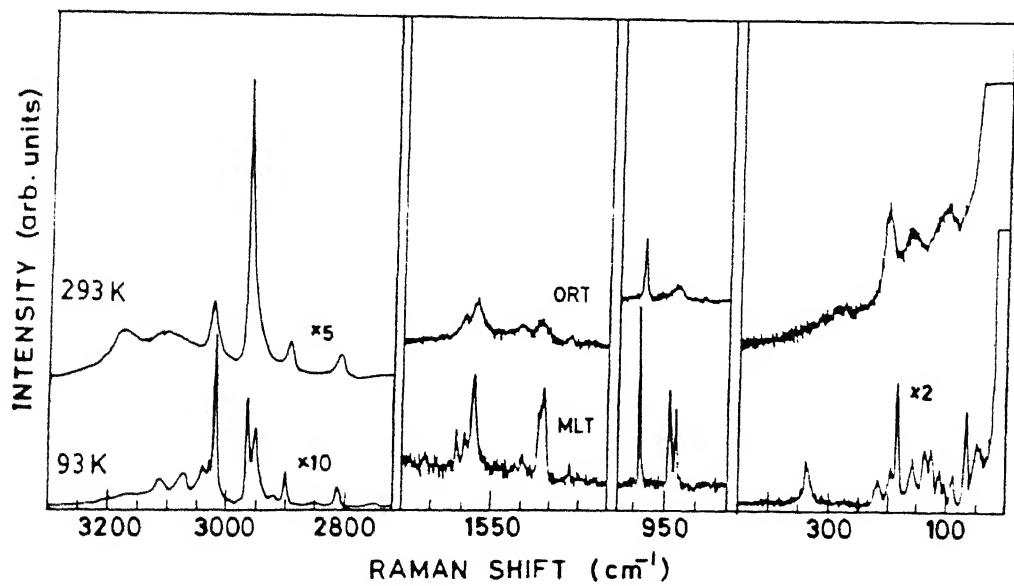Fig 3.10 Typical thermal variations of C_1CdCl in (a) lattice and
(b) $\nu(CN)$ mode region.

Fig 3.11 The Raman spectra of C_1CdCl in ORT and MLT phases.

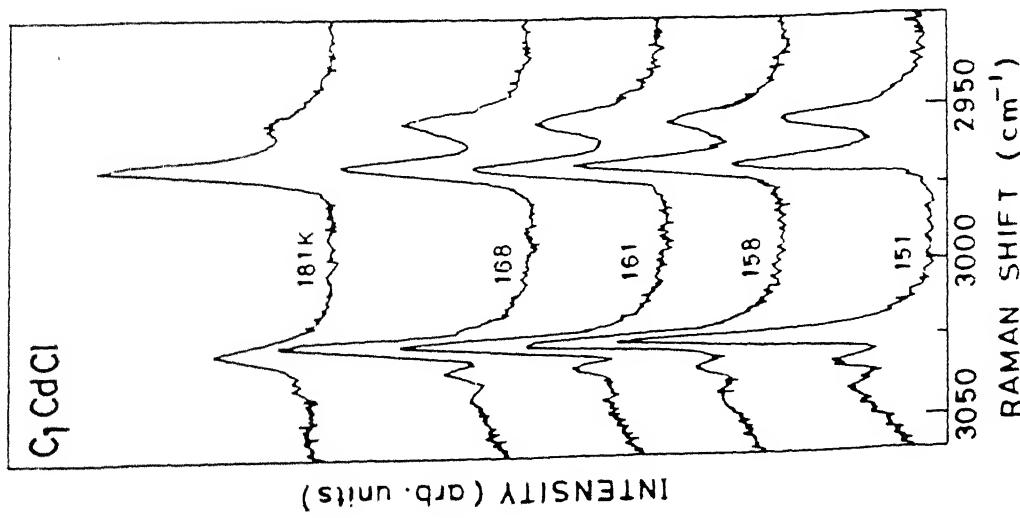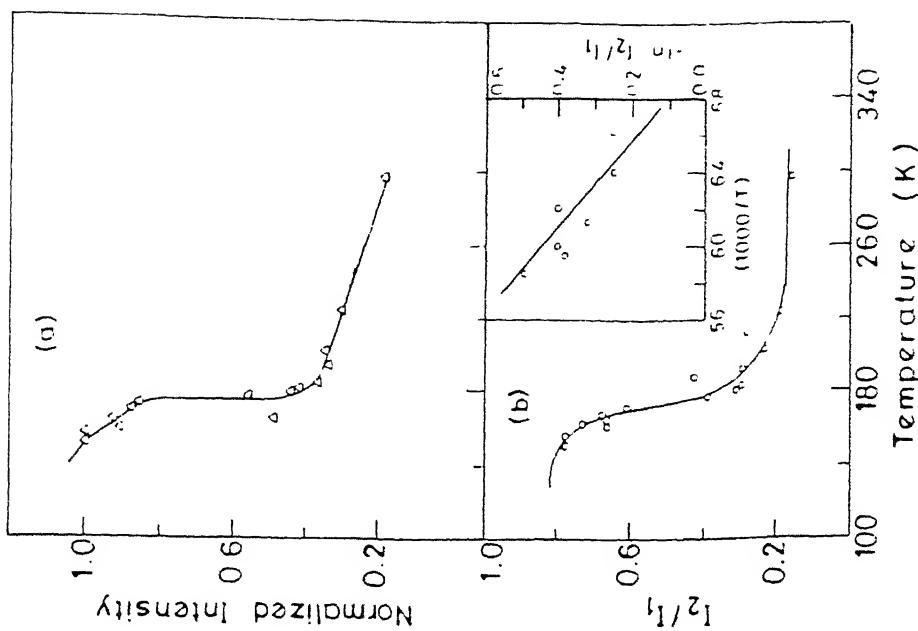Fig 3.13 Thermal variation of a) normalized peak intensity of ν_8 and (b) peak intensity ratio of ν_2 bands. Inset is the Arrhenius plot for the ν_2 components.

Fig 3.12 Temperature dependent Raman spectra in 2900 – 3075 cm^{-1} region.
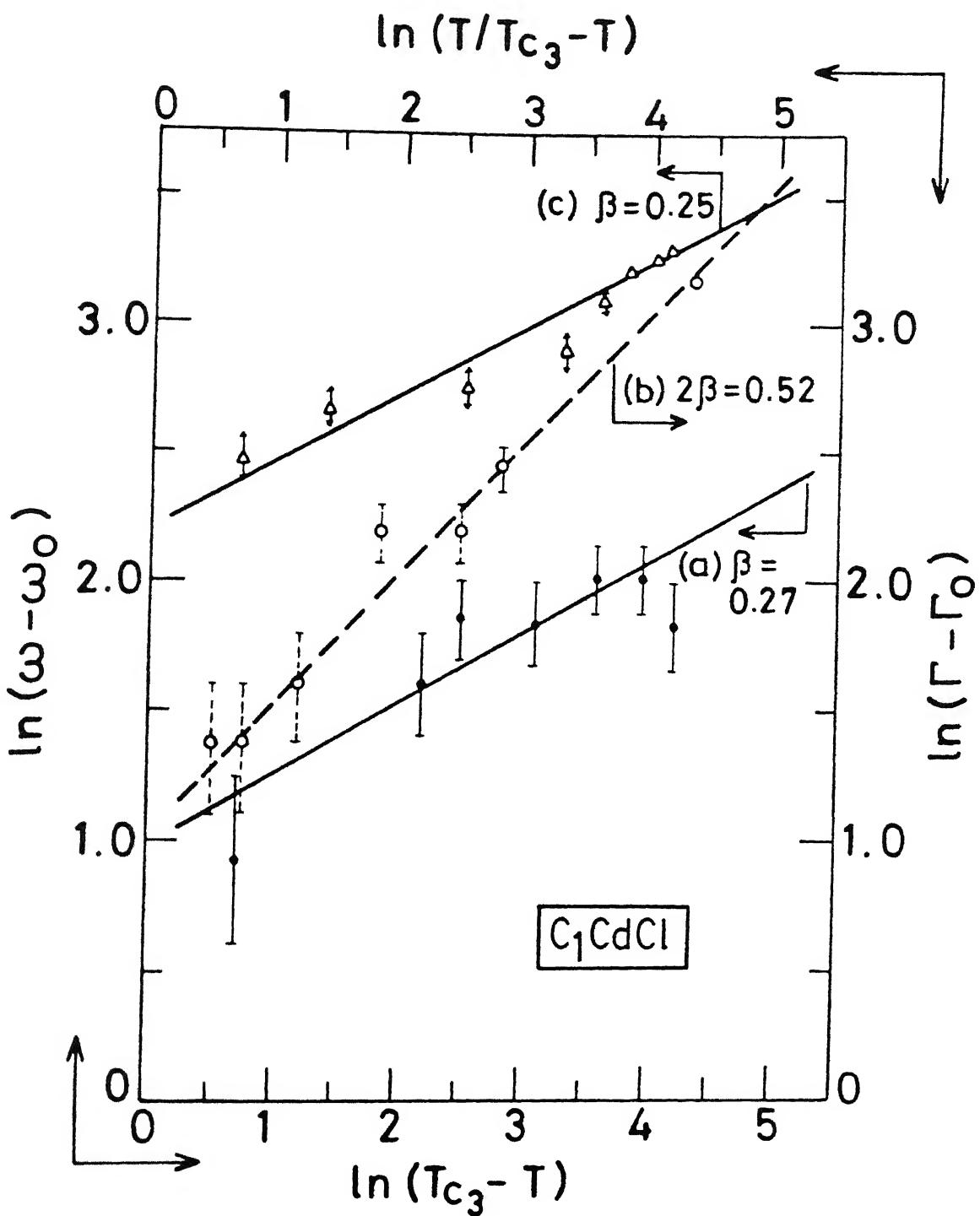
Fig 3.14 (a) & (c) are ln-ln plots of the peak frequency difference $(\omega-\omega_0)$ [left hand scale] vs (Tc_3-T) [bottom scale] for the ν_{12} and ν_{11} modes respectively.

(b) A graph of $\ln(\Gamma-\Gamma_0)$ [right hand scale] vs $\ln(T/(Tc_3-T))$ for the ν_{12} mode.

Fig 3.16 The Raman spectra of C_1ZnCl in above room temperatures.

Fig 3.15 DSC plot of C_1ZnCl in 313 – 573 K range.
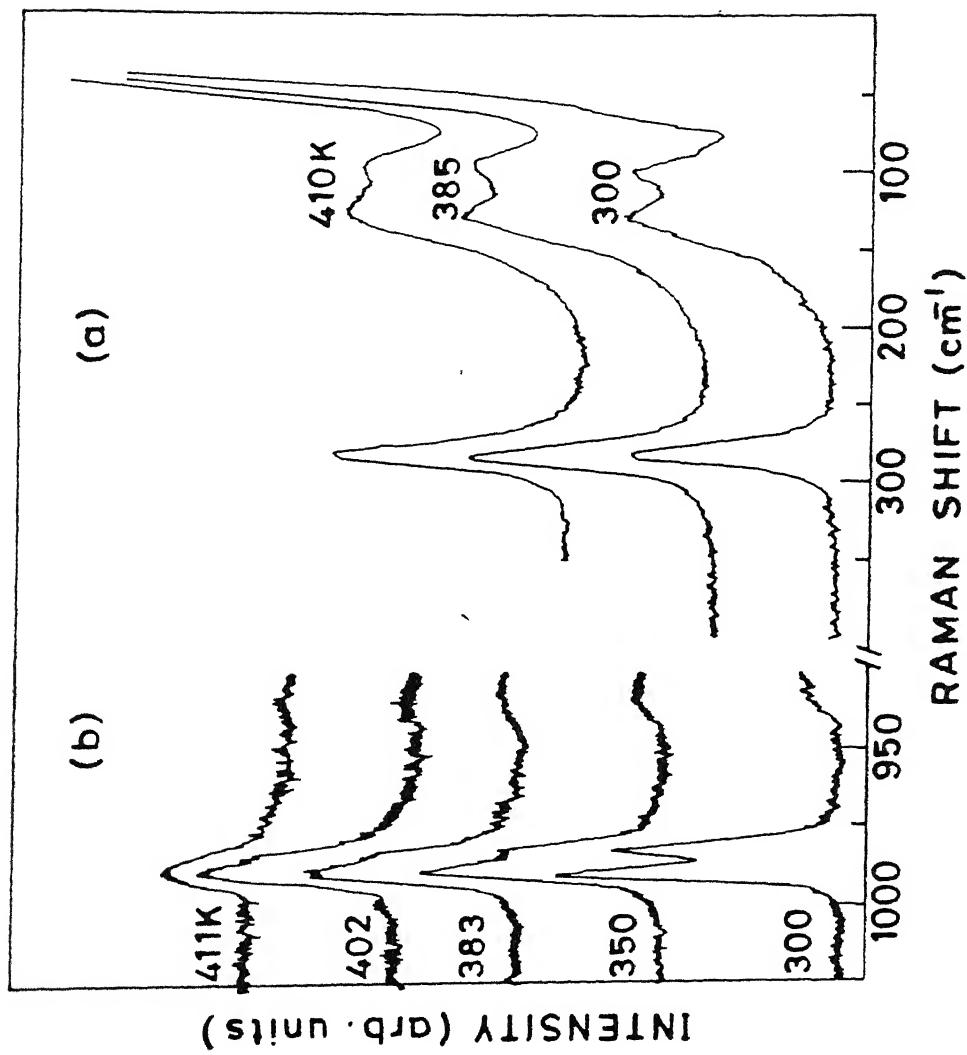
Fig 3.17 Typical thermal evolution of (a) lattice and (b) $\nu(CN)$ mode region in C_1ZnCl.

Fig 3.19 Thermal variations of (a) peak intensity
ratio and (b) peak frequency difference
of ν(CN) doublet. Inset is the Arrehenius
plot.
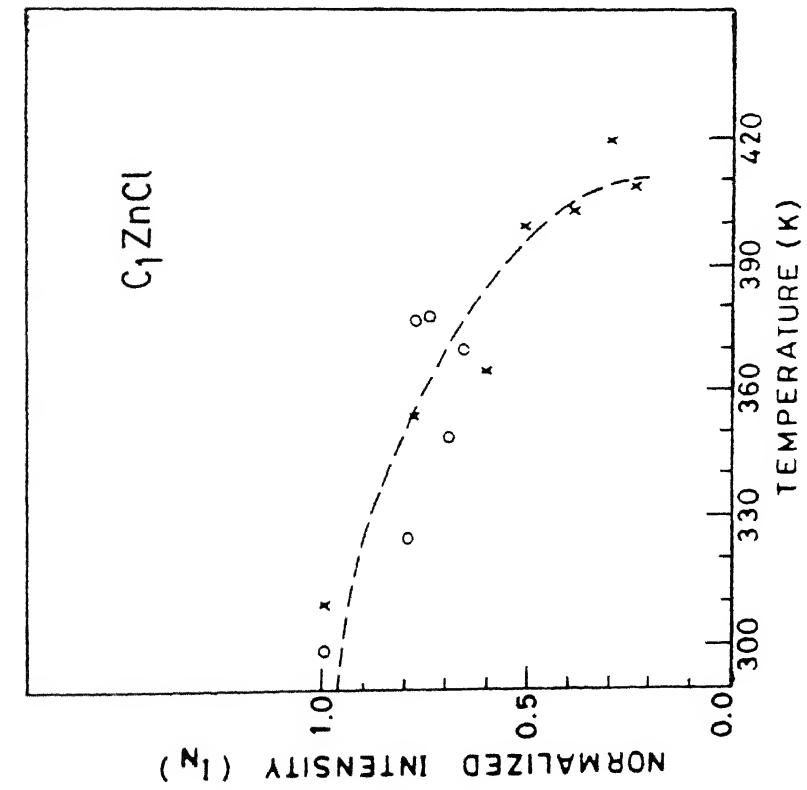
g 3.18 Peak intensity change with temperature of
ν(ZnCl) mode. Two symbols (x & o) are
from different experiments.

Fig 3.20 DTA plot of C_1HgCl in the high temperature range.
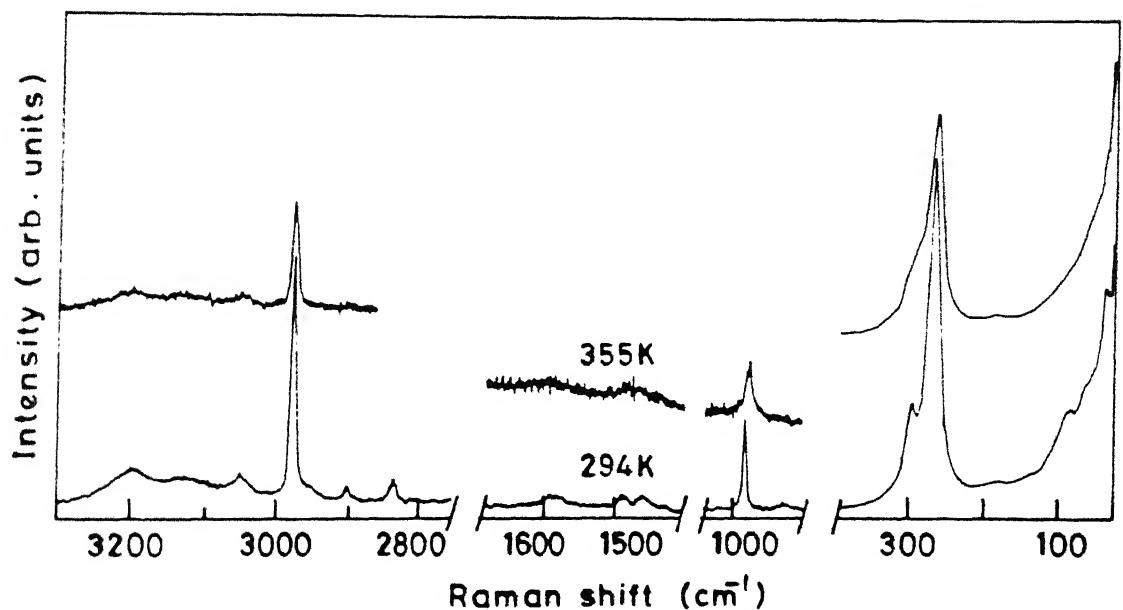
Fig 3.21 The Raman spectra of C_1HgCl at 294 and 355 K.
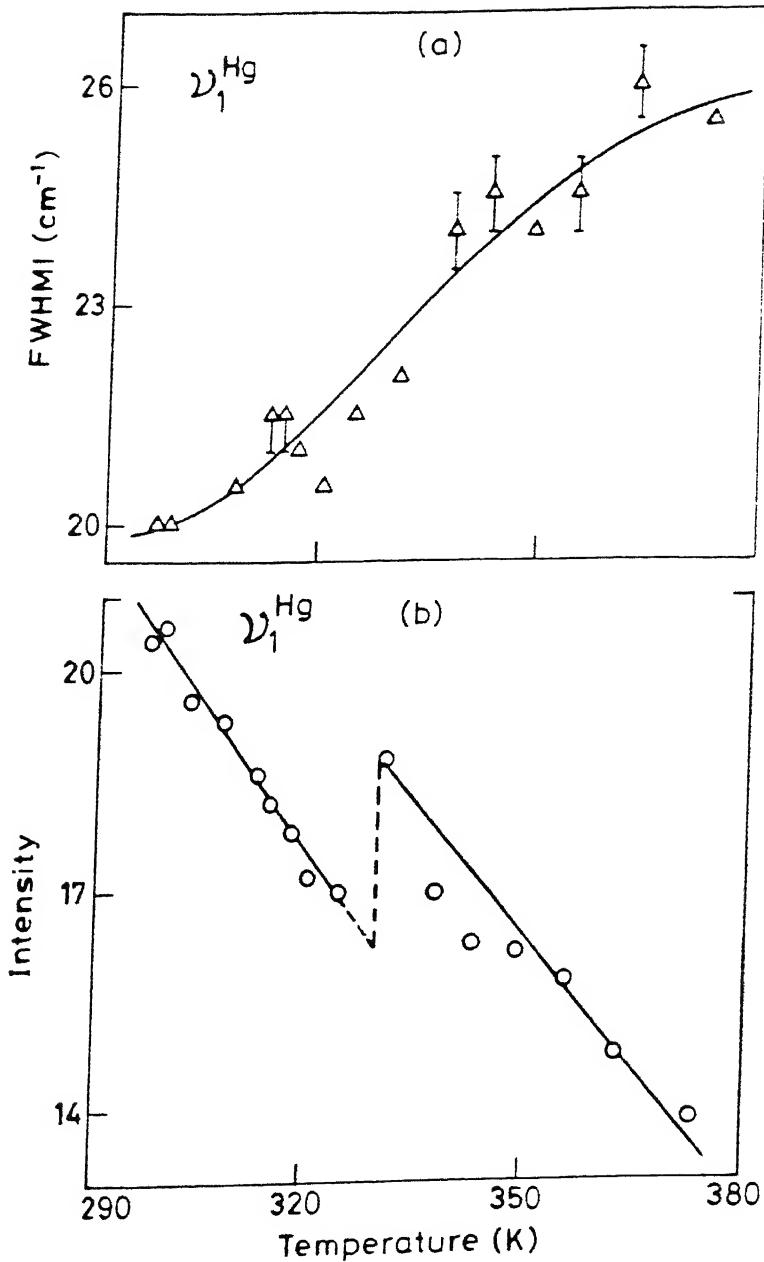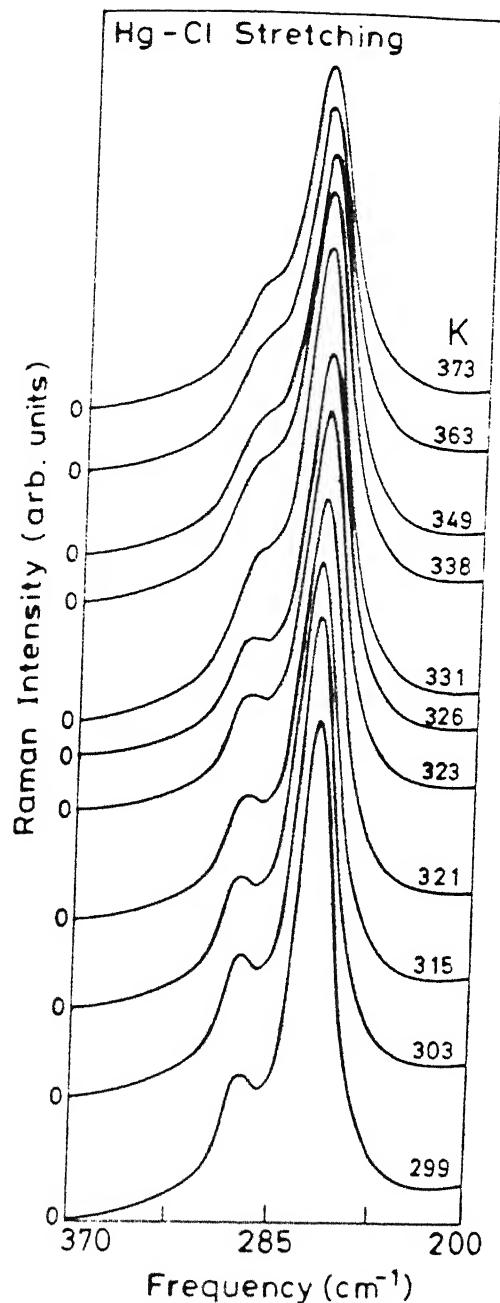
Fig 3.22 Thermal evolution of the Raman spectra in $\nu(HgCl)$ mode region.

Fig 3.23 (a) Linewidth and (b) peak intensity variation of $\nu(HgCl)$ mode in 290 - 380 K.
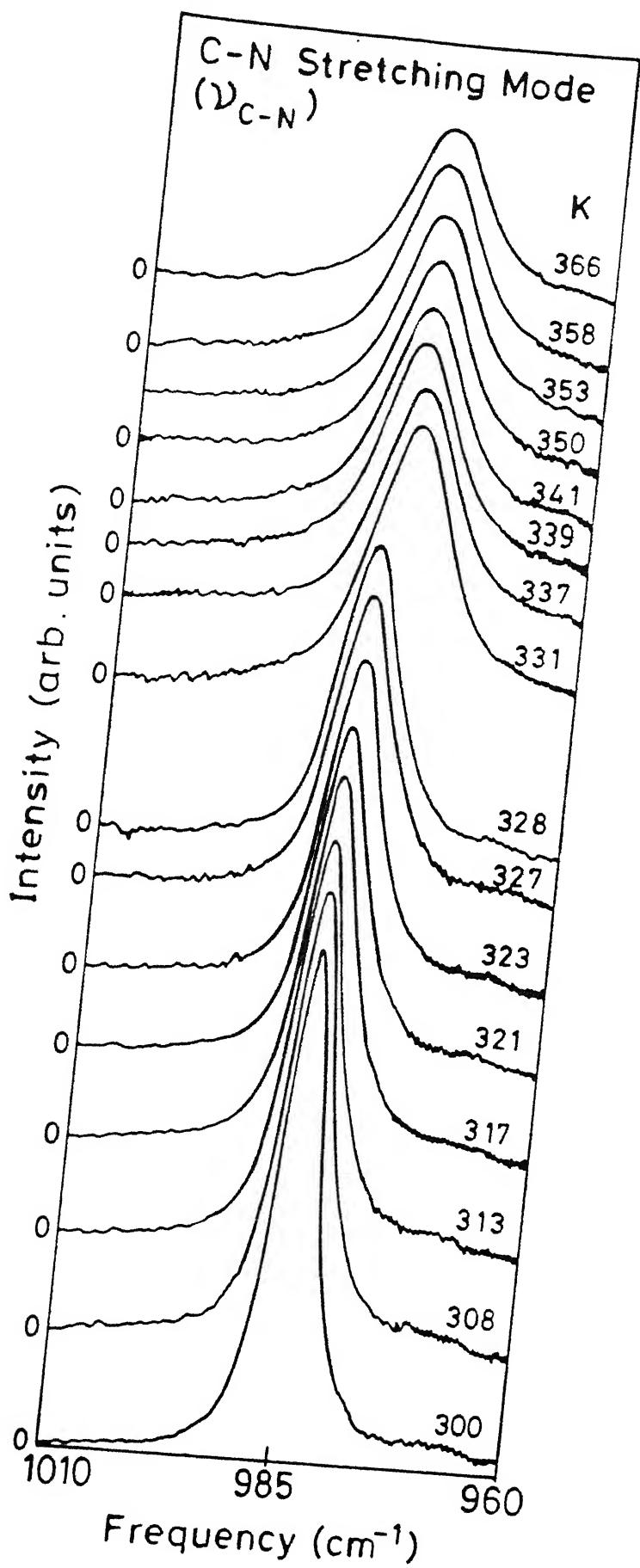
Fig 3.24 Typical thermal variations of $\nu(CN)$ mode of C_1HgCl.
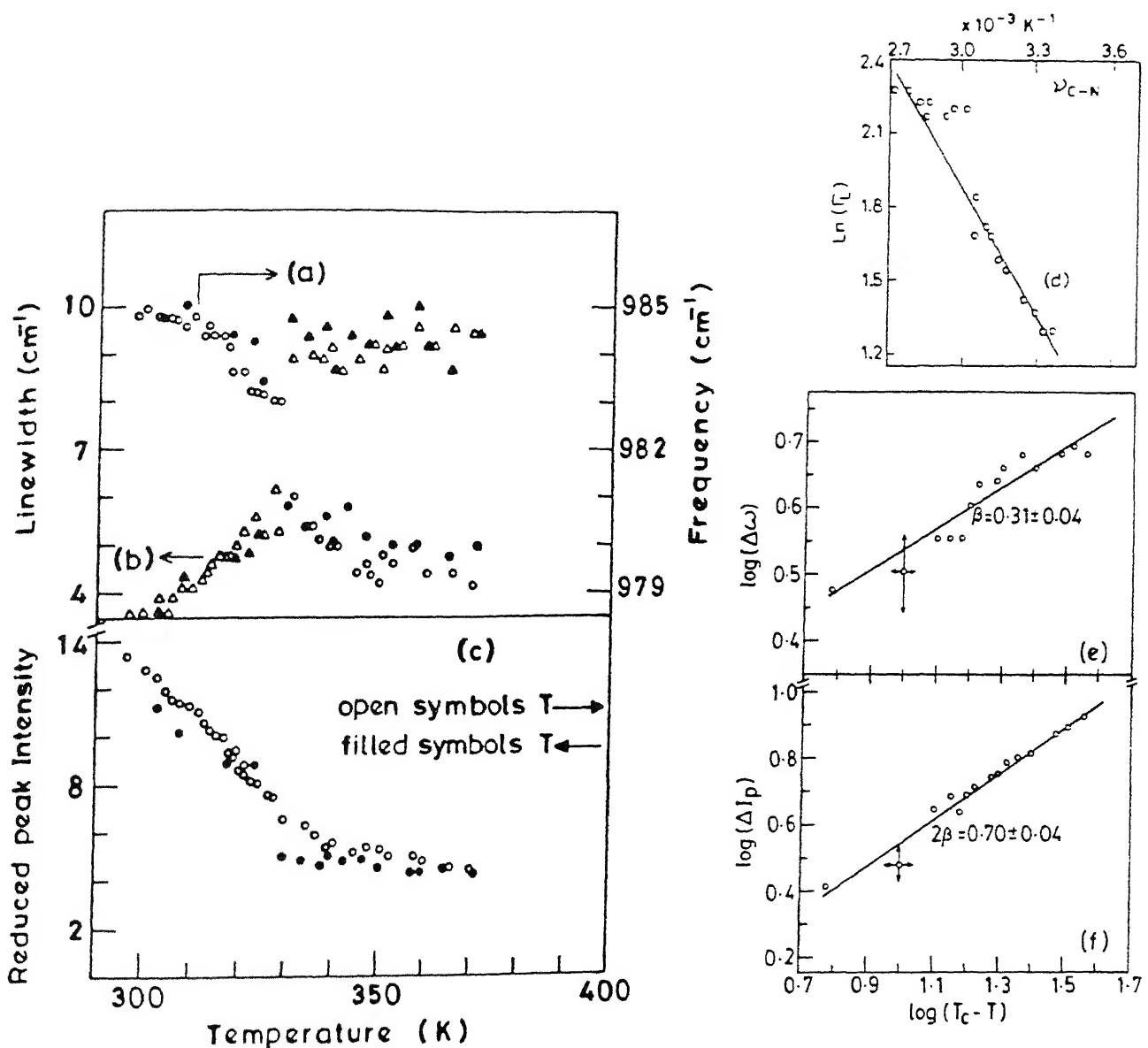
Fig 3.25 (a) Frequency ω, (b) linewidth Γ and (c) reduced peak
intensity I_p variation plots of ν(CN)mode. (d) is the
Arrhenius plot of Γ and a log - log plot for Δω, I_p
are shown in (e),(f) respectively in 294 - 332 K
range.

INDUCED DEFECTS IN $(CH_3NH_3)_2ZnCl_4$ CRYSTAL NEAR PHASE TRANSITION TEMPERATURE

INTRODUCTION

Formation of defects in the three dimensional lattices of alkali halides is a well known phenomena [1]. However, similar effects in a two dimensional lattice like that of $(C_nH_{2n+1}NH_3)_2MCl_4$ (M = Cd and Mn) is known to be thermally less stable [2-4]. The defects in these two dimensional crystals are known to be due to V_k centers [2-4]. Optical absorption and EPR studies reveal that these are stable till 200 K, after which they dissociate forming metallic clusters at room temperatures. The absorption due to Cl_2^- ions of these lie at 26000 cm^{-1} at 77 K. On approaching room temperature this band becomes weaker and broader.

Presently, an anomalous increase in the *background* signal in the Raman spectra is observed. The appearance of it is checked considering various possibilities. Attempts of characterizing this anomalous signal is described in the following paragraphs.

EXPERIMENTAL

The crystals of $(CH_3NH_3)_2ZnCl_4$ (abbreviated as C_1ZnCl) were prepared by the procedure described in § 2.1. The samples were purified by repeated recrystallization and single crystals in random orientation were used to record the Raman spectra. The description of the Ramalog system is already given in § 2.2. The excitation wavelength is 514.5 nm with the powers ranging between 80 to 3 mW.

RESULTS AND DISCUSSION

The temperature dependent Raman spectra of C_1ZnCl was recorded initially by using the laser power of 80 mW with the aim of studying the reported phase transition at 426 K. But a large increase in the background masks the well resolved Raman lines around 378 K. This was thought to be due to thermal decomposition and/or damage due to long exposure of laser irradiation. In another attempt the laser power was cut down to 13 and 3 mW. Now, the increased background was observed at 411 and 426 K, respectively. Just before this anomalous background (typically below $2°$) the spectral changes attributed to the transition are observed (see § 3.5.2). Typical recorded spectra with constant irradiation is shown in Fig 3.16. The broad background signal increases by many times on irradiating continuously for about an hour at that temperature, after which

the signal decreases. Further irradiation caused a local damage. However, the room temperature spectra is reproduced (with increased background) on cooling the sample. The following experiment is performed to attribute this background to the damage caused due to long exposure.

A virgin sample of C_1ZnCl is irradiated with the laser light with about 80 mW power (at the sample) for about 16 hours. This is the normal time required to complete one cycle of temperature variation. The increased background is not observed in this attempt. Moreover, the recorded spectra after such long irradiation is very much similar to the one recorded at the beginning. This experiment suggests that the anomalous increase in the background is not because of longer exposure.

The increased background just after the spectral variations occurring near the transition leads us to believe that these two could be related to each other. The Raman spectra of a fresh C_1ZnCl crystal is recorded after getting the EPR of the same. The recorded Raman and EPR spectra are shown in Fig 1 and Fig 2 respectively. EPR spectra of virgin C_1ZnCl gave no signal at room temperature. The Raman spectra does not show any strong background. The temperature of the sample is now increased slowly without irradiating continuously. This signal is monitored occasionally. There is no sharp increase in the background till 420 K. The recorded spectra at 426 K, without continuous irradiation, show an increasing background. Reproducible Raman spectra at room temperature discards the

possibility of thermal decomposition. The other possibility is the trapping of defect centers. In such a case EPR is a good method of checking such centers. The EPR spectra of the irradiated sample is very complex (see Fig 2b). Presently, it is very difficult to analyze the spectra. However, qualitative features show that the spectra resembles much with the one obtained from the V_k centers in $(C_nH_{2n+1}NH_3)_2CdCl_4$ (n=1,2) crystals [3].

In conclusion, the anomalous increase in the background of the Raman spectra indicate that this could be due to the trapping of defects. Qualitative features indicate that this could be similar to Cl_2^- defects in $(C_nH_{2n+1}NH_3)_2CdCl_4$ (n=1,2) crystals [3]. Further, the development of very faint saffron coloured line along the irradiation path could be due to clustering of metal. This diffuses uniformly throughout the crystal typically in about 36 hours. Further, optical absorption measurements are necessary to characterize these centers.

REFERENCES

1. "Physics of Color Centers" Ed WB Fowller, Academic Press, New York (1968).

2. T Yoshinari, T Matsuyama, N Achiwa, H Yamaoka and K Aoyagi, J Phy Soc Japan, **56**, 3354 (1987).

3. T Yoshinari, T Matsuyama, N Achiwa, H Yamaoka and K Aoyagi, Nucl Instrum & Methods, **32B**, 201 (1988).

4. T Yoshinari, T Matsuyama, H Yamaoka and K Aoyagi, J Phy Soc Japan, **58**, 4222 (1989).

5. CP Slichter, "Principles of Mag Res." Harper and Row, New York (1963).
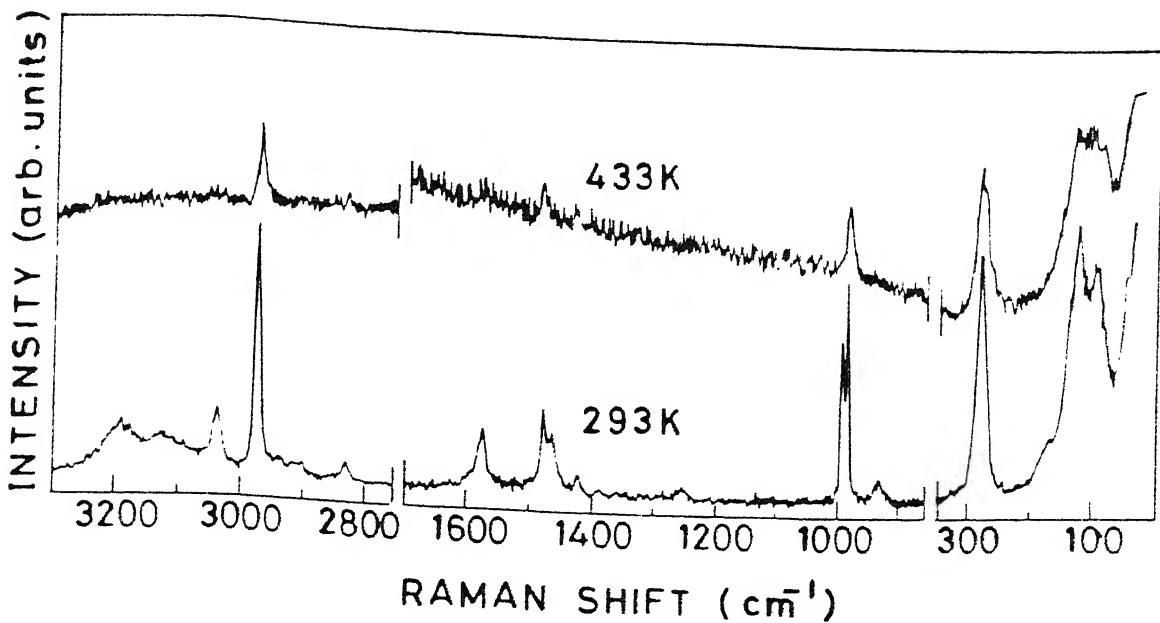
Fig 1   The Raman spectra of $(CH_3NH_3)_2ZnCl_4$ crystal. The spectra
at 433 K is recorded without irradiating the sample
continuously.
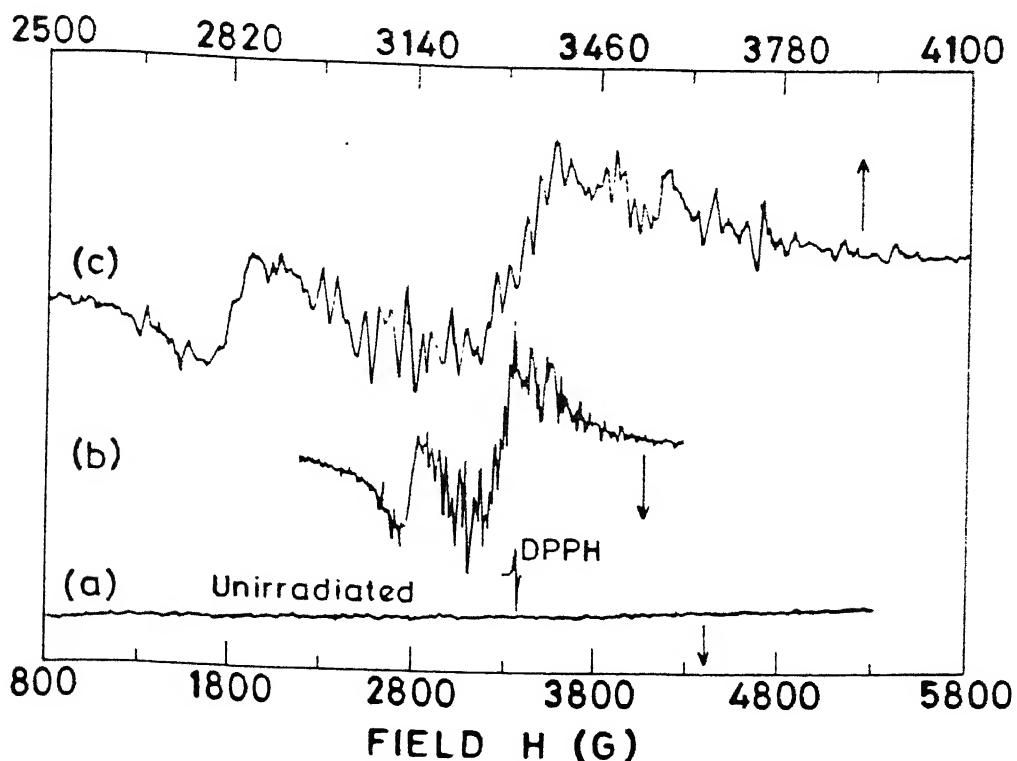
Fig 2 The ambient temperature EPR spectra of $(CH_3NH_3)_2ZnCl_4$
(a) before and (b,c) after exposing the sample with the
laser light.

CHAPTER IV

VIBRATIONAL SPECTRA AND PHASE TRANSITIONS IN $C_2H_5NH_3Cl$ AND $(C_2H_5NH_3)_2\,CdCl_4$ CRYSTALS

ABSTRACT

A detailed spectroscopic investigation of $C_2H_5NH_3Cl$ and $(C_2H_5NH_3)_2CdCl_4$ crystals have been reported in this chapter. Vibrational assignments are proposed on the basis of infrared and the Raman studies. Anomalous spectral variations in internal and lattice modes of $C_2H_5NH_3Cl$ corroborates the phase transition at 345 K.

Temperature variation induces many changes around 216 and 113 K in both infrared and the Raman spectra of $(C_2H_5NH_3)_2CdCl_4$. From the spectral evolution of few thermosensitive modes, the activation energy for the order-disorder transition at 216 K is calculated to be 0.06 eV. The order parameter exponent (β) is calculated to be 0.26 ± 0.04, based on the spectral variations in the modes around 405 and 1192 cm^{-1}.

4.1 INTRODUCTION

The ethylammonium compound which is the second member of the large family $(C_nH_{2n+1}NH_3)_2CdCl_4$ undergoes several structural phase transitions in 77 - 485 K range (see Table 1.2). These transitions are mainly due to the ordering of the alkylammonium ions and the change in the hydrogen bonding strength.

Previous studies reveal that the $D_{4h}^{17} \rightarrow D_{2h}^{18}$ at 485 K is second order and other two $i.e.$, $D_{2h}^{18} \rightarrow D_{2h}^{15} \rightarrow C_{2h}^{5}$ are first order in nature. The thermal decomposition under ambient conditions is estimated to be 450 K [1]. So, the study of $D_{2h}^{18} \rightarrow D_{4h}^{17}$ transition has not been feasible (see § 3.4.2). The other two sub-ambient phase transitions have been studied in the past using various techniques like crystallography [1] calorimetry [2], NMR [3], infrared [4-6] and the Raman scattering [7,8].

The transition at 216 K, $(D_{2h}^{18} \rightarrow D_{2h}^{15})$ is an order-disorder type (evident from the large entropy change). In C_1CdCl it was observed that the CH_3, NH_3 rocking modes are sensitive to such changes (see § 3.4) and many modes of this kind show sharp spectral variations around order-disorder transitions [9-11]. It was suggested that information regarding the changes in the strength of hydrogen bonding could be probed by $\delta_{asy}(NH_3) + \tau(CN)$ mode [12] (see § 1.4.3). With this knowledge, few thermosensitive modes have been selected for probing the transitions.

It is observed that the spectra of C_2CdCl consists of a complex structure owing to a large number of atoms in its unit cell. To get a better understanding of this system, it is useful to study ethylammonium chloride (abbreviated as C_2Cl) which is a starting material for C_2CdCl. Additionally, it undergoes SPTs at 345 and 221 K. These two transitions were previously observed by Rao *et al* [6], but earlier reports [13] claim no transitions. A systematic Raman spectroscopic study is carried out to characterize the transitions (if any) in ethylammonium chloride.

4.2 CRYSTAL STRUCTURE AND PHASE TRANSITIONS

The free ion symmetry of ethylammonium ion is C_s. The expected phonon distribution under this symmetry is shown in Table 4.1. The 27 internal modes are distributed as (16A'+11A"). The external modes consisting of translations and rotations of the ethylammonium ion are distributed as 2A'+A" and A'+2A", respectively. Various modes of ethylammonium (A) can be separated from that of $CdCl_6$, by having prior knowledge of ethylammonium chloride.

4.2.1 Ethylammonium Chloride

C_2Cl is iso-structural with the corresponding bromide salt at room temperature [14]. It crystallizes in the C_{2h}^5 space group

with two molecules in the unit cell (Z=2). The lattice parameters are a = 8.36, b = 5.19, c = 4.51 Å and β = 93.2° [14]. The factor group analysis is summarized in Table 4.2, using C_s site symmetry for the ethylammonium ion.

The differential scanning calorimetric (DSC) experiments by Tasu and Gilson in 1968 [13] claim no phase transitions in C_2Cl. Rao *et al* [6] in their subsequent DSC experiments have observed two transitions at 221 and 345 K. The transition entropy values for these two transitions are estimated to be 0.3 and 7.4 kJ mol^{-1} respectively.

4.2.2 Di(Ethylammonium) Tetrachlorocadmate (C_2CdCl)

C_2CdCl is orthorhombic with the space group D_{2h}^{18} (Z=2) between 484 and 216 K. The lattice parameters in this phase are a = 7.464, b = 7.565 and c = 21.879 Å [1]. The space groups in sub-ambient phases are D_{2h}^{15} and C_{2h}^{5} respectively [1]. The transition at 216 K is of special interest because of the large entropy change. The site symmetries for ethylammonium group in these phases are $C_s \rightarrow C_1 \rightarrow C_1$, respectively. The factor group analysis results following the usual site symmetry approach have been summarized in Table 4.3.

Previous Raman spectroscopic studies have mainly been confined to the low frequency region [7,8]. IR studies have not been very systematic to draw any specific conclusions regarding

phase transitions [4,6]. The salient features of those studies have been summarized as follows:

The earlier Raman spectroscopic observations reveal that the metal-chloride stretching mode around 214 cm^{-1} was not affected much by $D_{2h}^{15} \rightarrow C_{2h}^{5}$ transition [8,15]. Many low frequency modes suddenly appear around 113 K. The linewidth of $\tau(NH_3)$ mode show sharpening around this temperature. These changes have been attributed to the strong first order nature of the transition [15]. However, Rao *et al* [6] have not observed any significant changes around this temperature.

The transition at $D_{2h}^{18} \rightarrow D_{2h}^{15}$ show a hysteresis of 1 K. The most significant changes observed around the transition are in the linewidths. Few FIR modes show a small shift and sharpening near the transition [5,16]. The broad and structureless $\delta_{asy}(NH_3)$ IR mode at room temperature splits and narrows abruptly [4]. The rocking modes show little variation in frequencies in both the phases [6].

4.3 VIBRATIONAL SPECTROSCOPIC STUDY AT ROOM TEMPERATURE

Ethylammonium Chloride

The ethylammonium chloride is monoclinic with space group C_{2h}^{5} at ambient temperature. So under $C_s \rightarrow C_s \rightarrow C_{2h}^{5}$ correlation, one should find every mode with an infrared and a Raman active component. The observed Raman and infrared frequencies are noted in Table 4.4a, along with the recorded spectra in Fig 4.1.

The five Raman modes at 80, 86, 119, 155 and 192 cm^{-1} appear in the region below 200 cm^{-1}. The two low lying modes at 80 and 86 cm^{-1} are found to be inert to the deuteration and are assigned to the translational modes of the chloride [17]. Other modes at 119, 155 and 192 cm^{-1} are broader and found to be effective to deuteration [17]. These modes are intense in the lattice mode region. Considering these facts, we could assign these modes to the librations of ethylammonium ion. Further, the mode at 119 cm^{-1} could be compared with the librational mode of ethylammonium group at 116 cm^{-1} found in C_2CdCl [7].

The skeleton bending mode, $\delta(CCN)$ is found at 413 cm^{-1} in the Raman spectra with a IR component at 425 cm^{-1}. The torsional modes of CH_3 and NH_3 are found at 293 and 459 cm^{-1} in the Raman spectra respectively. The corresponding IR components are found at 325 and 470 cm^{-1}. The symmetric stretching (CC) mode of skeleton is found at 869 cm^{-1} in RS as a strong mode and the corresponding mode in IR is found at 885 cm^{-1} as a weak mode. The rocking modes of CH_3, CH_2 and NH_3 species have been found in both the Raman and IR at different positions and all these observations broadly corroborate the previous reports [6,17]. The stretching mode region of the CH_3, CH_2 and NH_3 groups in IR form a broad band centered around 3100 cm^{-1} containing many combinations. However, the Raman spectra in this region is comparably well resolved.

Di(ethylammonium) Tetrachlorocadmate

Properly polished and cut crystal of C_2CdCl of typical dimensions $3 \times 3 \times 0.5$ mm^3 is used for the polarization study. The sample was excited at about 80 mW. The crystal axes were identified with the help of polarizing microscope (see § 2.3.1).

The previous polarization studies [7,8] are mainly concentrated in the low frequency region i.e., modes upto 300 cm^{-1}. The observed spectra in this region broadly agree with the previous reports [7]. The observed Raman spectra in six different polarizations are depicted in Fig 4.2. The frequencies are noted in Table 4.4b along with the most probable assignments. The previous group theoretical studies considered ethylammonium ions as a rigid entity [18,19] and the experimental studies identify the translational (T) and librational (R) modes [7,8]. Extending the similar group theoretical analysis by taking the free ion symmetry of the ethylammonium group as C_s and using $C_s \rightarrow C_s \rightarrow D_{2h}^{18}$ correlations, it is expected that the A' modes would appear as A_g and B_{3g} modes in the Raman spectra (see Table 4.3). The A" modes would appear as B_{1g} and B_{2g} modes.

According to this correlation, one expects each fundamental mode of the ethylammonium ion to have a component in both the Raman and IR spectra. In the low frequency region, external modes of the ethylammonium ion were observed at 116, 98 and 56 cm^{-1}. The broad mode at 116 cm^{-1} could be assigned as

librational (R) mode of the organic ion whereas the other two *i.e.*, at 98 and 56 cm^{-1} could be assigned as translational (T) modes. The Cd-Cl stretching (ν) and Cl-Cd-Cl bending (δ) modes are observed at 214 and 160 cm^{-1} respectively [7]. The skeleton bending mode of δ(CCN) which belong to A' symmetry in C_s point group was found in all geometries as a weak mode. The corresponding IR mode is (407 cm^{-1}) strong. The torsional modes which belong to A" symmetry are allowed in (B_{1g}) α_{xy} and (B_{2g}) α_{xz} orientations. But the broad structure near 260 cm^{-1} is also clearly observed in α_{xx} and α_{yy} polarization, violating $K = 0$ selection rules. The infrared component of this was not observed. However, a weak combinational mode δ_{as}(NH$_3$) + τ(NH$_3$) has clearly been observed at 1860 cm^{-1}.

In 600-1600 cm^{-1} range, a strong band at 868 cm^{-1} with weak infrared component at 872 cm^{-1} could be assigned to ν(CC). The rocking (ρ) modes of NH$_3$ and CH$_3$ are observed as weak modes in the Raman spectra at 967 and 1214 cm^{-1} respectively. The corresponding IR modes are observed to be strong at 875 and 1217 cm^{-1}. The ρ(CH$_2$) mode is observed as strong at 795 cm^{-1} in IR spectra. Other fundamentals of the organic ion *i.e.*, wagging (ω), twisting (γ) and bending modes are identified in the present study taking the help of other reports [6,17].

The stretching modes of NH$_3$ and C$_2$H$_5$ groups form a very broad structure around 3100 cm^{-1} in IR spectra. Many combinations of the bending modes are also possible in this

region. The Raman spectra in this region, however, show well resolved structure. The $\nu_{as}(NH_3)$ appear as a weak and broad band at 3170 cm^{-1} in all the polarizations except α_{yz}. The symmetric stretching component of it is observed at 3075 cm^{-1} as a weak mode. The other fundamental modes $i.e.$, $\nu(CH_3)$ and $\nu(CH_2)$ are also observed at 2975 and 2940 cm^{-1} respectively as a strong mode.

The polarization studies clearly reveal the fact that $C_2H_5NH_3^+$ is weakly coupled with MCl$_6$ octahedra. The Raman and IR spectra show many common modes within the experimental uncertainties (see Table 4.4b). From this observation it is clear that the effective symmetry of the $C_2H_5NH_3^+$ ion is C_s and the factor group effects are weaker.

PHASE TRANSITION STUDIES

The two systems under consideration, $i.e.$, ethylammonium chloride (C_2Cl) and di(ethylammonium) tetrachlorocadmate (C_2CdCl) undergo one and two phase transitions, respectively, below the ambient temperature. In the following, a systematic study of few of the Raman and infrared bands have been probed across the phase transition temperatures. As THT phase occurs much above the thermal decomposition temperature in C_2CdCl, no efforts have been made to probe it (see § 3.4.2).

4.4 TEMPERATURE DEPENDENT RAMAN STUDY OF C_2Cl

The Raman spectra of C_2Cl in three different phases are shown in Fig 4.3. The lattice modes were monitored continuously across the two transitions in separate experiments using different cells (see § 2.2.4). The typical variation of these modes are shown in Fig 4.4. The peak frequency, relative intensity and linewidth variations of 119 and 155 cm^{-1} (RT) modes are shown in Fig 4.5 and 4.6 respectively. The ν(CC) and ν(CN) modes are also monitored in sub-ambient temperature. A few typical recorded spectra along with spectral parameters are shown in Fig 4.7 and 4.8 respectively. The CH_3 stretching mode region has been monitored across the high temperature phase and the spectral evolution is shown in Fig 4.9. The spectral parameter variations for the two strong modes, $\nu(CH_2)$ and $2\delta(CH_3)$ are depicted in Fig 4.10.

4.4.1 Variations at Low Temperatures

The Raman spectra (see Fig 4.3) show that the modes at low temperature are sharper and stronger. The chloride translational doublet shows an additional band at 98 cm^{-1} below 228 K. This band is seen as a slight asymmetry of 92 cm^{-1} band at 225 K and is clearly resolved at lower temperatures. From Fig 4.4a and Fig 4.5 the librational modes of the ethylammonium ion are observed to shift towards the higher frequency side on lowering the temperature. The variation is about 5% for all

these modes. No sharp discontinuity is observed in the frequency positions. The linewidths (see Fig 4.6b) vary linearly down to 90 K with a slope of 0.04 cm^{-1} K^{-1}. On the basis of the observations at 300 and 173 K Rao *et al* [8] have argued that the variations in the linewidths in IR spectra are due to the ordering of ethylammonium groups. However, from the observed linewidth variations of the librational modes (see Fig 4.6b) it is evident that the anharmonicity effects are responsible for these changes.

The torsional modes also do not show any discontinuities which could be attributed to the phase change [20]. The $\tau(NH_3)$ and $\tau(CH_3)$ modes are observed to shift downward at a rate of 0.0427 and 0.0386 $cm^{-1}K^{-1}$ on increasing the temperature and is attributed to the lattice expansion [20]. The only interesting change occurring around 221 K is that the two librational modes at 119 and 155 cm^{-1} show an increment in the peak intensity (see Fig 4.6). But this intensity variations in the absence of other convincing evidences, are difficult to understand in terms of phase change. The $\nu(CC)$ and $\nu(CN)$ modes (see Fig 4.7) also show no discontinuous changes down to 90 K. The linewidths remain almost constant (see Fig 4.5b).

4.4.2 Spectral Variations at Above Ambient Temperatures

The typical variations of lattice and CH_3 stretching mode region in the range of 290-350 K are shown in Fig 4.4b and 4.9

respectively. The lattice modes continue to show downward frequency shift on approaching 350 K (see Fig 4.5). The linewidth of the librational modes at 119 and 155 cm^{-1} also increases linearly till 340 K; however, the pattern changes close to 345 K and shows a jump. Similar changes are observed for $\nu(CC)$ and $\nu(CN)$ modes (see Fig 4.8). The two halogen translational modes seem to merge around 345 K. The lattice spectra which show a gradual decrease, suddenly disappears at about 346 K and reappears at about 343 K on cooling. The Rayleigh wing shows an increase around this temperature.

The internal $\nu(CC)$ and $\nu(CN)$ modes show a sudden jump in linewidth around this temperature. The other internal mode which shows maximum change is $\nu(CH_2)$. This mode is strong and sharp at room temperature (see Fig 4.9). On increasing the temperature, this mode does not show shift, but it becomes very weak and shows a large jump in linewidth. The first overtone of $\delta(CH_3)$ shows similar variations (see Fig 4.10). The well resolved structure consisting of at least five bands at RT is replaced by three at high temperature. This broad band spectrum at high temperatures and the sudden disappearance of the lattice modes is attributed to the phase transition at 345 K.

The compound melts at 383 K, which is rather close to the transition temperature. This makes the study difficult at still higher temperatures (in Phase I).

4.5 PHASE TRANSITIONS IN C_2CdCl

The Raman and infrared spectra of C_2CdCl are shown in Fig 4.11 in sub-ambient phases. Attractive changes for the $\nu(CC)$ (866 cm^{-1} in ORT) and $\delta(CCN)$ (at 405 cm^{-1}) were observed in the Raman spectra. The three rocking modes $\rho(CH_2)$ (at 796 cm^{-1}), $\rho(NH_3)$ (at 972 cm^{-1}) and $\rho(CH_3)$ (at 1218 cm^{-1}) in IR spectra show maximum changes during ORT-OLT transition. The other IR mode which shows variations in the same temperature range is $\delta_{asy}(NH_3) + \tau(NH_3)$ (at 1850 cm^{-1}).

The typical thermal variation for $\nu(CC)$ and δ (CCN) modes in X(ZZ)Y polarization are shown in Fig 4.12. The $\nu(CC)$ mode shows a small shift in frequency and broadening around 216 K. The $\delta(CCN)$ mode which is weak and broad at ORT, splits around the same temperature and becomes sharper. The two components are deconvoluted according to the procedure described in § 2.4.3.

The typical IR spectra in 720-1120 cm^{-1} and 1100-1375 cm^{-1} region are shown in Fig 4.13. Apart from the spectral parameter variations for the strong rocking modes, weak mode $\nu(CC)$ at 872 cm^{-1} in this range shows sharpening and gains intensity down to liquid nitrogen temperature. The weak $\omega(CH_2)$ band at 1334 cm^{-1} becomes sharper in OLT phase. The broad and weak band at (1275 cm^{-1}) sharpens and its intensity is comparable to that of $\omega(CH_2)$. At about 115 K the $\rho(CH_3)$ mode splits. The relative intensity of this mode decreases and the

splitted component can be seen clearly. Also, the $\tau(NH_3)$ is clearly seen in MLT phase.

The low frequency Raman spectra becomes complex in MLT phase. The modes upto 350 cm^{-1} have been assigned in the past [7,8,15]. The $\tau(NH_3)$ mode at 260 cm^{-1} (ORT) becomes sharper at liquid N_2 temperature. It also throws light on phase changes by discontinuous jump of 30 and 10 cm^{-1} around 216 and 113 K respectively, corroborating the previous reports [7,8]. Marginal changes in the relative intensities for $\rho(NH_3)$ and $\nu(CH_2)$ modes at 970 cm^{-1} and 2950 cm^{-1} occur down to phase IV.

It has been observed that few internal modes show drastic linewidth change around 216 K. In Fig 4.14, the Raman spectral variation for the peak frequency (a) and linewidth (b) has been shown for $\nu(CC)$ mode. The filled and open rectangles represent cooling and warming cycles respectively. On approaching OLT transition from ORT it is observed that the peak frequency shows very small ($\cong$ 2 cm^{-1}) but systematic shift to high frequency side around 216 K. At the same temperature, it is also observed that the linewidth of this mode decreases very rapidly. The Lorentzian linewidths have been deduced by the procedure described in § 2.4.2.

The rocking modes, $\rho(CH_2)$, $\rho(CH_3)$ and $\rho(HH_3)$ which are strong in IR spectra also show the similar changes around 216 K. The frequency and linewidth changes for $\rho(CH_2)$ mode are shown in Fig 4.15. The same for $\rho(NH_3)$ and $\rho(CH_3)$ modes are shown in Fig 4.16. The circles and the triangles in Fig 4.16a and b

represent the frequencies and linewidth changes for these modes. It has been observed that all these four modes $i.e.$, $\nu(CC)$, $\rho(CH_2)$, $\rho(NH_3)$ and $\rho(CH_3)$ show similar variations around ORT-OLT transition.

The weak and broad $\delta(CCN)$ mode at 405 cm^{-1} splits into two components near 216 K. The peak frequency shifts to higher frequency (412 cm^{-1}) as the temperature is decreased down to 100 K. The corresponding changes in the linewidth of this mode is shown in Fig 4.17b by triangles. The open and filled symbols represent warming and cooling cycles. Similar changes for 1192 cm^{-1} IR active combinational mode has been observed. The frequency and linewidth variations for this mode are depicted by circles in Fig 4.17a and b, respectively. Both these modes show a jump in the linewidths around 216 K. These changes can be attributed to the fluctuations in the order parameter (see § 1.7.3).

It has been known that the phase transition at 216 K is associated with a change in Hydrogen bonding [1]. Such changes should be reflected in the Raman and IR spectra through $\tau(NH_3)$, $\delta(NH_3)$ and $\nu(NH_3)$ modes [12,21]. Fig 4.18 shows the typical IR spectra in 1750-2000 cm^{-1} range. It has been observed that the mode around 1850 cm^{-1} due to $\delta_{asy}(NH_3)$ + $\tau(NH_3)$ [12] shifts ($\cong$ 30 cm^{-1}) to higher frequency side as shown in Fig 4.19a at about 216 K. Also, it becomes sharp (Fig 4.19b, curve 1) and strong (Fig 4.19b, curve 2) as the temperature is decreased to 100 K.

4.5.1 Order-Disorder Transition in C_2CdCl

The disorder of ethylammonium ions at room temperature is well known in C_2CdCl type systems [1]. The ethylammonium ions occupy the gaps created by the two dimensional corner shared $CdCl_6$ octahedral layers by N-H..Cl type Hydrogen bond. These ions in ORT phase have been known to exist in two equivalent orientations to fulfill the *orthorhombic Hydrogen bonding* scheme [1]. However, this kind of disorder has not been seen in OLT phase. Observed high entropy change 9.7 J mol^{-1} K^{-1} ($\cong$ R ln3) indeed corroborates the order-disorder nature of the transition at 216 K [2].

Considering this behaviour in C_2CdCl, we can treat the liberating $C_2H_5NH_3^+$ ions to be *Brownian particles* undergoing self diffusion (random jumps) among the possible orientations in ORT phase. The general theory for the variation in the linewidths for such phonons has been developed by PdaR Andrade *et al* [22] and is summarized in § 1.7.3. Recalling eqn 1.36,

$$\Gamma(T) = \Gamma_0 + AT + BT^2 + C \ (\tau_c/(1+\omega^2\tau_c^2))$$

where Γ_0, A and B are the usual intrinsic linewidth, cubic and quartic anharmonicity constants, respectively and τ_c represents the correlation time. The last term in eqn 1.36 represents the temperature dependence of the linewidths for Brownian particles. If $\omega^2\tau_c^2 \gg 1$ and in the absence of quartic anharmonicity, eqn 1.36 takes the simple form:

$$\Gamma(T) = \Gamma_0 + AT + C\omega^{-2}Exp(-\Delta U/k_B T)$$

4.1

By knowing the linewidth variations with temperature one can calculate the activation energy barrier or vice versa.

From NMR studies on this system it is shown that disorder originates from the hydrogen atoms of the ethylammonium ion [3]. In this case one would expect that the vibrational modes involving hydrogen atoms would show maximum linewidth changes during ORT-OLT transition.

In Fig 4.14, 4.15 and 4.16, it can be clearly seen that the linewidths of $\nu(CC)$ mode in the Raman along with the $\rho(CH_2)$, $\rho(NH_3)$ and $\rho(CH_3)$ modes in IR absorption exhibit drastic changes near 216 K. Similar experimental results have been obtained previously by Hagemann and Bill [8] for $\nu(CC)$ mode in C_2CdCl. They concluded that the discontinuous change in the linewidth of this mode could be due to the first order nature of the transition. If the linewidth changes are triggered by the transition alone, its temperature evolution could provide some information about the order parameter [23-25]. However, our attempts to apply the pseudo-spin model to explain the linewidth changes has failed (see § 1.7.3). In fact the linewidth changes could be understood well in terms of disorder induced changes. The linewidth changes for this mode are fitted well with eqn 4.1, using the least square minimization procedure described in § 2.4.3. The values of the different parameters in eqn 4.1 for $\nu(CC)$ mode are A = 0.0015, C = 0.35×10^8 and $\Delta U/k_B$ = 667. The activation energy calculated form this analysis is 0.058 eV.

To check the validity of our assumption that the linewidth variations of the disorder affected mode could be explained by the eqn 4.1, the observed linewidth variations of $\rho(CH_2)$ mode are analyzed in a similar way. The calculated curve using the following parameter values, Γ_0 = 5.09, A = 0.02, C = 0.99×10^8 and $\Delta U/k_B$ = 635 is shown in Fig 4.15b as continuous line. The calculated activation energy (0.055 eV) from this mode is again consistent with the one found from $\nu(CC)$ mode.

The ethylammonium ion is known to undergo reorientational motion in ORT phase [1]. So, one would expect similar changes for $\rho(NH_3)$ and $\rho(CH_3)$ modes. Indeed, our observations on linewidth changes for these modes (see Fig 4.16) yield similar results. The linewidth change takes place in a small temperature range (i.e., 170-220 K) above and below which the change is almost linear. A fit to eqn 4.1 results in large (above experimental uncertainty) variation in the *critical temperature range*. Considering this fact, it has been assumed that these variations in Γ are predominantly from the third term of eqn 4.1. i.e.,

$$\Gamma(T) \propto C\omega^{-2} \exp(-\Delta U/k_B T) \qquad 4.2$$

Simple linear regression analysis in 170-220 K range is made with the help of Lotus 1-2-3 to verify the validity of eqn 4.2 for $\rho(CH_3)$ and $\rho(NH_3)$ modes. The regression curves are shown as continuous lines in the inset of Fig 4.16 and the activation

energy is calculated to be 0.058 and 0.062 eV respectively for these two modes.

From these observations we conclude that the ethylammonium ions as such undergo reorientational motions. The activation energy for this is computed to be 0.06 eV. These results are remarkably closer to NMR results [3].

The other interesting changes are observed for δ(CCN) mode. This mode is a broad singlet in ORT phase at 405 cm^{-1}. On approaching ORT-OLT transition a new mode appears at 409 cm^{-1}. The 409 cm^{-1} band shifts to 412 cm^{-1} on further decreasing the temperature. The mode at 405 cm^{-1} does not show any appreciable change. The linewidth of this mode also shows a jump. Normally, an order parameter like frequency shift for a hard mode is unusual. However, such a behaviour could be expected if a soft mode is coupled to it (see § 1.7.3). In such case the frequency and the corresponding linewidth show the following temperature dependence [23-25].

$$\omega \propto (T_c-T)^{\beta} \qquad\qquad 4.3$$

$$\Gamma \propto \{T/(T_c-T)\}^{2\beta} \qquad\qquad 4.4$$

The inset of Fig 4.17 shows the logarithmic variation in peak frequency and linewidth with $\log(T_c-T)$, with T_c = 216 K. The exponent values 0.26 ± 0.04 and 0.45 ± 0.05, respectively, were calculated from the frequency and linewidth variations of δ(CCN) mode in 100-216 K range by following the procedure

described in § 3.5.5. The best fitted line resulting in this β value are shown by triangles and rectangles in the inset of Fig 4.17. The infrared active mode at 1192 cm^{-1} (at 300 K) also shows a similar frequency and linewidth change. By fitting eqns 4.3 and 4.4 for this mode, we get the exponent values 0.22 and 0.47, respectively. The open and filled circles in the inset of Fig 4.17 denote logarithmic values of frequency and linewidth changes with $log(T_c-T)$ respectively. The computed β ($\cong$ 0.26 $\pm$ 0.04) is comparable with that found by the birefrengence studies of C_2CdCl [26].

The change in the hydrogen bonding scheme has been reflected by the downward frequency shift for NH_3 stretching modes in the Raman spectra. The same has been demonstrated by the upward shift of $\tau(NH_3)$ mode by Hagemann and Bill [8] and is also corroborated by the present study. Infrared evidence for the same was clearly seen from $\delta_{asy}(NH_3) + \tau(NH_3)$ mode (see Fig 4.18). On decreasing the temperature, this mode shifts to higher frequency side showing a jump of 40 cm^{-1} at 216 K. The band becomes sharper as shown in curve 1 of Fig 4.19b below T_c. This shift could be attributed to the shift in $\tau(NH_3)$ mode. The frequency of $\delta_{asy}(NH_3)$ mode does not show any change. In the Raman spectra a broad band at 3174 cm^{-1} which could be due to $\nu_{as}(NH_3)$ shows a downward shift of 70 cm^{-1} and gains intensity in Phase III. All these facts corroborate the stronger Hydrogen bonding in OLT phase.

4.6. CONCLUSIONS

The spectral variations of the thermosensitive modes of C_2Cl does not provide any convincing evidence of phase changes around 221 K. However, the transition at 345 K show many precursor effects in the Raman spectra. Disappearance of well resolved lattice modes, diverging nature of the librational modes could be attribute to the transition. Further, the broad and weak modes at higher temperature ($\gg$ 345 K) show that the ethylammonium ions are highly disordered.

The $D_{2h}^{18} \rightarrow D_{2h}^{15}$ transition in C_2CdCl take place at 216 K. The present study corroborates the order-disorder nature of the transition. The anomalous linewidth changes for certain internal modes provide valuable information about the dynamical nature. The activation energy calculated from the linewidth variations of $\nu(CC)$, $\rho(CH_2)$, $\rho(CH_3)$ and $\rho(NH_3)$ is comparable with NMR results. The $\delta(CCN)$ and 1192 cm^{-1} IR mode show order parameter like frequency shifts in 100-216 K region. The calculated exponent value is in accordance with soft-hard mode coupling scheme. The order-disorder transition is associated with the strengthening of hydrogen bonding. This fact is clearly shown by temperature variations of spectral parameters for the infrared active $\delta_{asy}(NH_3) + \tau(NH_3)$ mode. Further evidence for this is provided by downward frequency shift for $\nu_{as}(NH_3)$ mode in the Raman spectra. All these observations confirm that the hydrogen bonding is stronger in OLT phase.

REFERENCES

1. G Chapuis, Phys Stat Sol., **43a**, 203 (1977).

2. C Filipic and A Levstik, Phys Stat Sol., **57a**, K55 (1980).

3. R Blinc, M Burgar, B Lozar, J Seliger, J Slak, H Arend, R Kind and V Rutar, J. Chem Phys., **66**, 278 (1977).

4. IA Oxton, J. Mol Struct., **54**, 11 (1979).

5. M Peyrar and R Perret, Phys Stat Sol., **52a**, 521 (1979).

6. CNR Rao, S Ganguli, H Ramachandra Swamy and IA Oxton, J. Chem Soc., Faraday Trans. 2 **77**, 1825 (1981).

7. R Mokhlisse, M Couzi and CH Wang, J. Chem Phys., **77**, 1138 (1982).

8. H Hagemann and H Bill, J. Phys., **18C**, 6441 (1985).

9. AD Bruce, W Taylor and AF Murray, J. Phy., **13C**, 483 (1980).

10. M Schlaak, M Couzi and PV Houng, Ben. Bunsenges Physik. Chem., **80**, 881 (1976).

11. JHM Stoelinga and P Wyder, J. Chem. Phys, **64**, 4612 (1976).

12. W Depmeier and IA Oxton J. Mol Struct., **77**, 91, (1981).

13. J Tasu and DFR Gilson, J. Phy Chem., **72**, 4082 (1968).

14. F Jellinek, Acta Cryst., **11**, 626 (1958).

15. H Hagemann and H Bill, Chem Phy Lett., **87**, 45 (1982), *ibid* **93**, 582 (1982).

16. M Peyrard and M Remoissenet, J. Chem Phys **71**, 2732 (1979).

17. H Hagemann and H Bill, J. Chem Phys., **80**, 111 (1984).

18. J Petzel, J. Phys Chem Solids, **36**, 1005 (1977).

19. R Geick and K Strobel, J. Phys., **10C**, 4221 (1977).

20. CI Ratcliffe, WF Sherman and GR Wilkinson, J. Raman Spectrosc., **11**, 205 (1981).

21. JC Decius and RM Hxeter, "Molecular Vibrations in Crystals." McGraw-Hill International Co., New York (1977).

22. P da R Andrade and SPS Porto, Solid StateCommu., **13**, 1249 (1973)

23. F Gervais, Ferroelectrics, **13**, 555 (1976).

24. I Lavlicht, J. Phys Chem Solids, **39**, 901 (1978).

25. PSR Prasad and HD Bist J. Phys Chem Solids, **50**, 1033 (1989).

26. E Karajamki, R Laiho, T Levola, W Kleemann and FJ Schafer, Physica, **111B**, 24 (1981).

TABLE 4.1 Classification of modes of $C_2H_5NH_3^+$ ion under point group symmetry of C_s.

C_s	E	σ	n(vib)	n(tr)	n(rot)	Raman	IR
A'	1	1	16	2	1	A	A
A"	1	-1	11	1	2	A	A
ω_R	11	5					
ϕ	0	0					

TABLE 4.2 Factor group analysis of $C_2H_5NH_3Cl$ in C_{2h}^5 phase

C_{2h}^5	A_g	B_g	A_u	B_u
n_{int}^A	16	11	11	16
n_T^A	2	1	1	2
n_R^A	1	2	2	1
n_T^{Cl}	2	1	1	2
n(Acostic)	-	-	1	2
n(Optical)	5	4	3	3
n(Total)	21	15	15	21
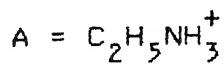
$A = C_2H_5NH_3^+$

TABLE 4.3 Factor group analysis of $C_2H_5NH_3^+$ in $(C_2H_5NH_3)_2CdCl_4$ crystal in sub-ambient phases.

Phase/Mode		A_g	B_{1g}	B_{2g}	B_{3g}	A_u	B_{1u}	B_{2u}	B_{3u}
	n_{int}	16	11	11	16	11	16	16	11
D_{2h}^{18}	n_R	1	2	2	1	2	1	1	2
	n_T	2	1	1	2	1	2	2	1
	n_{int}	27	27	27	27	27	27	27	27
D_{2h}^{15}	n_R	3	3	3	3	3	3	3	3
	n_T	3	3	3	3	3	3	3	3
Activity		$\alpha_{xx}, \alpha_{yy}, \alpha_{zz}$	α_{xy}	α_{xz}	α_{yz}	–	$\varepsilon\|z$	$\varepsilon\|y$	$\varepsilon\|x$

		A_g	B_g	A_u	B_u
	n_{int}	27	27	27	27
C_{2h}^{5}	n_R	3	3	3	3
	n_T	3	3	3	3
Activity		$\alpha_{xx}, \alpha_{yy}, \alpha_{zz}, \alpha_{xy}$	α_{yz}, α_{xz}	$\varepsilon\|z$	$\varepsilon\|y, \varepsilon\|x$

int = internal R = librational and T = translational

TABLE 4.4a Comparision of band positions of $C_2H_5NH_3Cl$ at different temperatures.

RAMAN			IR	Assignments[†]
358 K	298 K	80 K	298 K	
--	3030	3028	a	$\nu_{as}(NH_3)$
--	2986	2984	a	$\nu_{as}(CH_3)$
2977	2972	2970	a	$\nu(CH_2)$
2937	2943	2934	a	$\nu_{sy}(CH_3)$
--	1590	1594	1610	$\delta(NH_3)$
			1645	
--	1471	1476	--	$\delta(CH_2)$
1457	1457	1456	1480	$\delta_{as}(CH_3)$
	1461	1463		
--	1450	1448	1410	$\delta_{sy}(CH_3)$
--	1368	1366	1377	$\omega(CH_2)$
1329	1340	1340	1345	$\gamma(CH_2)$
--	1220	1218	1225	$\rho(CH_3)$
1188	1192	1190	1200	
1048	1041	1038	1050	$\nu(CN)$
976	979	978	980	$\rho(NH_3)$
--	966	962	970	
870	869	870	885	$\nu(CC)$
--	798	802	802	$\rho(CH_2)$
--	459	468	470	$\tau(NH_3)$
416	413	412	425	$\delta(CCN)$
--	298	302	325	$\tau(CH_3)$
--	192	208	--	R(A)
--	155	166	--	R(A)
--	119	130	--	R(A)
--	86	98	--	T(Cl)
--	--	90	--	
--	80	82	--	T(Cl)

[†] $A = C_2H_5NH_3^+$ a = A part of the broad band, b = Broad, m = Medium, s = Strong, sh = Shoulder, v = Very, w = Weak, ν = Stretch, δ = Bend, ρ = Rock, τ = Torsion, ω = Wagg, γ = Twist,
R = Librational and T = Translational.

TABLE 4.4b The Raman and Infrared frequency positions in $(C_2H_5NH_3)_2CdCl_4$

α_{xx}	α_{yy}	α_{zz}	α_{xy}	α_{xz}	α_{yz}	Infrared	Assignment[+]
A_g			B_{1g}	B_{2g}	B_{3g}		
3156 w	3156 w	3176 vw	3174 w	3170 w	--	a	$\nu_{as}(NH_3)$
3076 w	3075 w	--	--	--	--	a	$\nu_s(NH_3)$
2977 s	2975 s	2985 s	2976 s	2984 s	2986 s	a	$\nu(CH_3)$
2935 s	2932 s	2941 s	2938 s	2940 s	2944 s	a	$\nu(CH_2)$
--	--	2930 sh	--	--	2933 sh	a	
2883 m	2882 m	2884 m	2886 m	2865 m	2886 w	a	$\nu(CH_3)$
2783 w	2782 w	2784 vw	2787 w	--	--	a	
1574 vw	1574 vw	1576 vw	1580 w	--	1580 w	1590 s,b	$\delta_{as}(NH_3)$
1454 w	1454 w	1454 w	1458 m	1456 m	1455 m	1490 s	$\delta_{as}(CH_3)$
--	--	1394 vw	--	--	--	1410 sh	$\delta_{as}(CH_2)$
--	--	1374 vw	--	--	--	--	$\gamma(CH_2)$
1328 vw	--	1330 vw	1333 w	1330 w	1332 w	1337 m	$\omega(CH_2)$
--	--	1214 vw	--	--	1214 w	1217 sh	$\rho(CH_3)$
1184 vw	1183 vw	1186 vw	1186 vw	--	1186 w	1195 s	
1042 vw	1042 vw	1040 vw	1042 w	1040 w	1040 w	1052 w	$\nu(CN)$
968 vw	970 vw	967 vw	968 w	963 vw	968 w	975 s	$\rho(NH_3)$
866 w	864 w	866 s	868 m	866 s	866 s	872 w	$\nu(CC)$
--	--	--	--	--	--	795 s	$\rho(CH_2)$
404 vw	404 vw	407 w	402 w	405 vw	405 w	407 s	$\delta(CCN)$
252 sh	256 sh	--	258 sh	--	--	--	$\tau(NH_3)$
214 m	214 s	214 s	214 s	213 m	213 s	--	$\nu(CdCl)$
--	160 w	--	--	--	159 w	--	$\delta(CdCl)$
--	115 w	116 sh	--	--	--	--	R(A)
98 w	--	98 s	96 w	99 s	99 s	--	T(A)
--	--	56 sh	--	53 sh	--	--	T(A)

[+] $A = C_2H_5NH_3^+$ a = A part of the broad band, b = Broad, m = Medium, s = Strong, sh = Shoulder, v = Very, w = Weak, ν = Stretch, δ = Bend, ρ = Rock, τ = Torsion, ω = Wagg, γ = Twist, R = Librational and T = Translational.
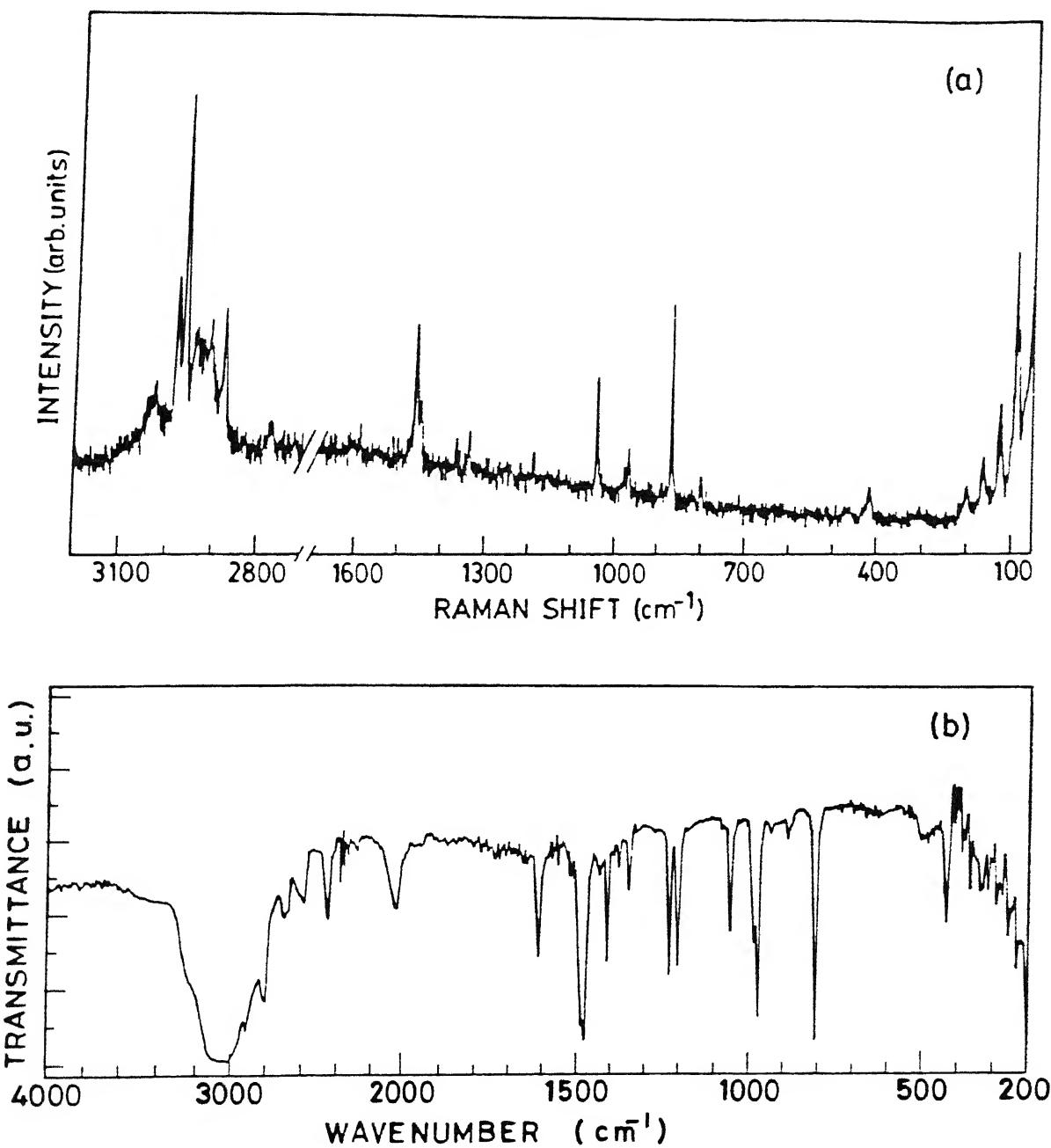
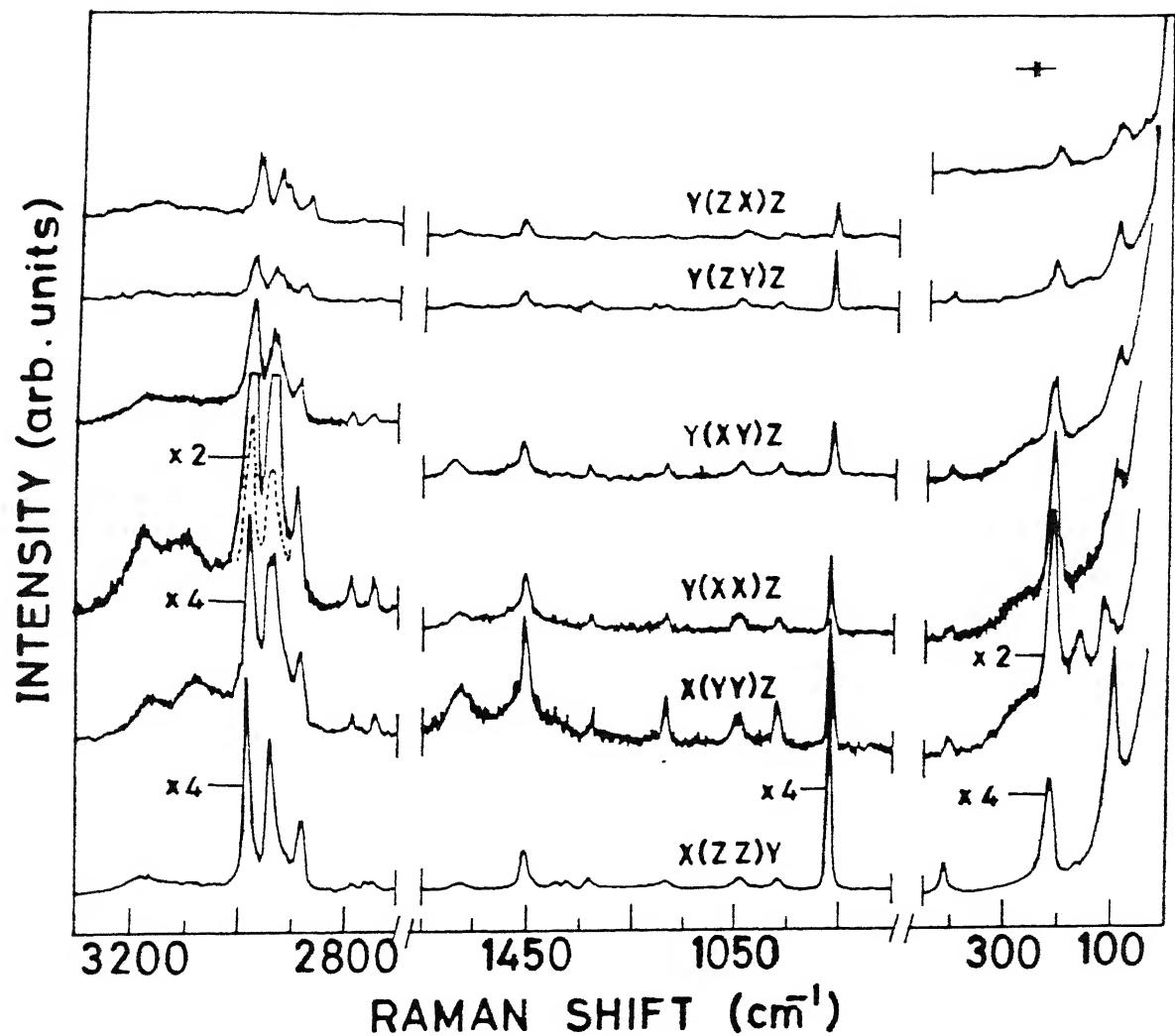Fig 4.1 (a) The Raman and (b) infrared spectra of C_2Cl at 300 K.

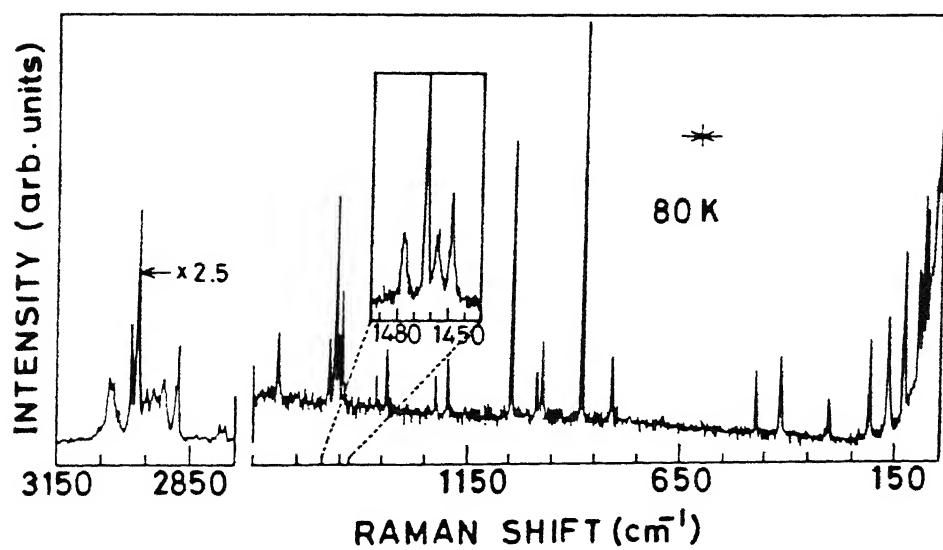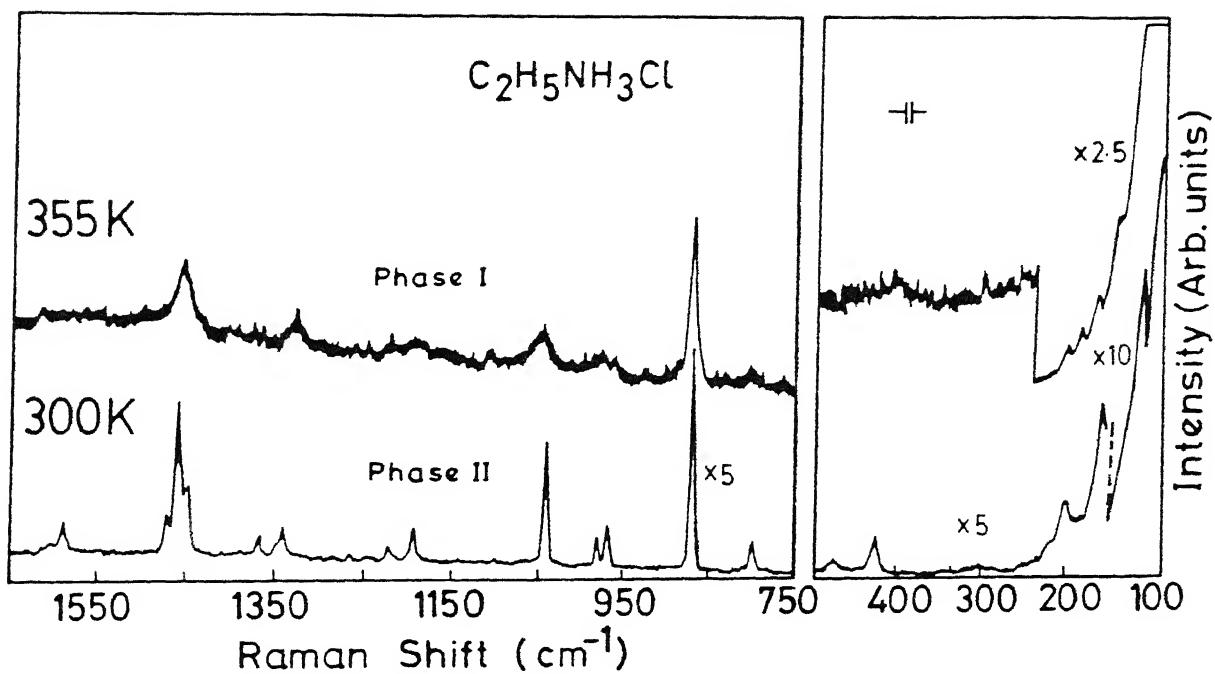Fig 4.2 Single crystal Raman spectra of C_2CdCl at room temperature.

Fig 4.3 The Raman spectra of C_2Cl in different phases.

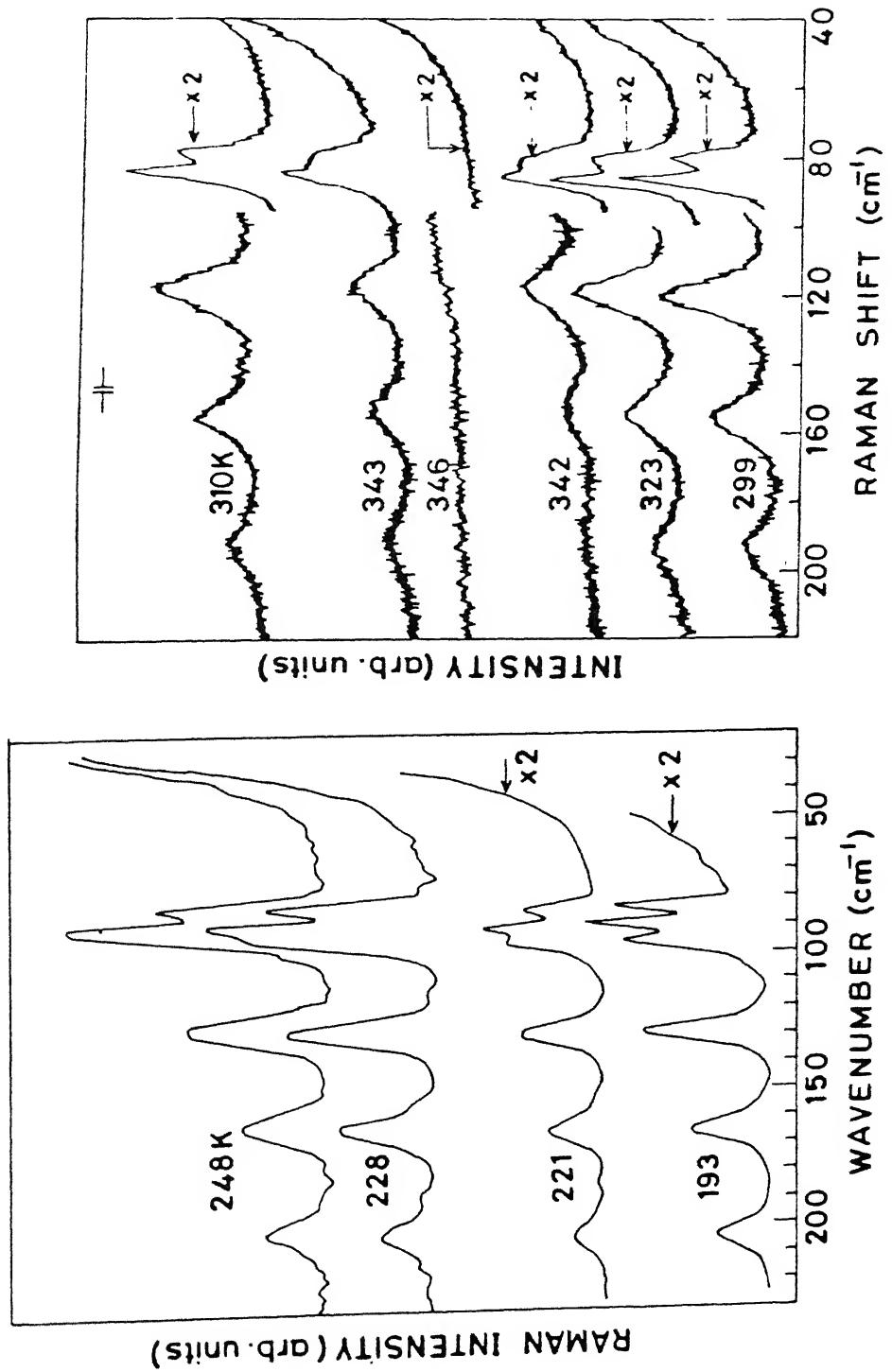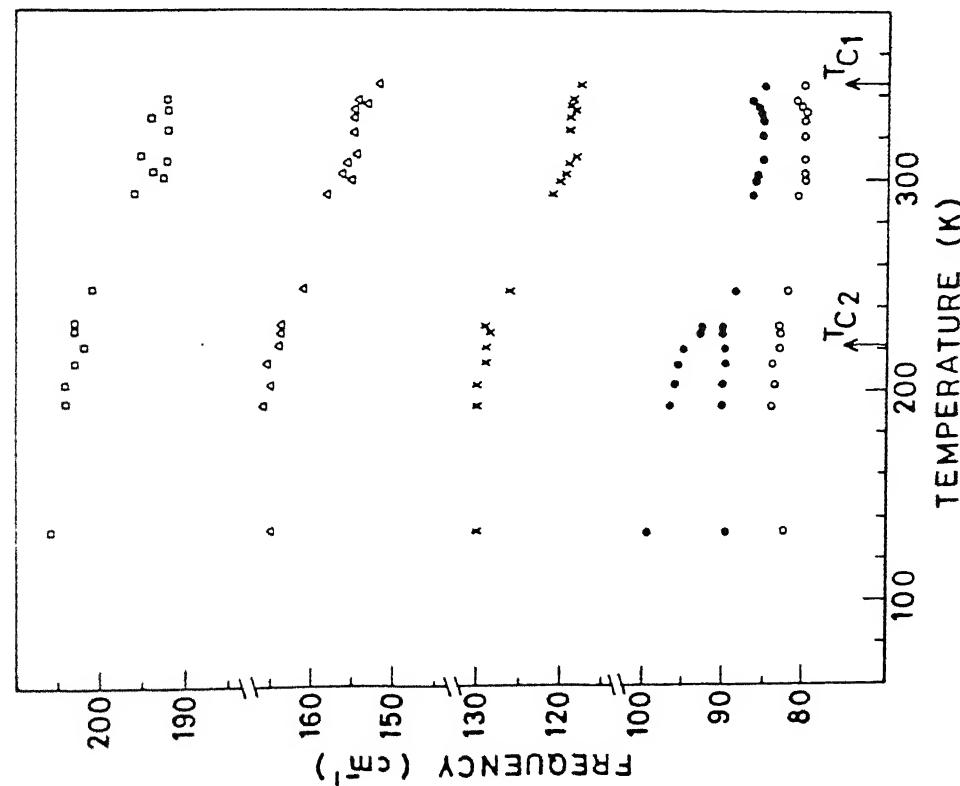Fig 4.4 The Raman spectra of C_2Cl in the lattice mode region at different temperatures.

179

Fig 4.6 (a) Normalized intensity and (b) linewidth variations for 119 and 155 cm^{-1} (RT) modes of C_2Cl.

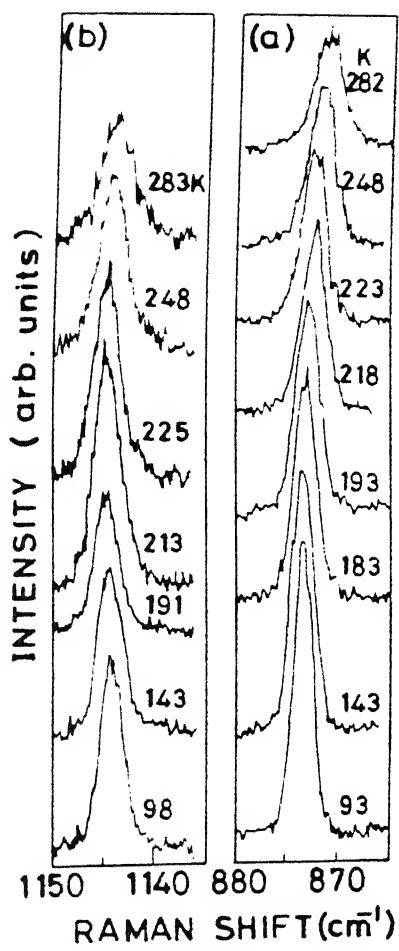Fig 4.5 Frequency variation of the lattice modes of C_2Cl_4.
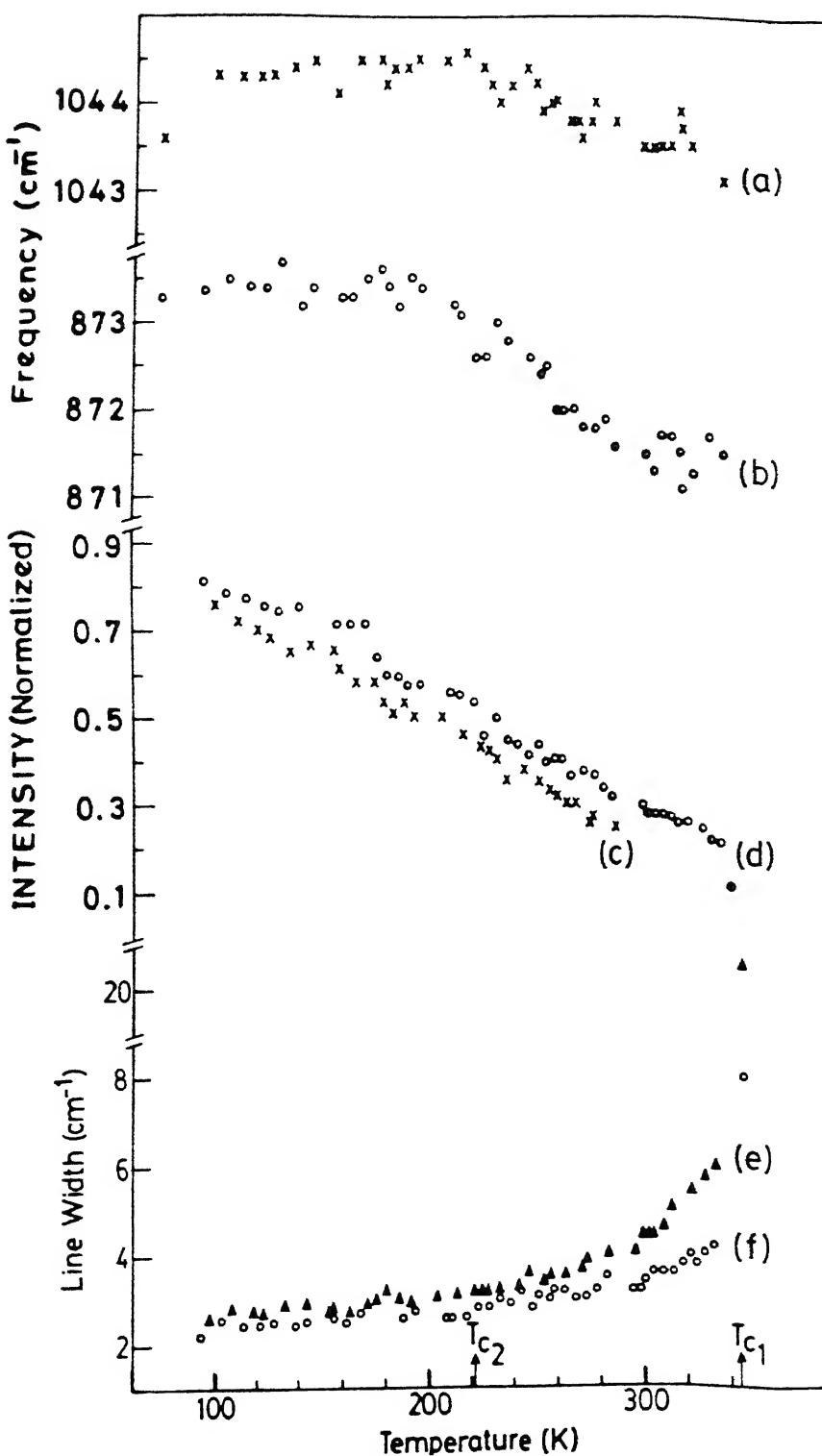
Fig 4.7 Typical thermal evolution of $\nu(CC)$ and $\nu(CN)$ modes of C_2Cl.

Fig 4.8 Peak frequency (a,b), intensity (c,d) and linewidth (e,f) variation plots of $\nu(CN)$ and $\nu(CC)$ modes of C_2Cl.
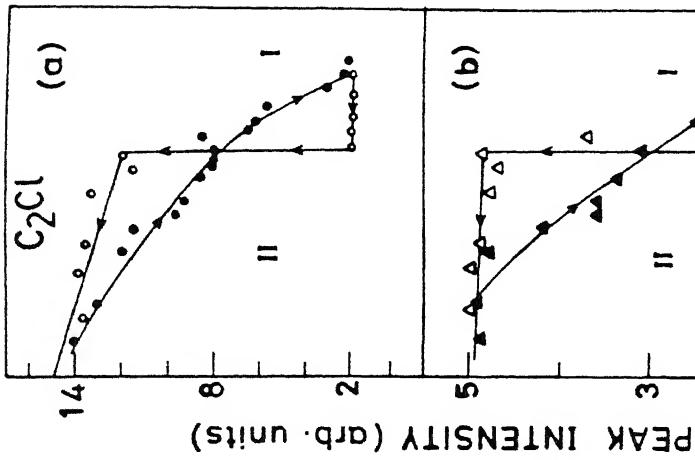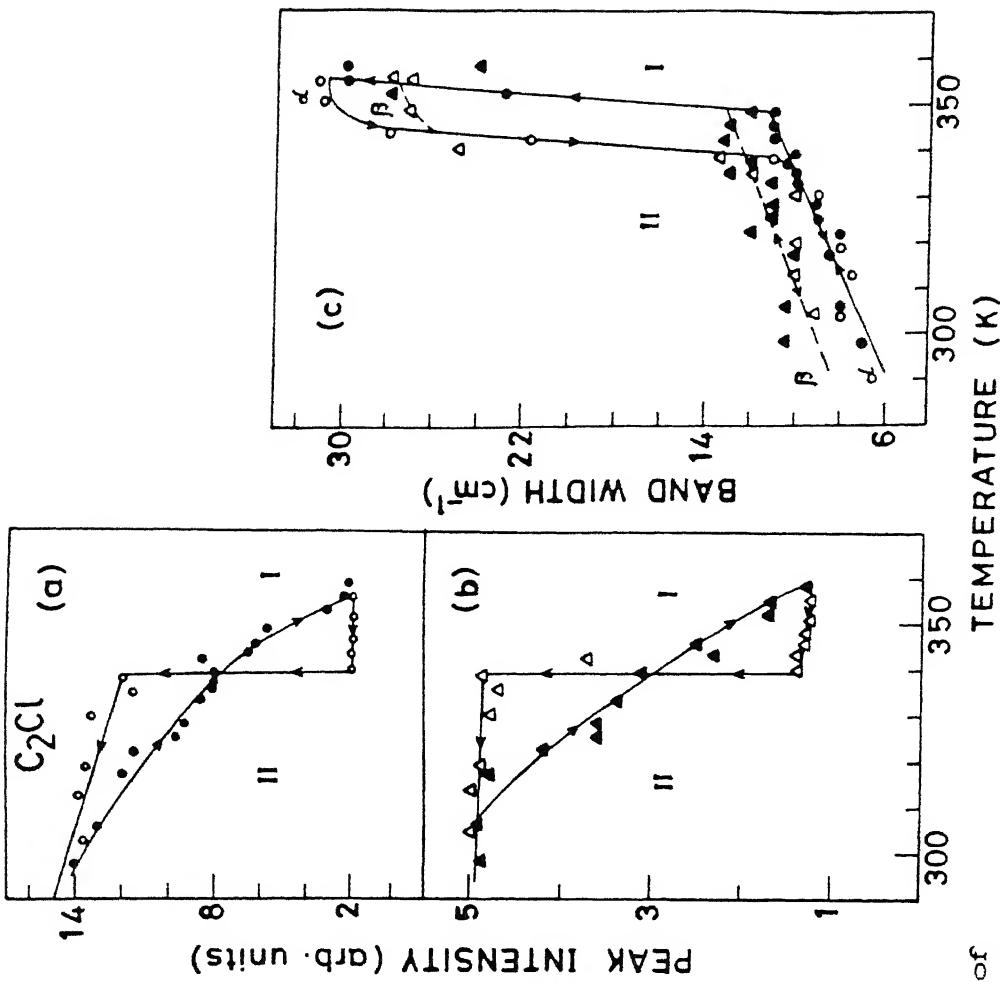
Fig 4.10 Peak intensity (a,b) and linewidth (c_α, c_β) variations of $\nu(CH_2)$ and $2\delta(CH_3)$ modes. Filled and open symbols represents heating and cooling respectively.

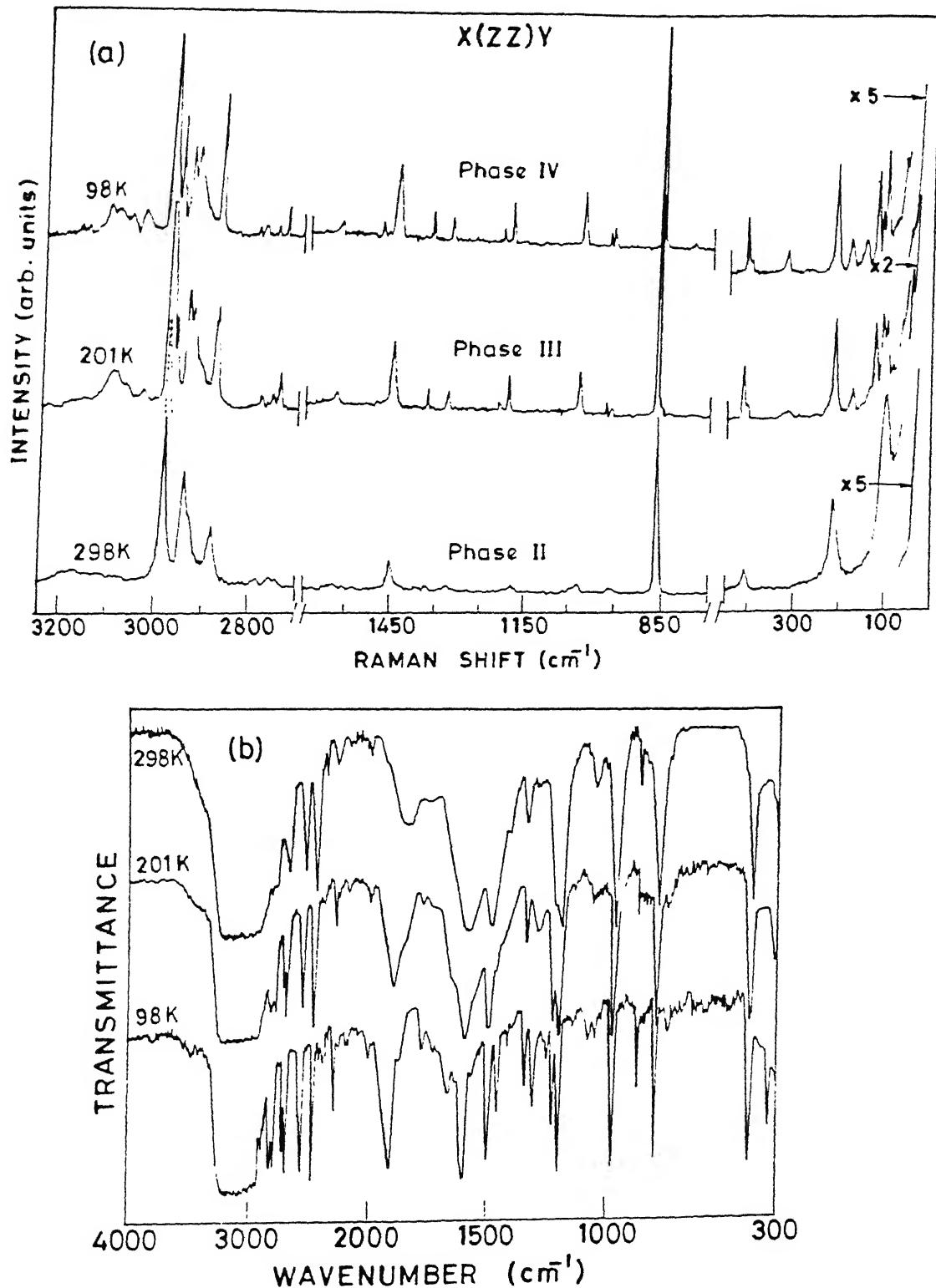Fig 4.9 Few representative Raman spectra of C_2Cl in the stretching mode region.

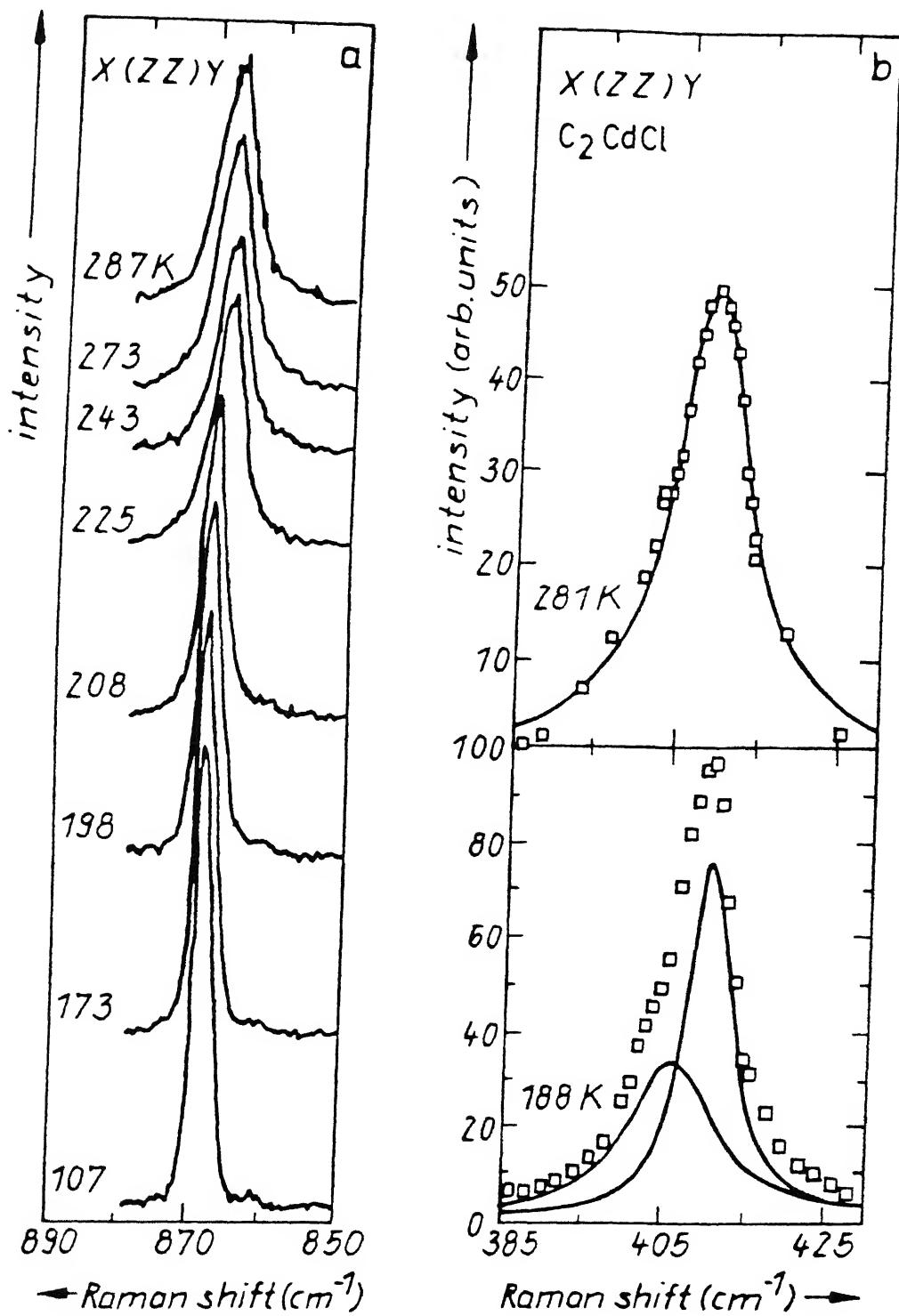Fig 4.11 (a) The Raman and (b) infrared spectra of C_2CdCl crystal in sub – ambient phases.

Fig 4.12 Thermal evolution of (a) $\nu(CC)$ and (b) $\delta(CCN)$ Raman

modes in X(ZZ)Y polarizition. The continious lines in

(b) are the calculated Lorentzian curves using least

square method.
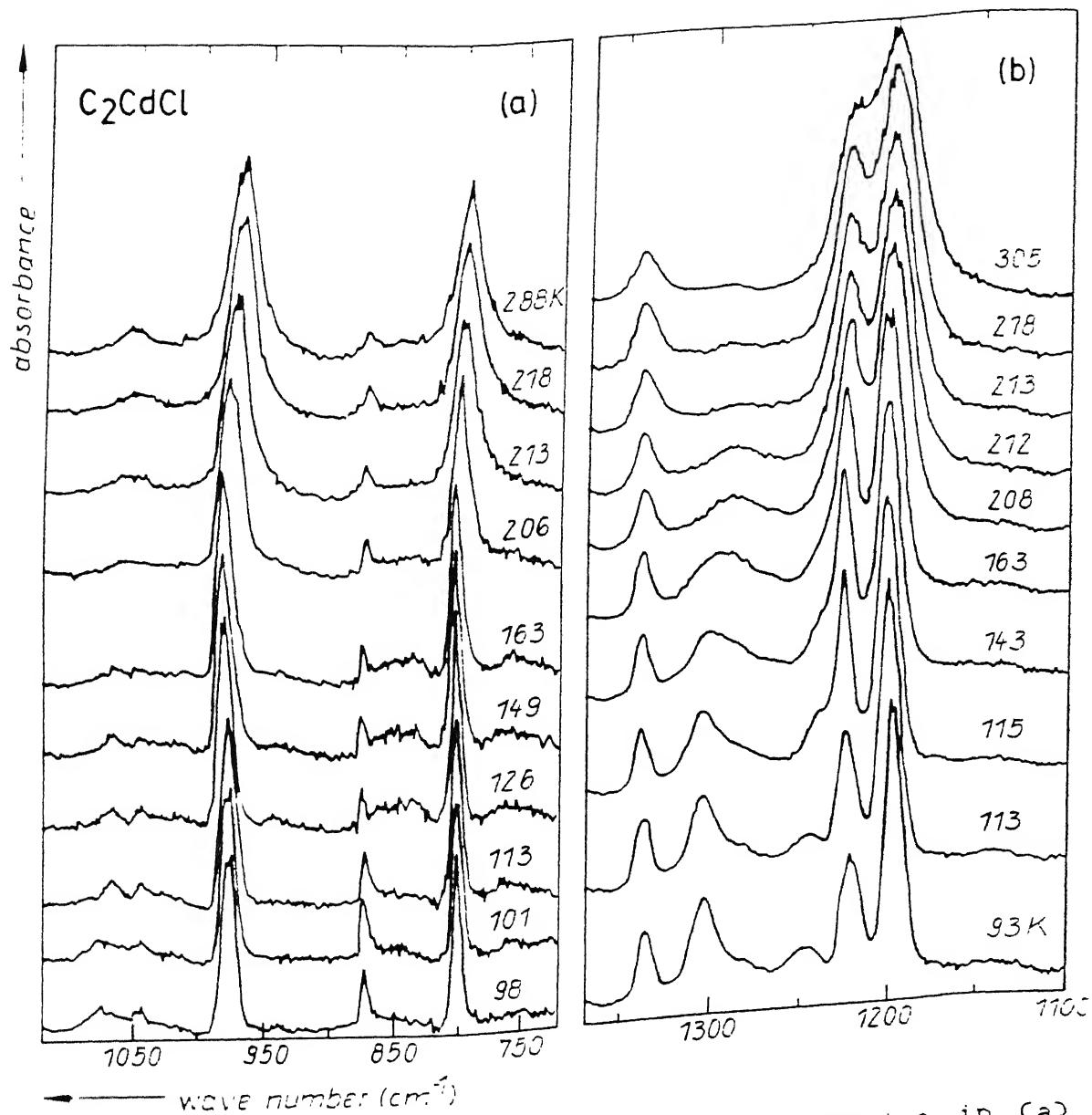
Fig 4.13 The thermal evoluation of infrared spectra in (a) 720 – 1120 and (b) 1100 – 1375 cm^{-1} region.
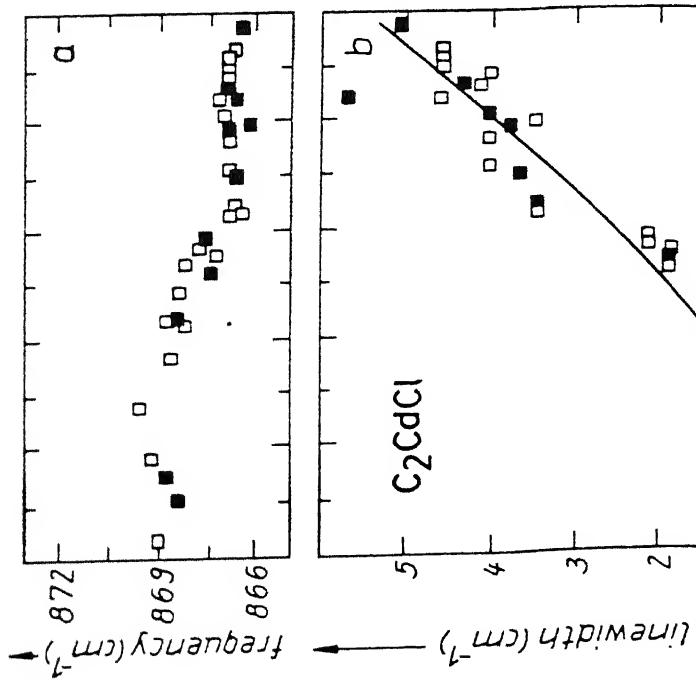
Fig 4.14 Temperature dependence of (a) frequency and (b) linewidth for $\nu(CCl)$ (RS) mode. Filled and open symbols represent cooling and warming cycles, respectively.
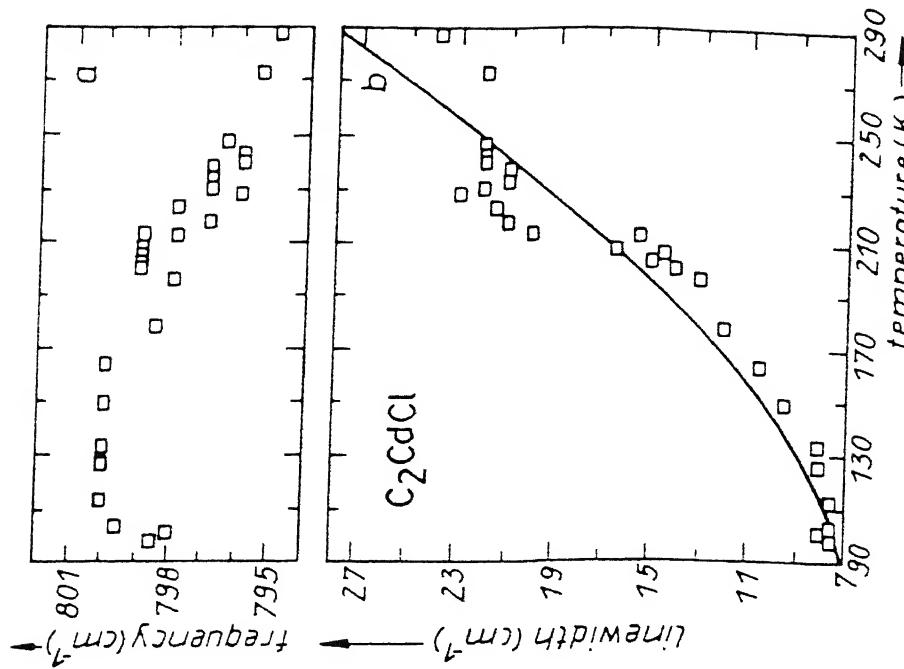
Fig 4.15 The (a) frequency and (b) linewidth changes for $\rho(CH_2)$ IR mode in 100 - 290 K region.
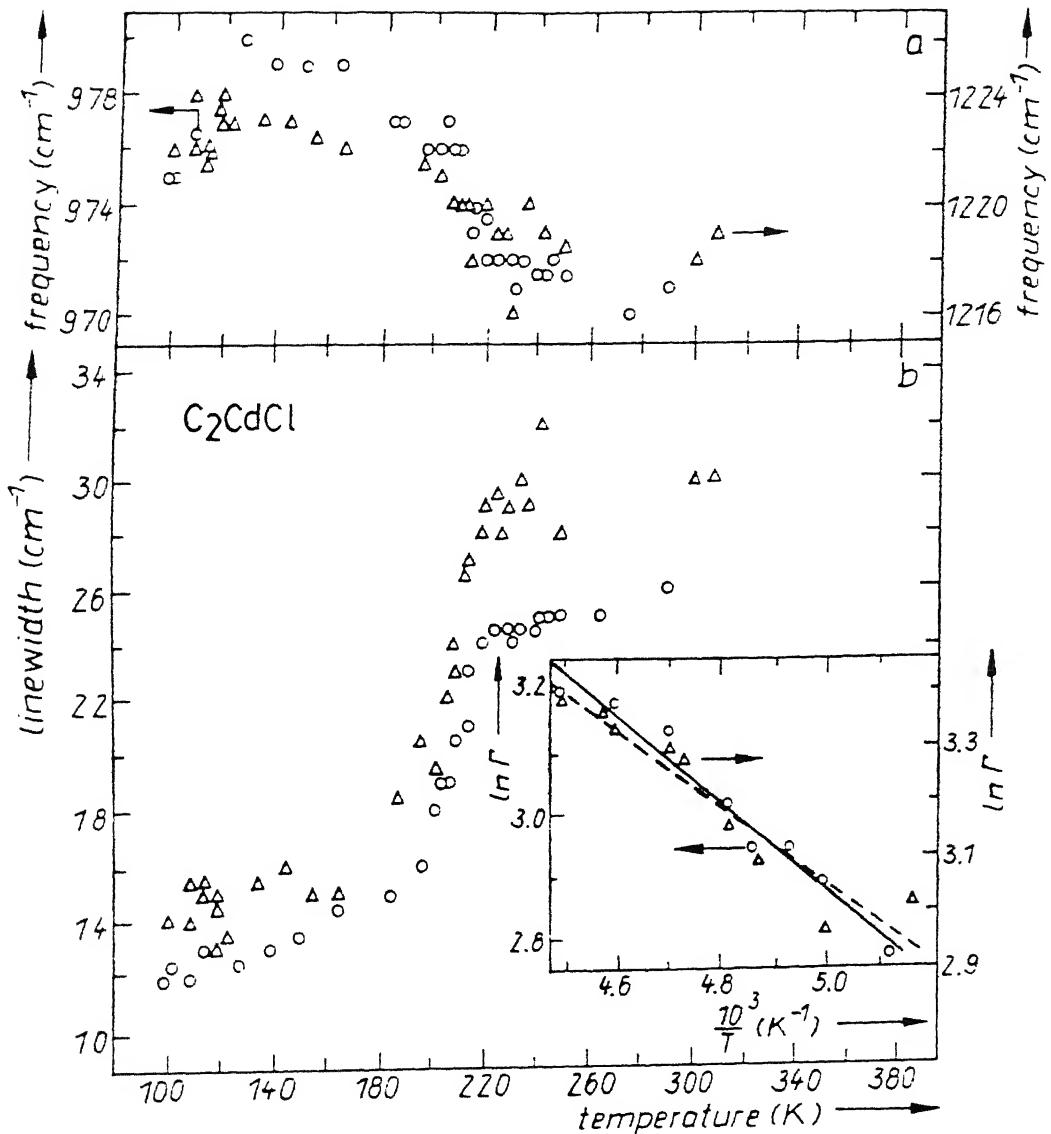
Fig 4.16 The (a) frequency and (b) linewidth changes for ρ(NH₃) (circles) and ρ(CH₃) (triangles) modes in 100 - 300 K range. In the inset a plot of lnΓ vs. [10³/T] is shown for the same modes in the 160 - 220 K range.
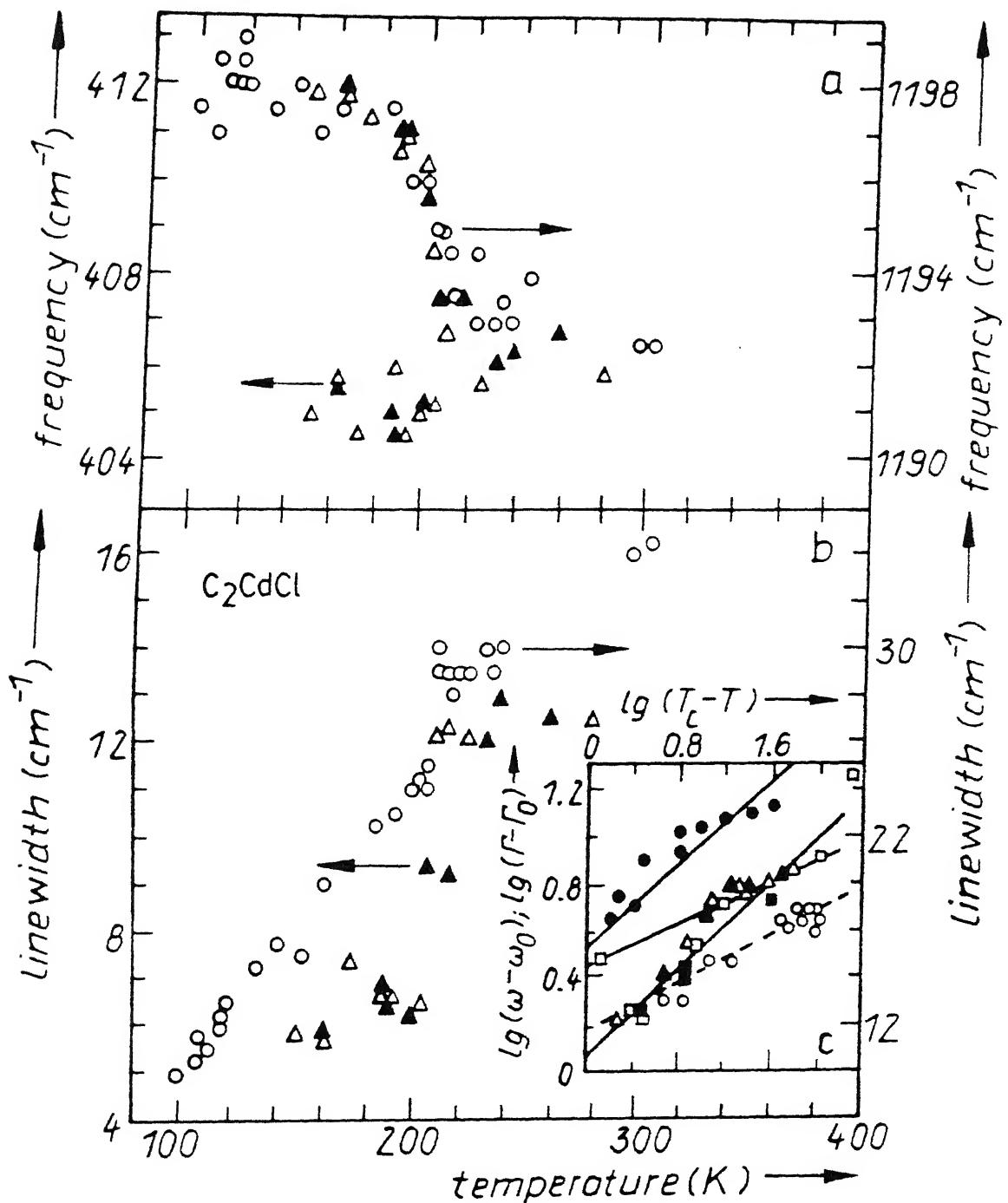
Fig 4.17 The thermal variations of (a) frequency and (b)
linewidth for δ(CCN) Raman and 1192 cm⁻¹ IR modes. The
filled and open triangles are for δ(CCN) mode in
cooling and heating cycles, the circles represent
changes for 1192 cm⁻¹ IR mode. (c) Shows a plot of
log(ω−ω₀) vs. log(T_c−T) for these modes by same
symbols. The filled circles and squares represent the
plot of log (Γ−Γ₀) vs. log(T/(T_c−T)) for the same modes.

Fig 4.19 Spectral parameter varitions for $\delta_{asy}(NH_3) + \tau(NH_3)$ mode in 100 – 300 K range.

Fig 4.18 Typical IR spectra in 1750–2000cm^{-1} range at different temperatures.

CHAPTER V

VIBRATIONAL SPECTROSCOPIC STUDY OF $C_3H_7NH_3CL$ AND $(C_3H_7NH_3)_2CdCL_4$ CRYSTALS

ABSTRACT

In this chapter detailed vibrational assignments of n-propylammonium chloride (C_3Cl) and di(propylammonium) tetrachlorocadmate (C_3CdCl) are reported. The Raman study in C_3Cl were carried out in 90-385 K range. From the spectral evolution of $\nu(CC)$ and $\nu(CN)$ Raman modes in C_3Cl the transition at 188 ± 2 K can be characterized to an order-disorder type. From the anomalous variations in the intensity of these modes below 188 K, the order parameter exponent (β) is calculated to be 0.35 ± 0.04.

Thermal evolution of a few modes in IR and Raman (in $X(ZZ)Y$ and $X(YY)Z$ polarizations) spectra of C_3CdCl suggest that the transition around 158 K could mainly be due to the change in H-bonding strength. Split in many IR at 113 K is an evidence of the transition.

The following are based on this chapter:

1. Proc Solid St Sympo., **30**, 335 (1987).
2. Solid St Communications, **00**, 000 (1990).

5.1 INTRODUCTION

C_3CdCl, the last member in short chain compound of the family $(C_nH_{2n+1}NH_3)_2 CdCl_4$, undergoes a sequence of phase transitions (see Table 1.2). In 183-158 K range it is known to show an incommensurate phase, which is unique in these crystals [1]. However, spectroscopic studies have not provided any evidence for the transition. Apart from this, it undergoes an order-disorder transition near 158 K and to a monoclinic phase around 113 K [2-6]. There has been no systematic studies in this compound covering all the transitions. Presently, systematic infrared and Raman spectroscopic studies of the crystal in 100-300 K range are reported.

Similar to C_2CdCl, this crystal also contain a large number of atoms in its molecular units. Hence a study of its parent compound i.e., propylammonium chloride (abbreviated as C_3Cl hereafter) is found useful. Additionally, C_3Cl also undergoes an order-disorder transition around 188 K [7,8]. The Raman spectral study of the compound in 90-385 K region is also reported in this chapter.

5.2 CRYSTAL STRUCTURE AND PHASE TRANSITIONS

Di(propylammonium) tetrachlorocadmate (abbreviated as C_3CdCl) in its room temperature phase is iso-structural with n = 1, 2 crystals of the family $(C_nH_{2n+1}NH_3)_2 CdCl_4$ [3,4]. The large

number of atoms in the molecular unit makes a detailed assignment tedious. However, certain characteristic group frequencies could be identified by comparing the spectra with similar compounds. The organic entity *i.e.*, propylammonium ion has C_s point group and the classification of the modes under this symmetry is shown in Table 5.1. Expected vibrational, translation and rotational modes are distributed between A', A" irreducible representations as 21A' + 15A", 2A'+ A" and A' + 2A" respectively. Both A' and A" are active in the Raman and IR spectra.

5.2.1 n-Propylammonium Chloride (C_3Cl)

C_3Cl is iso-structural with the corresponding bromide and iodide salts. The space group and the lattice parameters of it at room temperature D_{4h}^7 (Z=2) phase are a = 6.22 and c = 7.377Å [8]. Crystal structure in this phase is similar to that of PbO, with the propylammonium ions (cations) occupying Pb site [8]. Wyckoff tables [9] suggest a site of C_{4v} to Pb ions. In order to find the activity of the modes using the group theoretical methods, a prime requirement is a clear knowledge about the atomic arrangement in the unit cell [10]. In C_3Cl, such clear picture does not exist [8]. Furthermore, suggested site C_{4v} is not a sub-group of the propylammonium ion under its point group symmetry C_s [11,12]. This fact further complicates the classification of modes using the site symmetry approach [10].

So, the classification of modes using $K = 0$ selection rules in this compound is not simple. To explain the observed spectra one has to consider the contribution from the modes which have non-vanishing K values [13,14]. In such orientationally disordered crystals, phonons with $K \neq 0$ could also appear or could strongly interact with $K = 0$ phonons. The intensity of such phonons is comparable to the allowed modes and their temperature variation is governed by the degree of disorder [14]. Differential scanning calorimetric study reveals two structural phase transitions at 408 and 188 K.

The space group of the prototype phase is not known while the same in the low temperature phase is C_{2h}^3 [8]. The lattice parameters for the low temperature monoclinic phase are $a = 9.06$, $b = 8.58$, $c = 7.34$ Å and $\beta = 98^\circ$ and the propylammonium ions occupy C_s site, which is also its point group [8]. Crystallographic studies reveal that the propylammonium ions are orientationally disordered and occupy a site of C_{4v} symmetry at room temperature while they confine to a particular orientation C_s (in C_{2h}^3) below 188 K [8]. Furthermore, NMR study on C_3Cl also show a large change in its second moment corroborating the order-disorder nature of the transition [15,16]. So, this system is rather useful to understand the effect of order-disorder transition on the Raman spectra.

5.2.2 Di(Propylammonium) Tetrachlorocadmate (C_3CdCl)

At ambient temperature C_3CdCl crystallizes into an orthorhombic with space group D_{2h}^{18} (Z=2). The lattice parameters in this phase are a = 7.607, b = 7.370 and c = 25.18 Å [3,4]. C_3CdCl undergoes transitions at 183, 158 and 113 K [2-6]. The first is characterized as an incommensurate phase and the second is an orthorhombic with the space group D_{2h}^{15} (Z=4). Propylammonium ions in this phase are in an ordered state. This transition is similar to the one found in C_2CdCl (see § 4.2.2). In the temperature dependent spectra, it would be interesting to look for similar variations (see § 4.5).

The factor group analysis of C_3CdCl for the low temperature phases is summarized in Table 5.2. There was no report of crystal structure below 113 K [4] and hence it is not feasible to extend the analysis to this phase. In the disordered and ordered phase the organic chain occupies a site C_s and C_1 respectively [6]. From Table 5.2a it is clear that the modes belonging to A', in free ion symmetry, would appear in A_g and B_{2g} in the Raman spectra, while that of A" would appear as B_{1g} and B_{3g}. In low frequency range (below 350 cm^{-1}) one would expect $6A_g$ modes, three each belonging to the organic and inorganic parts. However, in OLT phase, where the organic ion occupies C_1 site, all the modes are expected in A_g species. The

Raman spectra in different orientations reveal that strict selection rules are not applicable.

5.3 ROOM TEMPERATURE SPECTRA AND ASSIGNMENTS

n-Propylammonium Chloride

Observed modes in the Raman and IR spectra are tabulated in Table 5.3. Both the IR and Raman spectra at 300 K are shown in Fig 5.1. Precise assignments of the modes for C_3Cl would be difficult because all the 36 modes are active in both the Raman and IR spectra (see Table 5.1). However, we can identify the characteristic modes by comparing with other similar systems [11,12,17]. Very general remark is that, both C_2Cl and C_3Cl spectra show similarities at room temperature.

A large Rayleigh wing in the Raman spectra masks all the lattice modes at RT indicating the disordered nature of the propylammonium ion [5,8]. The weak skeleton bending $(\delta(CCCN))$ mode appears around 446 cm^{-1} after the wing followed by the strong stretching $(\nu(CC)$ and $\nu(CN))$ modes at 876 and 1050 cm^{-1} respectively. It is observed that $\nu(CN)$ is stronger than $\nu(CC)$ in C_3Cl. These modes are broader in this phase and become much sharper at lower temperatures.

The modes involving hydrogen atoms could be assigned with the help of previous studies [17]. In the stretching mode region, (2800-3400 cm^{-1}) IR spectra form a broad structure involving many modes. However, in the Raman spectra the same is

very complex. NH_3 stretching modes $\cong 3000$ cm^{-1} are very broad and weak. Other CH_3, CH_2 stretching and bending modes are identified (see Table 5.3).

Di(Propylammonium) Tetrachlorocadmate

The room temperature Raman spectra of C_3CdCl in different polarization geometries alongwith the IR spectra are shown in Fig 5.2. The crystals of C_3CdCl are very thin and soft making it difficult to handle. Typical size of the crystal used for the purpose is about $2 \times 2 \times 0.5$ mm^3. The polarization dependence has been recorded by exciting the sample with 514.5 nm Ar$^+$ laser line using a power of 60 mW and other recording conditions are similar to the one described in § 2.2.

The spectra below 300 cm^{-1} could be compared well with the previous reports [5]. The spectra corresponding to A_g species are well resolved and stronger while that in B_{ig} (i = 1,2,3) are weak and broad corroborating the earlier reports [5]. In Table 5.4, the Raman and IR modes observed in the present study are noted. A brief description of the modes are given in the following paragraphs.

All the A_g modes occurring because of $CdCl_6$ octahedra and the external modes of the propylammonium ions occur below 300 cm^{-1}. From Table 5.2, it is clear that there are six A_g modes, of which two and one each are internal and librational modes of $CdCl_6$, respectively. By comparing the modes with

C_1CdCl (see § 3.3.1) and C_2CdCl (see § 4.3), the band at 207 cm^{-1} can unambiguously be assigned to $\nu(CdCl)$. The bending mode of it is found at 174 cm^{-1} in X(YY)Z polarization [5,19]. The other mode belong to the $CdCl_6$ octahedra which was found in α_{zz} polarization as very weak around 75 cm^{-1} has not been observed in the present study; however, this is observed as a shoulder to the mode around 94 cm^{-1} at lower temperatures. The same is observed around 74 cm^{-1} in α_{xx} geometry, in which the strong 94 cm^{-1} band is not present. Of the three remaining A_g modes, two and one are due to translational and librational of propylammonium ion (see Table 5.2). Following the earlier assignments, we attribute the mode at 94 cm^{-1} (in α_{zz}) to the translations of the propylammonium ion. Other translational mode at 110 cm^{-1} is clearly observed at lower temperature. The librational mode at 45 cm^{-1} is broader in α_{zz} geometry. The other broad mode at 280 cm^{-1} could be due to $\delta(CCC)$ [11].

The internal modes of propylammonium group are found above 400 cm^{-1} range. Most probable assignments are proposed in Table 5.4 by taking the help from other similar systems [6,11,20-22]. The lowest of it is the skeleton bending mode found around 450 cm^{-1} in both the Raman and IR spectra. The $\nu(CC)$ and $\nu(CN)$ are observed in all polarization geometries around 860 and 1045 cm^{-1} respectively. The IR component of $\nu(CC)$ at 864 cm^{-1} is comparably closer to the Raman frequency. The rocking modes of CH_2, NH_3 and CH_3 groups are found strong in IR at 755, 1010, 1185 cm^{-1}. Specially the mode at 1010 cm^{-1} is broader and the $\nu(CN)$ component is merged with it. Other

wagging and twisting modes are observed to be very weak.

The bending and stretching modes of $C_3H_7NH_3^+$ group are observed in both the Raman and IR spectra similar to the propylammonium chloride. $\delta(CH_3)$ and $\delta(NH_3)$ modes are weak in all polarization geometries around 1450 and 1580 cm^{-1} respectively and IR components at 1480 and 1590 are broader. As in the other members of the family, stretching modes form a broad band centered around 3100 cm^{-1} in IR spectra. The Raman counterparts of it form a complicated structure involving many bands. The fundamentals are identified and tabulated in Table 5.4. The stretching modes of NH_3 group are very weak and broad.

PHASE TRANSITIONS

5.4 RAMAN STUDY IN n-PROPYLAMMONIUM CHLORIDE

C_3Cl is known to undergo two transitions in 400-100 K range [7,8]. In the present study, we monitored a few thermosensitive internal modes across the two transitions. Polycrystalline sample of C_3Cl, obtained from Aldrich Co., is used without further purification. The experimental conditions are the same as described in § 2.2. The sample is excited with about 50 mW of 514.5 nm Ar^+ laser line.

5.4.1 Changes in Higher Temperature Side

On the basis of DSC studies, C_3Cl is known to undergo a transition at 385 K [7]. However, to the best of our knowledge there are no other studies at higher temperatures. To throw some light on this transition, a temperature dependent Raman study is carried out. Temperature evolution of the thermosensitive $\delta(CCCN)$, $\nu(CC)$ and $\nu(CN)$ modes are shown in Fig 5.3. All the three modes do not show any marked variations upto 382 K. These modes have become weaker above 382 K. The well resolved spectral lines completely disappeared and the spectra was replaced by an unusual background at 385 K. The spectrum could not be reproducible on lowering the temperature to 300 K. It is also observed that the irradiated portion of the sample turned yellow in colour. A repetitive effort with less ($\cong$ 20 mW) power resulted in similar variations. So these changes could be attributed to the thermal decomposition occurring well below the transition temperature.

5.4.2 Spectral Variations in Lower Temperature Side

The transition at 188 K in C_3Cl is probed in the present study. The crystallographic studies reveal the transition to be an order-disorder type where the propylammonium ions are being arranged anti-parallel to each other at lower temperatures [8]. A large entropy change further corroborates this fact [7].

The Raman spectra of C_3Cl in 40-3300 cm^{-1} range at 300 and 93 K are shown in Fig 5.4. A broad Rayleigh wing which masks the lattice modes at 300 K, reduced considerably at lower temperature. The lattice vibrations are clearly observed at 93 K. The broad internal modes considerably sharpen on lowering the temperature. The stretching mode region 2800-3200 cm^{-1} shows many bands with relatively complex structure. Two strong Raman bands at 874 and 1047 cm^{-1} at RT, assigned to $\nu(CC)$ and $\nu(CN)$ respectively [11,12], are chosen for the temperature dependence study in 90-300 K range. Typical thermal evolution of these two modes are shown in Fig 5.5. Spectral parameter variations of $\nu(CC)$ and $\nu(CN)$ modes are systematically plotted as a function of temperature in Fig 5.6 and Fig 5.7 respectively. The open and filled circles in these two plots are the observed behaviour during the warming and cooling cycles. The peak frequency of $\nu(CC)$ mode shows (Fig 5.6b) a small ($\cong 3cm^{-1}$) but systematic upward shift on lowering the temperature. A weaker component assigned to the gauche conformer [12] of propylammonium ion is observed at 864 cm^{-1} in the ordered phase (see Fig 5.5). Additionally, $\nu(CN)$ mode which is a singlet at room temperature, splits into two components at about 188 K (see Fig 5.5). The two components of $\nu(CN)$ mode are deconvoluted according to the procedure described in § 2.4.3. The normalized reduced peak intensity (I_p) and linewidth of the stronger component (1048 cm^{-1} at 90 K) are plotted as a function of temperature in Fig 5.7a and c respectively. The linewidth of

these two modes show a very weak temperature dependence in the ordered state (see Fig 5.6c and Fig 5.7c). The linewidth ν(CC) mode as depicted in Fig 5.6c shows a discontinuous jump around 188 K, corroborating the transition. Most interesting changes are observed in the reduced peak intensities (I_p), of these modes (see Fig 5.6a and Fig 5.7a). I_p of ν(CC) and ν(CN) modes remain essentially constant till 188 K and increase sharply below this temperature. This anomalous variation of I_p in the ordered state have been attributed to the long range order. All these variations are reproducible without any measurable hysteresis.

5.4.3 DISCUSSION

In room temperature phase, the propylammonium (cations) ions are situated along c-axis (height) of the unit cell, while the chloride (anions) ions lie in ab-plane. Polar NH_3 ends of the successive cations point in opposite directions. To fulfill the tetragonal symmetry, the cations should show the orientational disorder [8]. On lowering the temperature this orientational disorder freezes gradually between 193-183 K. At lower temperature the cationic motion is arrested [8]. However, CH_3 and NH_3 group rotations are possible in the monoclinic phase [15].

The intensity of a mode which is allowed in the ordered state only, shows a diminution ($\propto \eta$) on approaching the

transition temperature. Other kind of modes which themselves are not directly involved in the transition (called the hard modes) and may have activity because of the disorder, also show interesting variations with the temperature. Deep in the ordered state, the Raman intensity of such modes is governed by the long range interactions. As the temperature approaches T_c, the order-disorder transition temperature, the intensity of such modes decreases and is proportional to η^2. On the other hand, the linewidth is linearly dependent on temperature indicating weak anharmonic forces in the crystal (see § 1.7).

The temperature dependence of the Raman intensities of two modes (i.e., $\nu(CC)$ and $\nu(CN)$) clearly show a dramatic variation in 80-186 K range (see Fig 5.6a and 5.7a). In these two plots, the reduced peak intensity $I_p = [\omega_{op}/(n(\omega)+1)] I_{op}$ is plotted as a function of temperature; here ω_{op} and I_{op} are peak frequency and intensity respectively. According to the hard mode theory (see § 1.7) the rate at which I_p decreases in the ordered state is mainly due to long range interactions and is proportional to η^2. Here, the variations in the reduced peak intensity instead of the total intensity are taken into consideration so that the dispersion effects would be minimized. Further, the validity of this assumption is demonstrated by a weak temperature dependence (in the range 90-186 K) of the linewidths of these modes. To verify this behaviour, a log-log graph of intensity changes against (T_c-T), with $T_c = 188$ K, is plotted in 90-186 K range. The plots are shown as insets in Fig 5.6 and Fig 5.7. A straight line is fitted through the

experimental points considering 2 K and 15 % uncertainties in measured temperature and intensity values respectively (using the least square fit method described in § 3.5.4). The best line is the one with slopes ($\cong 2\beta$) 0.70 ± 0.09 and 0.70 ± 0.07 respectively. This value of β ($\cong$ 0.35 ± 0.04) is significantly different from the mean field exponent, but is comparably closer to that observed in similar systems. Evidently, the linewidth of these modes (see Fig 5.6c and 5.7c) monotonically increase in the temperature range 90-186 K, giving a slope of 0.04 $cm^{-1}T^{-1}$. This shows the presence of weak anharmonicity in the crystal.

The band at 864 cm^{-1} in low temperature spectra could be due to gauche conformer. Absence of this mode at room temperature indicates negligible gauche population [12,15]. This mode however, gains intensity on decreasing the temperature. The relative intensity of this mode with respect to 877 cm^{-1} is 0.2, indicating a considerable gauche population at lower temperature.

5.5 TEMPERATURE DEPENDENT STUDY IN C_3CdCl

At room temperature, C_3CdCl belongs to the space group (D_{2h}^{18}) and undergoes three transitions at 183, 158 and 113 K in the sub-ambient temperatures. These were studied in past using x-rays in great detail [3,4]. The Raman study was in the lower frequency (< 350 cm^{-1}) region only [5]. No detailed temperature

dependent IR studies are available in literature [6]. We mainly concentrated on the temperature variations in a few internal modes to compare the changes with C_2CdCl.

5.5.1 Changes in the Raman Spectra

The Raman spectra of C_3CdCl in different phases are shown in $X(ZZ)Y$ and $X(YY)Z$ polarization geometries in Fig 5.8a and b, respectively. These spectra are recorded in two different experiments using a power of 65 and 50 mW (at the sample). There are no appreciable changes in $X(ZZ)Y$ geometry on decreasing the temperature. The broad $\delta(CCC)$ mode around 278 cm^{-1} became sharper. The two broad and weak peaks around 76, 110 cm^{-1} corresponding to librational modes of the $CdCl_6$ octahedra and $C_3H_7NH_3^+$ respectively, are observed clearly as shoulder to the translational mode of the organic ion. In Fig 5.9, the recorded portions in 128-288 K range of $\delta(CCCN)$ and $\nu(CC)$ modes in $X(ZZ)Y$ polarization are shown. Systematic plot of the frequency and the linewidth variations are shown in Fig 5.10. Open and closed symbols in this figure represent the observed variation in cooling and warming cycles. The true Lorentzian width are estimated (slit width 1.5 cm^{-1}) by the procedure described in § 2.4.2. There are no anomalous variations in this geometry near the reported transition regions of 183 and 158 K.

From Fig 5.8b, it is evident that modes in the internal modes in $X(YY)Z$ polarization geometry show very

marginal changes. The ν(CN) mode became relatively stronger (to ν(CC)) at lower temperatures. However, this change is gradual and does not show any anomalous variation similar to that observed in propylammonium chloride (see § 5.4.1). So, it is rather difficult to attribute this variation due to an order-disorder transition. Significantly, in the stretching mode region many bands appear at lower temperature. The temperature dependent study is extended to the mode at 174 cm^{-1} (which is assigned as librational mode of propylammonium ion) to throw light on the order-disorder transition. In Fig 5.11, spectral variations for this mode are shown. Temperature evolution of the spectral parameters are plotted in Fig 5.12. The shoulder peak around 174 cm^{-1} became sharper and is clearly observed at lower temperatures. The ν(CdCl) mode around 208 cm^{-1} does not show any remarkable variations with temperature.

5.5.2 Changes in Infrared Spectra

IR spectra of C_3CdCl at four different temperatures are shown in Fig 5.13. At lower temperature, many bands split and became sharp. To understand the variations near the reported transitions, IR spectra in 700-1120 cm^{-1} range have been monitored continuously. Typical variations in this region are shown in Fig 5.14. The ρ(CH_2) at 755 cm^{-1} and ν(CC) at 865 cm^{-1} modes show marginal changes till 120 K. However, these two modes split into two each at about 111 K which is close to the reported ORT-MLT transition. The parameters of ρ(CH_2) mode are

plotted in Fig 5.15. Similar splitting is also observed in $\rho(NH_3)$ mode.

The another mode which shows interesting variations is in 1750-2000 cm^{-1} range, which is due to $\delta_{asy}(NH_3) + \tau(NH_3)$. Thermal evolution in recorded spectra is shown in Fig 5.16 and its spectral parameters are depicted in Fig 5.17. Near 158 K this mode abruptly jumps by about 20 cm^{-1} to higher frequency and becomes sharper and stronger. These variations are similar to that of C_1CdCl (see § 3.4.1) and C_2CdCl (see § 4.5).

5.5.3 Discussion

The phase transitions in this compound have been attributed to the reorientational motion of propylammonium ions [4,5]. The lower temperature phase sequence i.e., $D_{2h}^{18} \rightarrow (INC)D_{2h}^{18} \rightarrow D_{2h}^{15} \rightarrow$ monoclinic is significantly different from the corresponding Mn salts. Specially, the transition to $D_{2h}^{18} \rightarrow D_{2h}^{15}$ could be compared with C_2CdCl [5,23]. The knowledge in C_2CdCl can be used to deduce the information regarding the transitions. Previous Raman data assign the transition at 158 K to an order-disorder type [5]. A careful comparison of the spectral variations with C_2CdCl suggest the following.

Changes Through the Transition at 158 K

A clear manifestation of the disorder in ethylammonium ions in C_2CdCl was observed through rocking and skeleton streching modes

in both IR and Raman (see § 4.5). However, from Fig 5.10a and d, it is clearly seen that the frequency and the linewidths of $\nu(CC)$ mode of C_3CdCl in $X(ZZ)Y$ geometry do not show similar changes. Moreover, the linewidth of $\nu(CC)$ varies linearly in 133-300 K range. Interestingly, another skeleton mode $(\delta(CCCN))$ also shows variations similar to $\nu(CC)$. From these observations it is concluded that the skeleton may not have the impact of the disorder. Another possible origin of the transition is due to the interaction of hydrogen atoms in the crystal. In that case it is expected that the rocking modes should vary drastically [6]. Indeed, the rocking modes show drastic variations in 140-220 K range. Specially, $\rho(CH_2)$ mode becomes sharper (see Fig 5.15a). This variation is spread over a wide range covering Tc_1 and Tc_2 i.e., 200-133 K. A trial fit to the eqn 4.2 gives the activation energy of 0.03 eV. However, the NMR gives the value to be 0.08 eV, which is significantly different from the present study [24]. $\rho(NH_3)$ mode which is broader at 300 K becomes sharper and contains many components at lower temperatures. In MLT phase it consists of at least five components corroborating the previous report [6].

The Raman spectra in both $X(YY)Z$ and $X(ZZ)Y$ geometries are studied by varying the temperature in order to detect the spectral variations during the order-disorder transition. From Fig 5.11 no anomalies are observed for the mode at 174 cm^{-1}. This mode which has been mainly assigned to librations of propylammonium group, is expected to show drastic variation near the order-disorder transition [19]. However, the linewidth

changes can be well understood in terms of anharmonicity effects (see § 1.7). These facts corroborate the fact that the orientational changes are not playing a significant role in the transition at 158 K. Surprisingly, the spectra at lower temperatures became weaker. However, as the two transitions (183 and 158 K) are very close, such variations cannot be attributed due to the incommensurate phase [25,26]. A sharp decrease in the Rayleigh wing around 160 K is corroborated by the present study [5].

In the IR spectra the combination mode of $\delta_{asy}(NH_3)$ + $\tau(NH_3)$ around 1850 cm^{-1} at RT, shows a very sharp jump of about 20 cm^{-1} near 158 K, indicating the transition (see Fig 5.17). This change is similar to that occurring in C_1CdCl (see § 3.4.1) and in C_2CdCl (see § 4.5). Further, from the Raman spectra the modes belong to NH_3 group also show a downward shift (see Fig 5.8) indicating the variation in H-bond strength. A detailed investigation using the deuterated analogue of C_3CdCl could provide useful information regarding the transition at 158 K.

Changes at 113 K

The transition at 113 K produces many drastic variations in both the Raman and IR spectra. Crystalline samples used in the present study are observed to become powder below 113 K. Many lattice modes appear out of the broad Rayleigh wing. Interestingly, $\nu(CC)$ mode splits into two in both the Raman and IR at about 111 K. Similar kind of splitting has been observed

in many modes including $\rho(CH_2)$ and $\rho(NH_3)$ (see Figs 5.14-5.16). The observations corroborate the transition at 113 ± 2 K [3-6].

5.6 CONCLUSIONS

The Raman spectroscopic study of C_3Cl reveal the transition at 188 ± 2 K, to be an order-disorder type. Anomalous increase in the Raman intensity of $\nu(CC)$ and $\nu(CN)$ modes show the dominance of long-range interactions in the ordered state. Absence of hysteresis and the value of the order parameter exponent (β) 0.35 ± 0.04 confirm the second order nature of the transition in C_3Cl around 188 K.

A clear spectral variations in $C_3H_7NH_3^+$ modes of C_3CdCl suggest that the transition at 158 K is mainly due to a change in the hydrogen bonding scheme. The splitting in the spectral lines of many modes indicates the transition at 113 K.

REFERENCES

1. W Depmeier, J. Solid St Chem., **29**, 15 (1979).

2. MA White, VM Granville, NJ Davies and LAK Staveley, J. Phys Chem Solids, **42**, 951 (1981).

3. G Chapuis, Acta Cryst., **34B**, 1506 (1978).

4. B Doudin and G Chapuis, Acta Cryst., **44B**, 495 (1988).

5. R Mokhlisse, M Couzi, NB Chanh, Y Haget, C Hauw and A Meresse, J. Phys Chem Solids, **46**, 187 (1985).

6. W Dipmeier and IA Oxton, J. Mol Struct., **77**, 91 (1981).

7. J Tasu and DFR Gilson, J. Phys. Chem. **72**, 4082 (1968).

8. MV King and WN Lipscomb, Acta. Cryst., **3**, 222, 227 (1950).

9. RWG Wyckoff, "Crystal structures" Interscience pub., New York, **1**, 134 (1963).

10. JR Ferraro and JS Ziornek, "Int. Group Theory and its App. to Molecular Struct." Plenum press, New York., **chap.2**, (1975).

11. JR Durig, WB Beshir, SE Godbey and TJ Hizer, J. Raman Spectrosc. **20**, 311 (1989).

12. H Hagemann, H Bill and J Mareda, J. Mol. Struct. **127**, 241 (1985).

13. E Whalle and JE Bertie, J. Chem Phys., **46**, 1264, 1271 (1967).

14. JM Loveluck and JB Sokoloff, J. Phys Chem Solids, **34**, 869 (1973).

15. S Albert and JA Ripmeester, J. Chem. Phys. **69**, 3967 (1978).

16. J Tasu and DFR Gilson, Can. J. Chem. **51**, 1990 (1973).

17. H Hagemann and H Bill, J. Chem Phys., **80**, 111 (1984).

18. PSR Prasad and HD Bist, Solid St Commu., **00**, 000 (1990).

19. H Hagemann and H Bill, J. Phys., **18C**, 6441 (1985).

20. A Ban Salah and A Daoud, J. Solid St Chem., **65**, 151 (1984).

21. DM Adams and DC Stevens, J. Phys., **11C**, 617 (1978).

22. L Ricard, R Cavagnat and MR Lafon, J. Phy Chem., **89**, 4887 (1985).

23. PSR Prasad and HD Bist, Phys. Stat. Sol., **116a**, 275 (1989).

24. R Blinc, M Burger, B Lozar, J Seliger, J Slak, V Rutar, H Arend and R Kind, J. Chem Phys., **66**, 278 (1977).

25. M Pal, A Agarwal, DP Hhandelwal and HD Bist, J Raman Spectrosc., **17**, 345 (1986).

26. RM Pick in "Recent Trends in Raman Spectroscopy" Ed SB Banerjee and SS Jha, World Scientific, Singapore, (1989).

TABLE 5.1 Classification of modes of $C_3H_7NH_3^+$ ion under point group symmetry of C_s.

C_s	E	σ	n(vib)	n(tr)	n(rot)	Raman	IR
A'	1	1	21	2	1	A	A
A"	1	-1	15	1	2	A	A
ω_R	14	6					
ϕ	0	0					

TABLE 5.2 Factor group analysis of $(C_3H_7NH_3)_2CdCl_4$ crystal in ORT and OLT phases.

(a) Orthorhombic Room Temperature (ORT) phase (D_{2h}^{18}; Z = 2)

i. $C_3H_7NH_3^+$
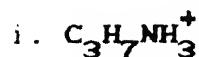
				SYMMETRY				
	Free ion			Site	Factor			
Modes							Modes	
T	R	V	C_s	C_s	D_{2h}^{18}	V	R	T
					A_g	21	1	2
					B_{2g}	21	1	2
2	1	21	A' —	A'	B_{1u}	21	1	2
					B_{3u}	21	1	2
					B_{1g}	15	2	1
					B_{3g}	15	2	1
1	2	15	A'' —	A''	A_u	15	2	1
					B_{2u}	15	2	1

ii. $CdCl_4^{-2}$
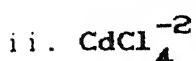
T	R	V	D_{4h}	C_{2h}	D_{2h}^{18}	V	R	T
0	0	1	A_{1g}					
0	0	1	B_{2g}		A_g	2	1	0
0	1	0	E_g	A_g	B_{3g}	2	1	0
0	1	0	A_{2g}	B_g	B_{1g}	1	2	0
0	0	1	B_{1g}		B_{2g}	1	2	0
1	0	2	E_u	A_u	A_u	2	0	1
					B_{3u}	2	0	1
1	0	1	A_{2u}	B_u	B_{1u}	4	0	2
0	0	1	B_{1u}		B_{2u}	4	0	2

(b) Orthorhombic Low Temperature (OLT) phase $(D_{2h}^{15}; Z = 4)$

i. $C_3H_7NH_3^+$
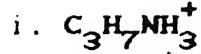
S Y M M E T R Y

			Free ion	Site	Factor			
Modes							Modes	
T	R	V	C_s	C_1	D_{2h}^{15}	V	R	T
2	1	21	A'		A_g	36	3	3
					B_{1g}	36	3	3
					B_{2g}	36	3	3
				A	B_{3g}	36	3	3
					A_u	36	3	3
					B_{1u}	36	3	3
					B_{2u}	36	3	3
1	2	15	A''		B_{3u}	36	3	3

ii. $CdCl_4^{-2}$

T	R	V	D_{4h}	C_i	D_{2h}^{15}	V	R	T
0	0	1	A_{1g}					
0	1	0	A_{2g}		A_g	3	3	0
0	0	1	B_{1g}	A_g	B_{1g}	3	3	0
0	0	1	B_{2g}		B_{2g}	3	3	0
0	1	0	E_g		B_{3g}	3	3	0
					A_u	6	0	3
1	0	1	A_{2u}		B_{1u}	6	0	3
0	0	1	B_{1u}	A_u	B_{2u}	6	0	3
1	0	2	E_u		B_{3u}	6	0	3

TABLE 5.3 Observed Raman and infrared band positions of
$C_3H_7NH_3Cl$ in different temperatures.

RAMAN 300 K	RAMAN 93 K	INFRARED 300 K	Assignment
--	3138 b	a	
3070 b,sh	3038 b,sh	a	$\nu_{as}(NH_3)$
2980 s	2972 vs	a	$\nu_{as}(CH_3)$
2924 vs	2920 s	a	$\nu(CH_2)$
--	2900 s	a	
--	2886 sh	a	$\nu_{sy}(CH_3)$
1550 w	1556 w	1571 vs	$\delta(NH_3)$
--	--	1511 vs	
1472 sh	1480 w	1476 vw	$\delta_{as}(CH_3)$
--	1464 m	--	
1454 m	1460 sh	1461 vw	$\delta_{sy}(CH_3)$
--	1452 vw	1421 vw	$\delta_{as}(CH_2)$
1386 vw	1388 vw	1398 w	$\omega(CH_2)$
1318 m	1313 m	1326 vw	$\gamma(CH_2)$
1290 sh	1284 vw	1296 vw	$\rho(CH_3)$
1186 w	1191 vw	1191 m	
1050 vs	1052 s	1051 sh	$\nu(CN)$
--	1046 sh	1041 sh	
998 w	996 w	996 m	$\rho(NH_3)$
876 s	876 bs	868 bw	$\nu(CC)$
--	862 vw	--	
--	--	761 w	$\rho(CH_2)$
446 w	440 vw	456 w	$\delta(CCCN)$
--	316 vw	--	$\delta(CCC)$
256 b	290 vw	--	
--	202 vw	--	
156 sh	184 vw	--	
--	116 vw	--	

a = A part of the broad band, b = Broad, m = Medium, s = Strong,
sh = Shoulder, v = Very, w = Weak. ν = Stretch, δ = Bend,
ρ = Rock, ω = Wagg and γ = Twist.

TABLE 5.4 Observed band positions (cm^{-1}) of $(C_3H_7NH_3)_2CdCl_4$ crystal at 300 K.

A_g			B_{1g}	B_{2g}	B_{3g}		
α_{xx}	α_{yy}	α_{zz}	α_{xy}	α_{xz}	α_{yz}	Infrared	Assignment
3170 w	3164 w	3180 vw	3170 vw	--	3166 vw	a	$\nu_{as}(NH_3)$
3100 vw	3082 w	--	--	--	--	a	$\nu_s(NH_3)$
2970 s	2968 vs	2967 vs	2971 s	2966 vs	2976 vs	a	$\nu(CH_3)$
2933 vs	2936 vs	2932 s	2931 s	2938 vs	2936 vs	a	$\nu(CH_2)$
2876 s	2876 s	2873 s	2876 m	2870 s	2874 m	2800	$\nu(CH_3)$
2780 vw	2784 vw	--	2784 vw	--	--	--	
2738 vw	--	--	2738 vw	--	--	2690	
1576 vw	1584 vw	1584 vw	1574 vw	--	1576 vw	1590 b	$\delta_{as}(NH_3)$
1450 vw	1456 w	1449 w	1450 w	1446 m	1455 m	1480 b	$\delta_{as}(CH_3)$
--	--	--	--	--	--	1407 sh	$\gamma(CH_2)$
1332 vw	--	1335 vw	1332 w	1330 vw	1336 vw	1330 m	$\omega(CH_2)$
--	1294 vw	1290 vw	1286 vw	--	--	1302 m	
1176 vw	--	1173 vw	1168 vw	1176 vw	1179 vw	1185 s	$\rho(CH_3)$
--	--	--	--	--	--	1010 s,b	$\rho(CH_2)$, $\nu(CN)$
1044 vw	1045 w	1044 s	1040 vs	1045 s	1042 s	--	$\nu(CN)$
862 w	861 w	861 vs	861 vs	860 s	861 vs	864 w	$\nu(CC)$
--	--	--	--	--	--	755 s	$\rho(CH_2)$
449 vw	--	447 m	450 m	447 w	448 w	447 s	$\delta(CCCN)$
266 b	--	284 b	270 b	260 b	262 b	285	$\delta(CCC)$
207 m	208 m	210 m	213 m	210 s	205 m	--	$\nu(CdCl)$
--	174 sh	--	--	--	--	185	$\delta(CdCl)$
--	--	90 vs	91 s	90 s	--	--	T(A)
74 sh	--	--	--	--	74 sh		R(CdCl)
--	--	48 vb	--	50 sh	--	--	R(A)

Abbreviations used are a = A part of the broad band, b = Broad, m= Medium, s = Strong, sh = Shoulder, v = Very, w = Weak. ν = Stretch, δ = Bend, ρ = Rock, τ = Torsion, ω = Wagg, γ = Twist, R= Librational, T = Translational and A = $C_3H_7NH_3^+$.
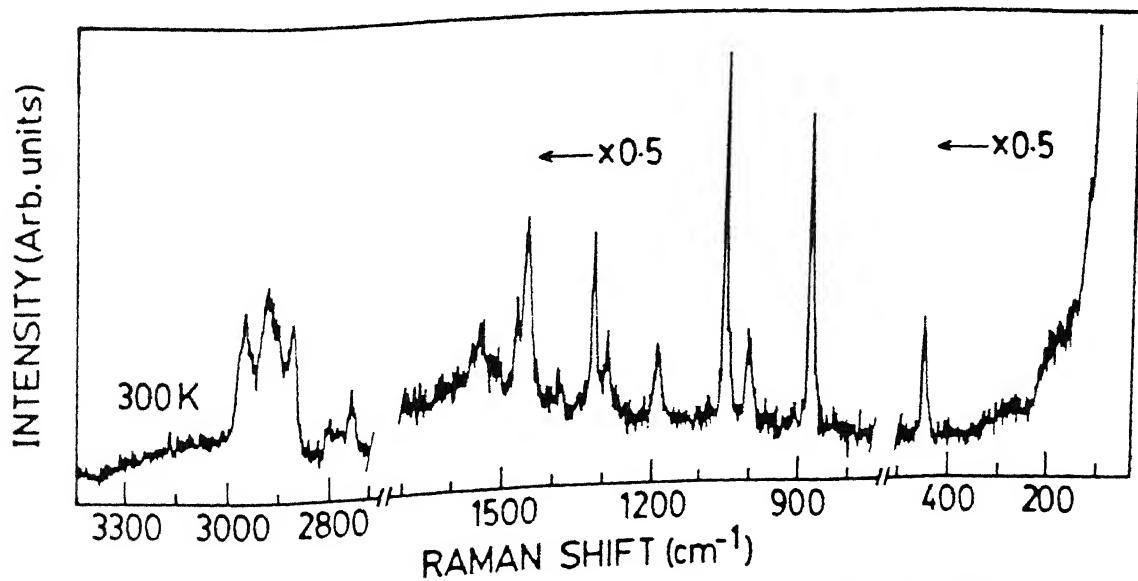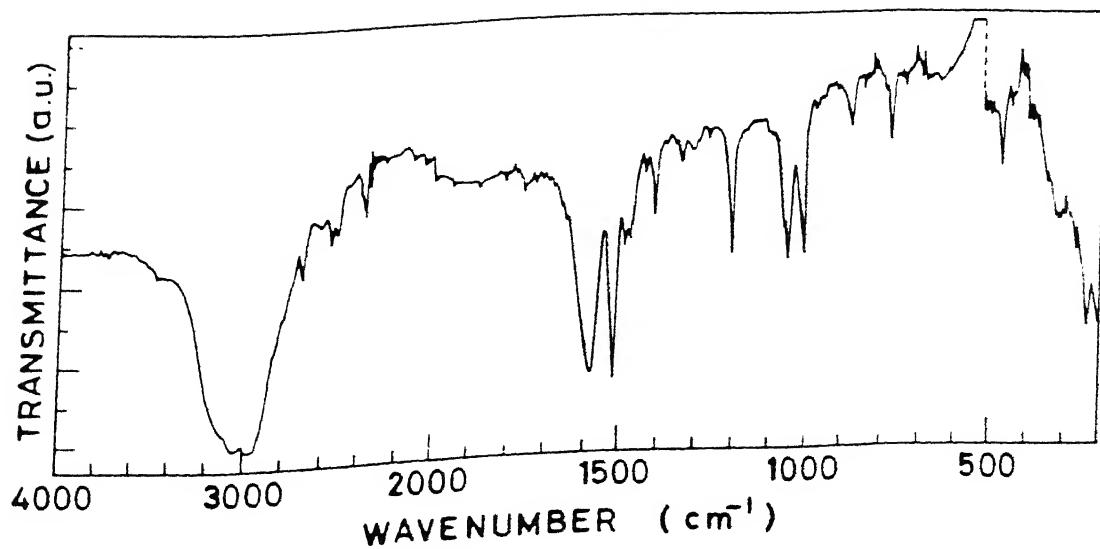
Fig 5.1 The Raman and infrared spectra of C_3Cl at 300 K.
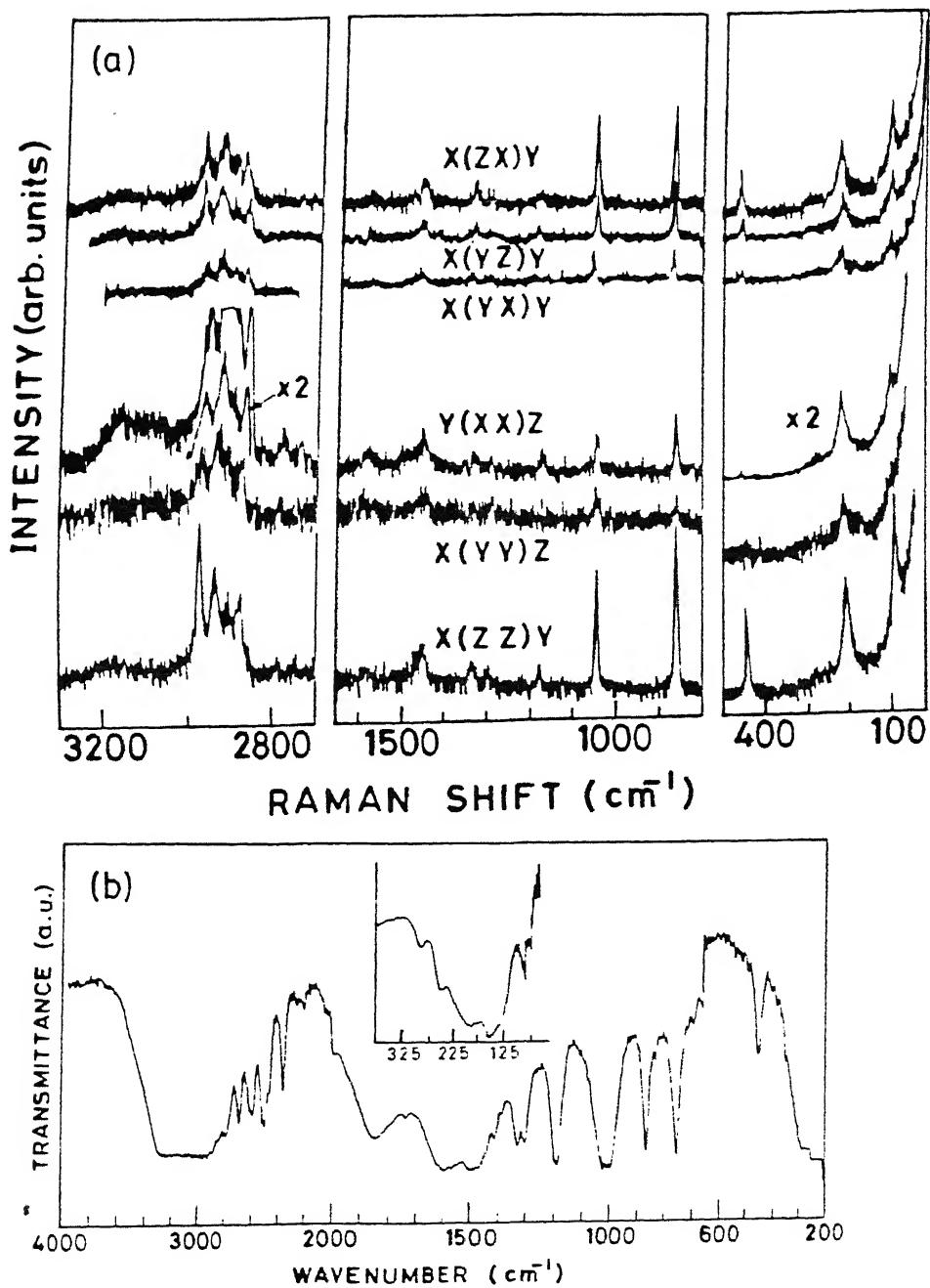
Fig 5.2 Single crystal (a) Raman and (b) IR spectra of C_3CdCl at 300 K.

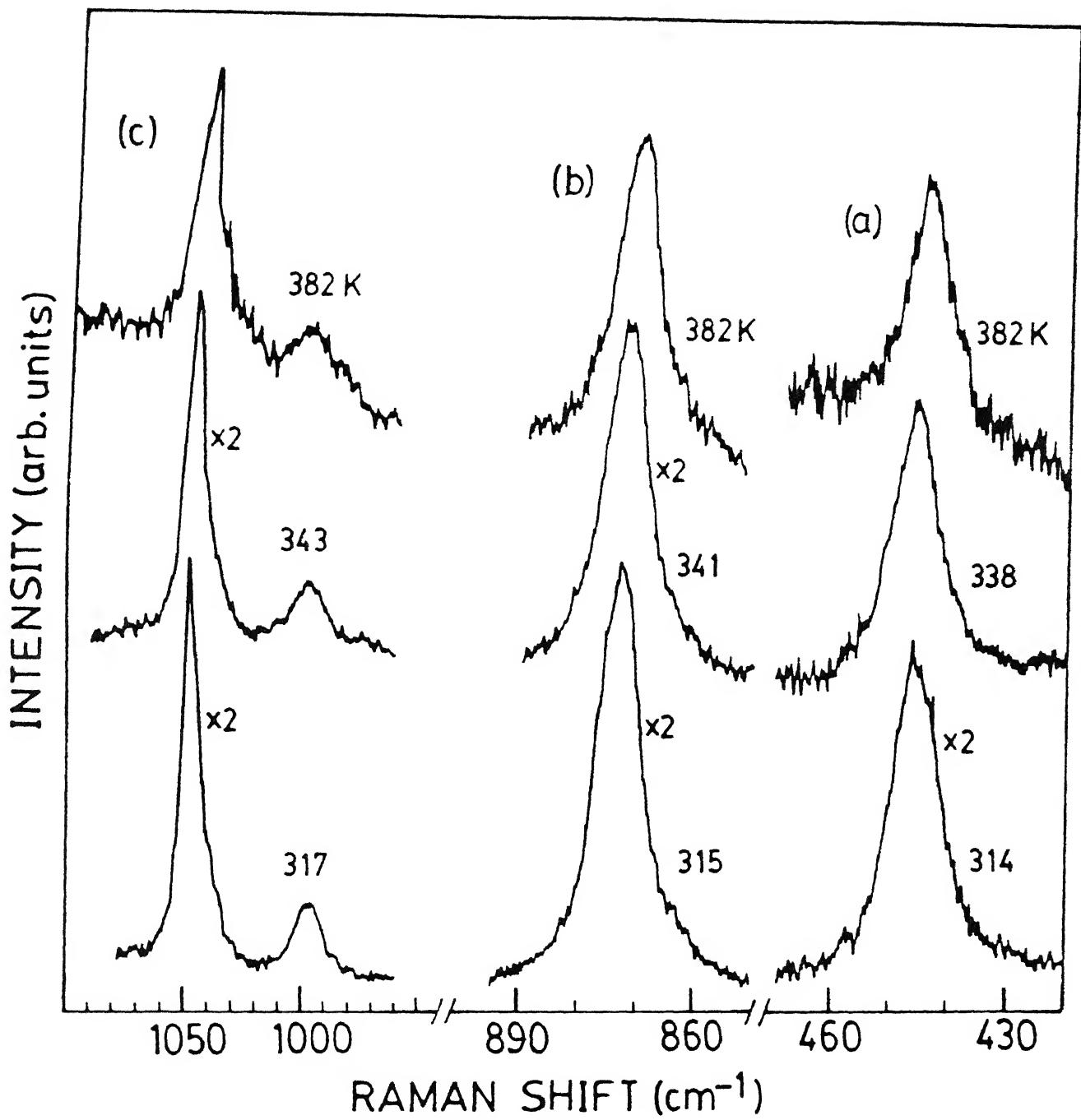Fig 5.3 Thermal evolution of (a) $\delta(CCCN)$, (b) $\nu(CC)$ and (c) $\nu(CN)$ modes of C_3Cl.
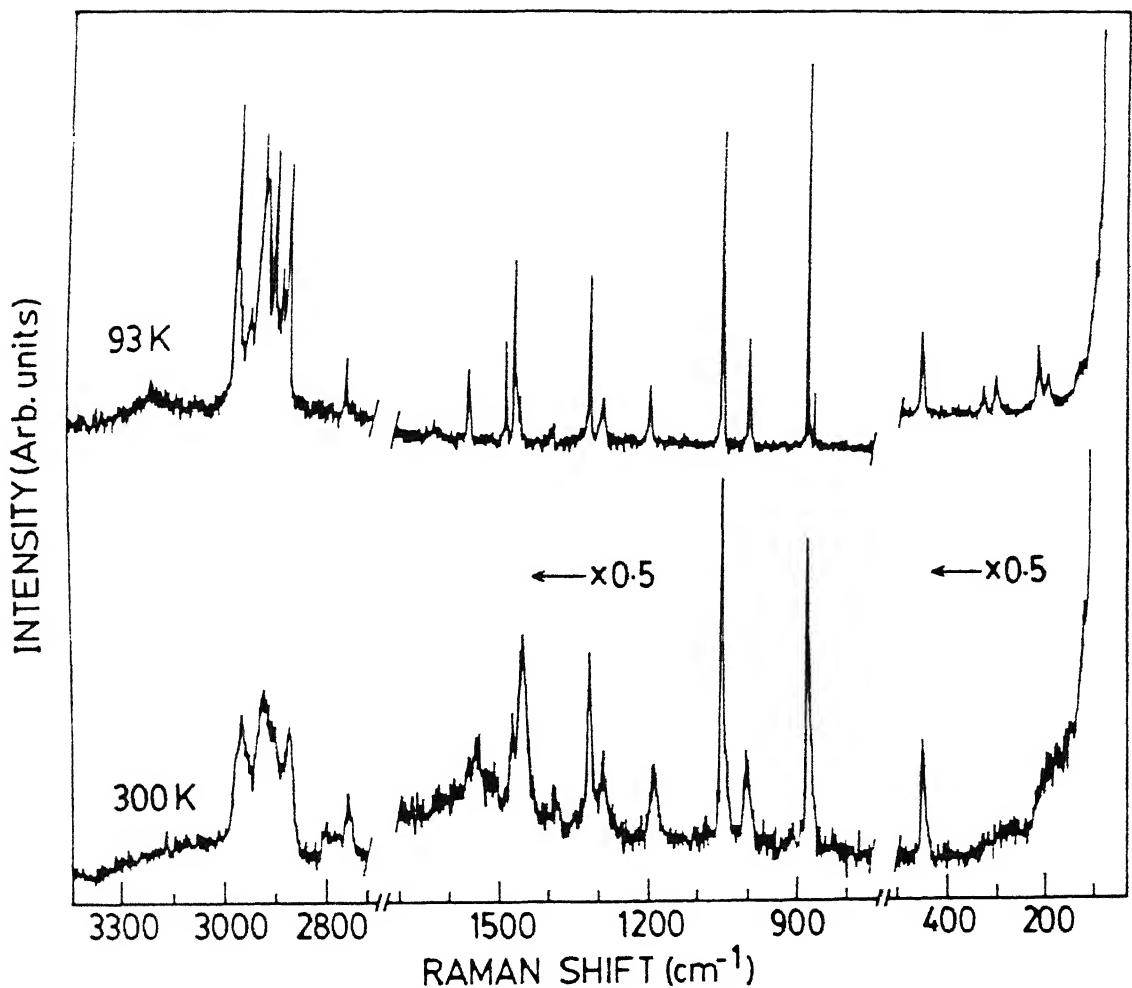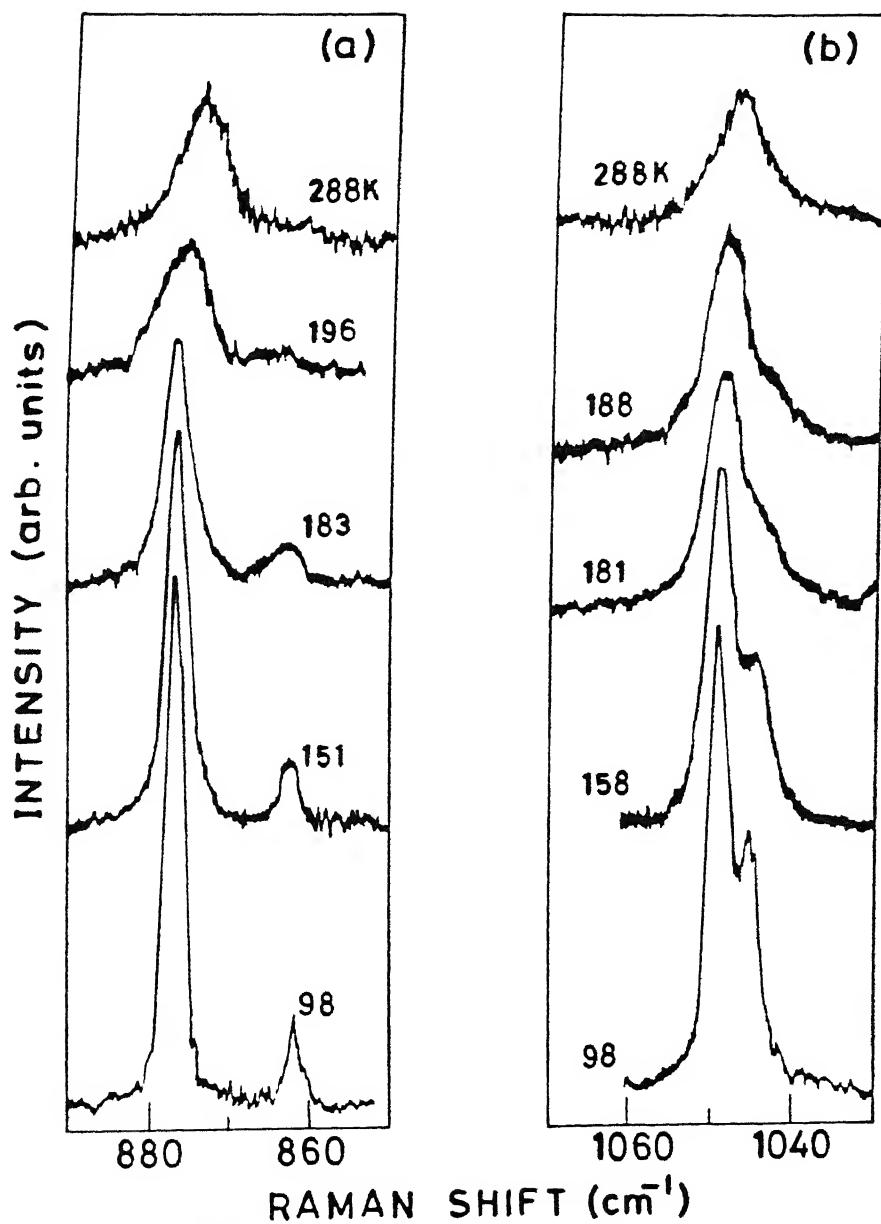
Fig 5.4 The Raman spectra of C_3Cl at 93 and 300 K.

Fig 5.5 Thermal evolution of (a) $\nu(CC)$ and (b) $\nu(CN)$ mode regions in C_3Cl.

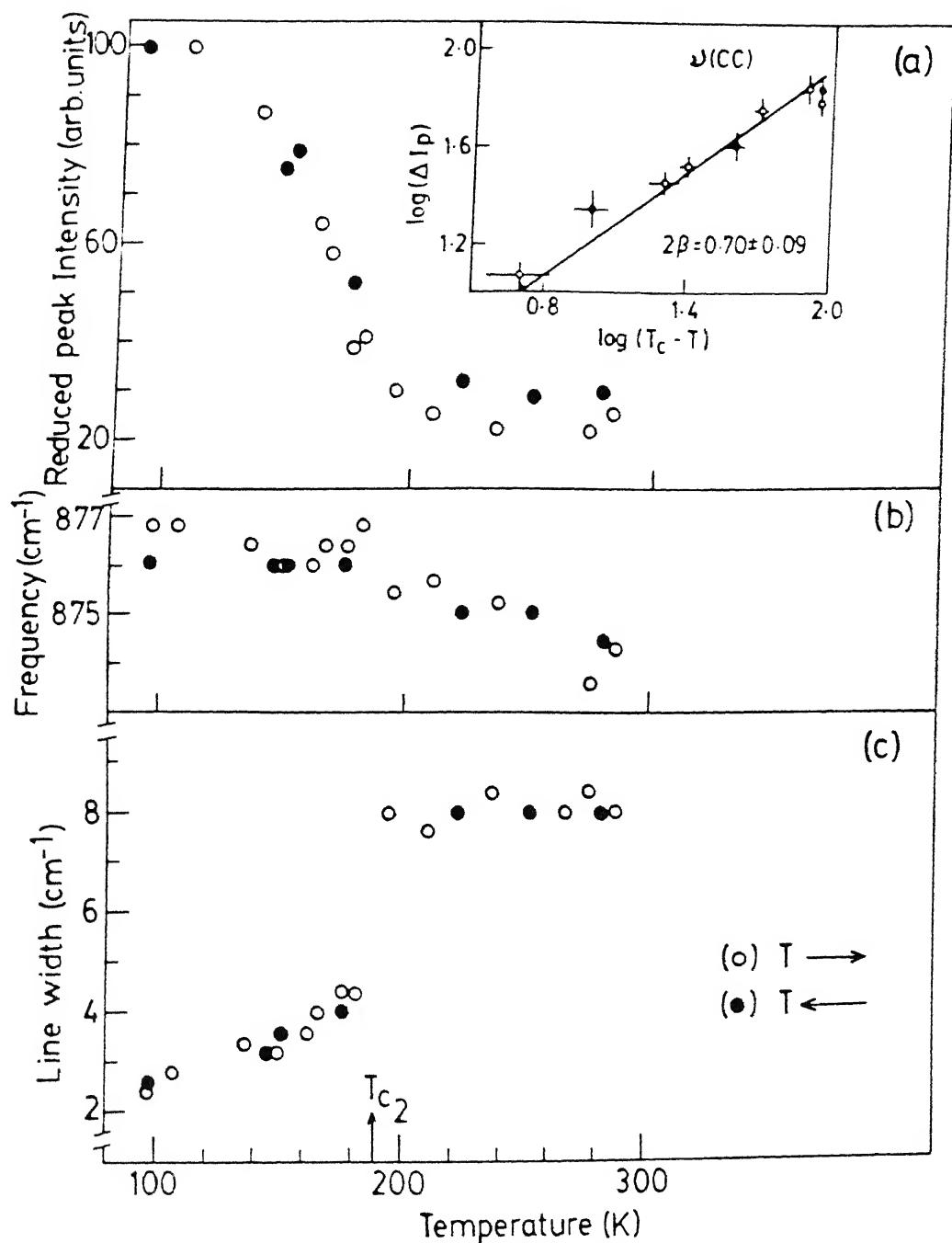Fig 5.6 Temperature dependence of (a) reduced peak intensity I_p, (b) peak frequency and (c) linewidth of $\nu(CC)$ mode of C_3Cl. Inset depicts the logarithmic variation of (ΔI_p) vs $(T_c - T)$.
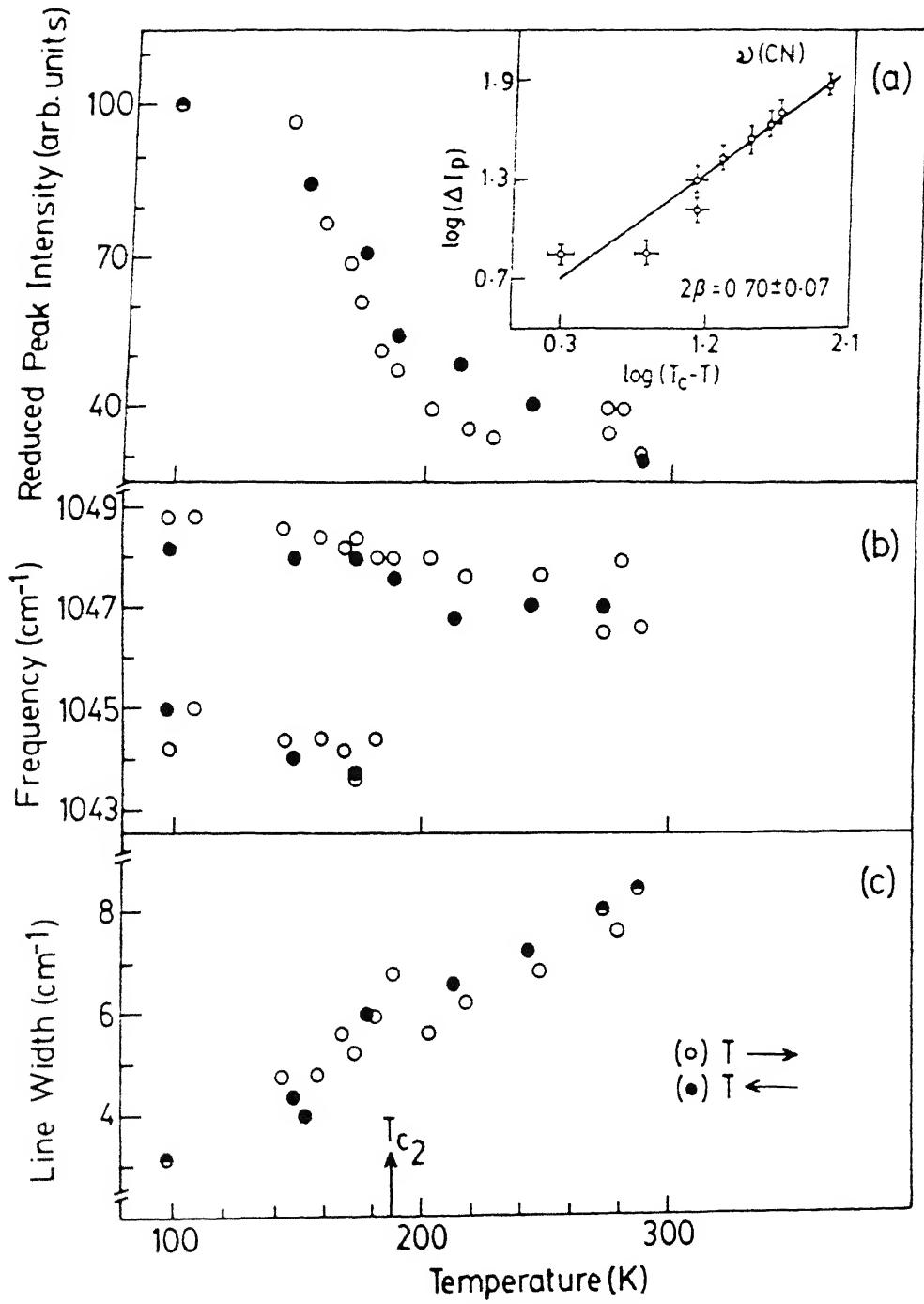
Fig 5.7 (a) Reduced peak intensity I_p, (b) peak frequency and (c) linewidth variations of $\nu(CN)$ mode of C_3Cl with temperature. Inset shows a plot of $\log(\Delta I_p)$ vs (T_c-T).
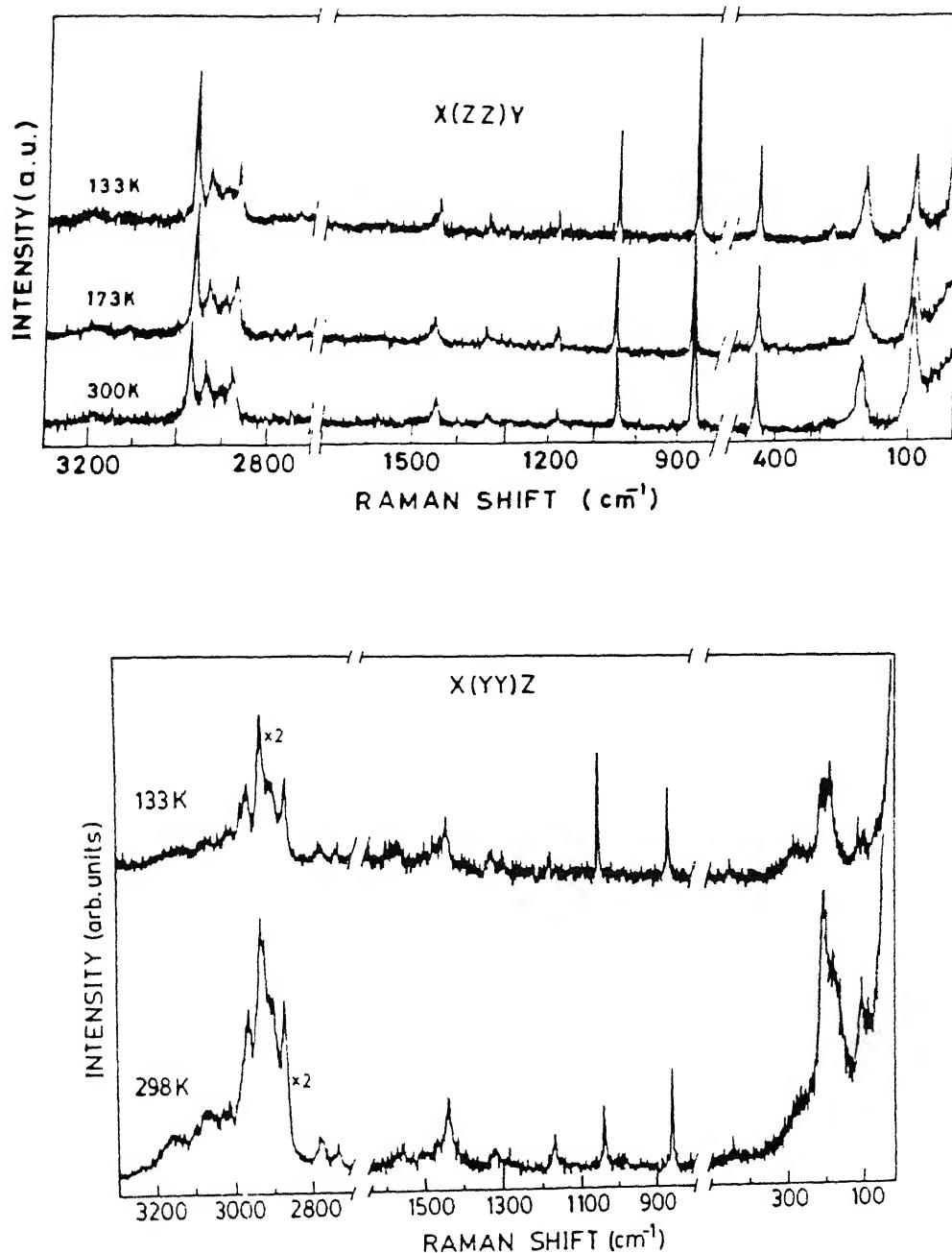
Fig 5.8 Temperature dependent Raman spectra of C_3CdCl in X(ZZ)Y and X(YY)Z polarization geometries.
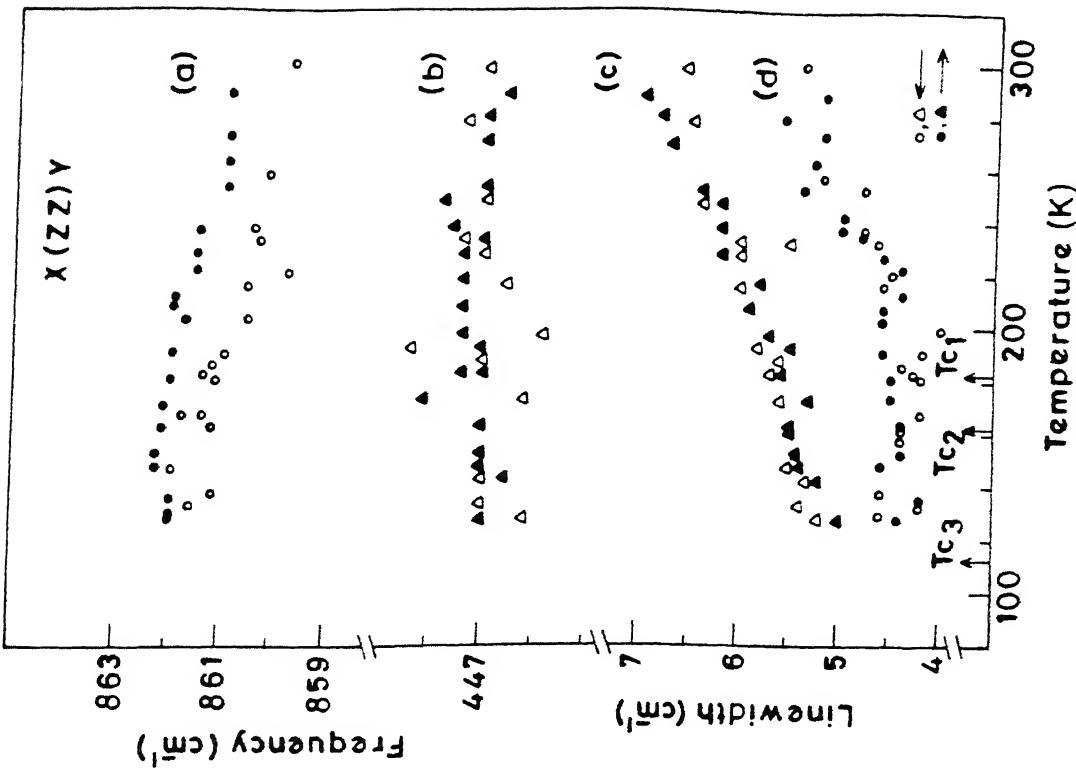
Fig 5.10 Temperature dependence of peak frequency (a,b) and linewidth (d,c) for $\delta(CCCN)$ and $\nu(CC)$ modes of C_3CdCl.
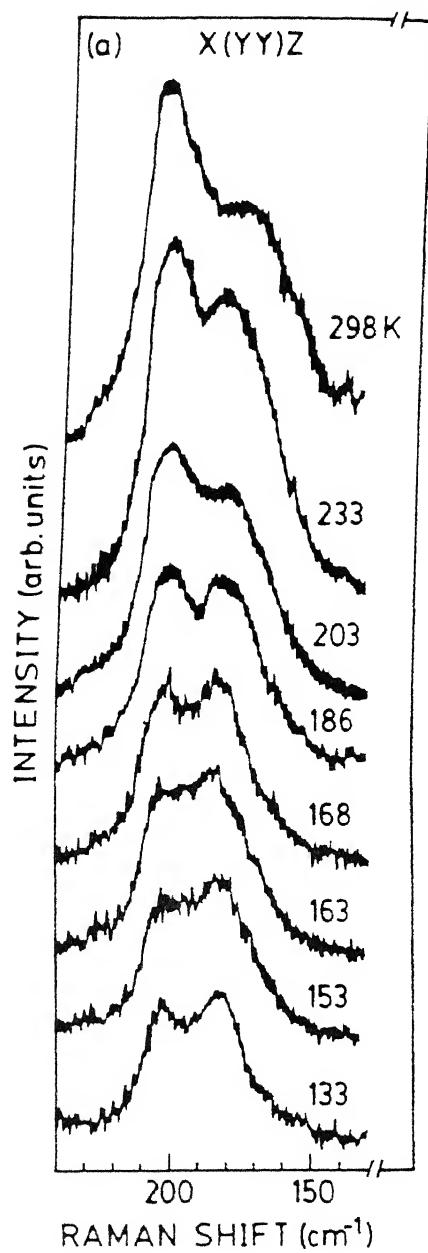
Fig 5.9 Thermal evolution of (a) $\delta(CCCN)$ and (b) $\nu(CC)$ modes of C_3CdCl.
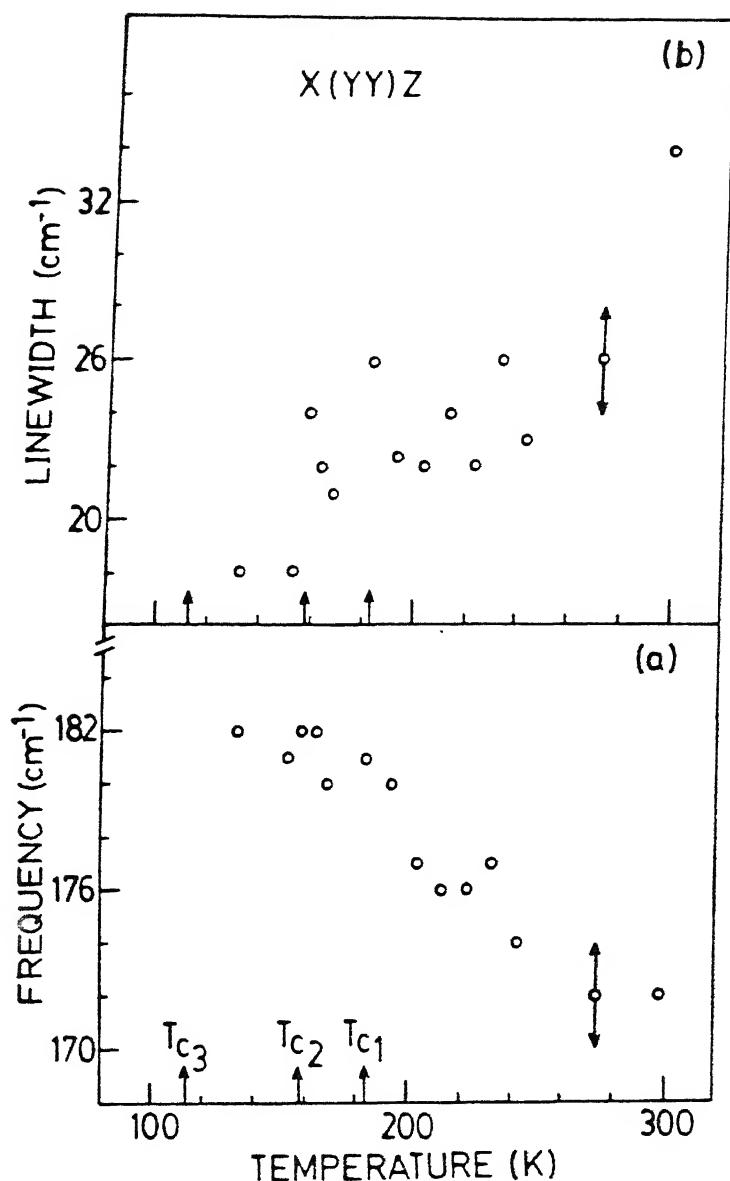
Fig 5.11 The Raman spectra of C_3CdCl in $\nu(CdCl)$ mode region in X(YY)Z geometry.

Fig 5.12 Thermal evolution of (a) peak frequency and (b) linewidth of the mode at 172 cm^{-1} (RT) of C_3CdCl in X(YY)Z geometry.
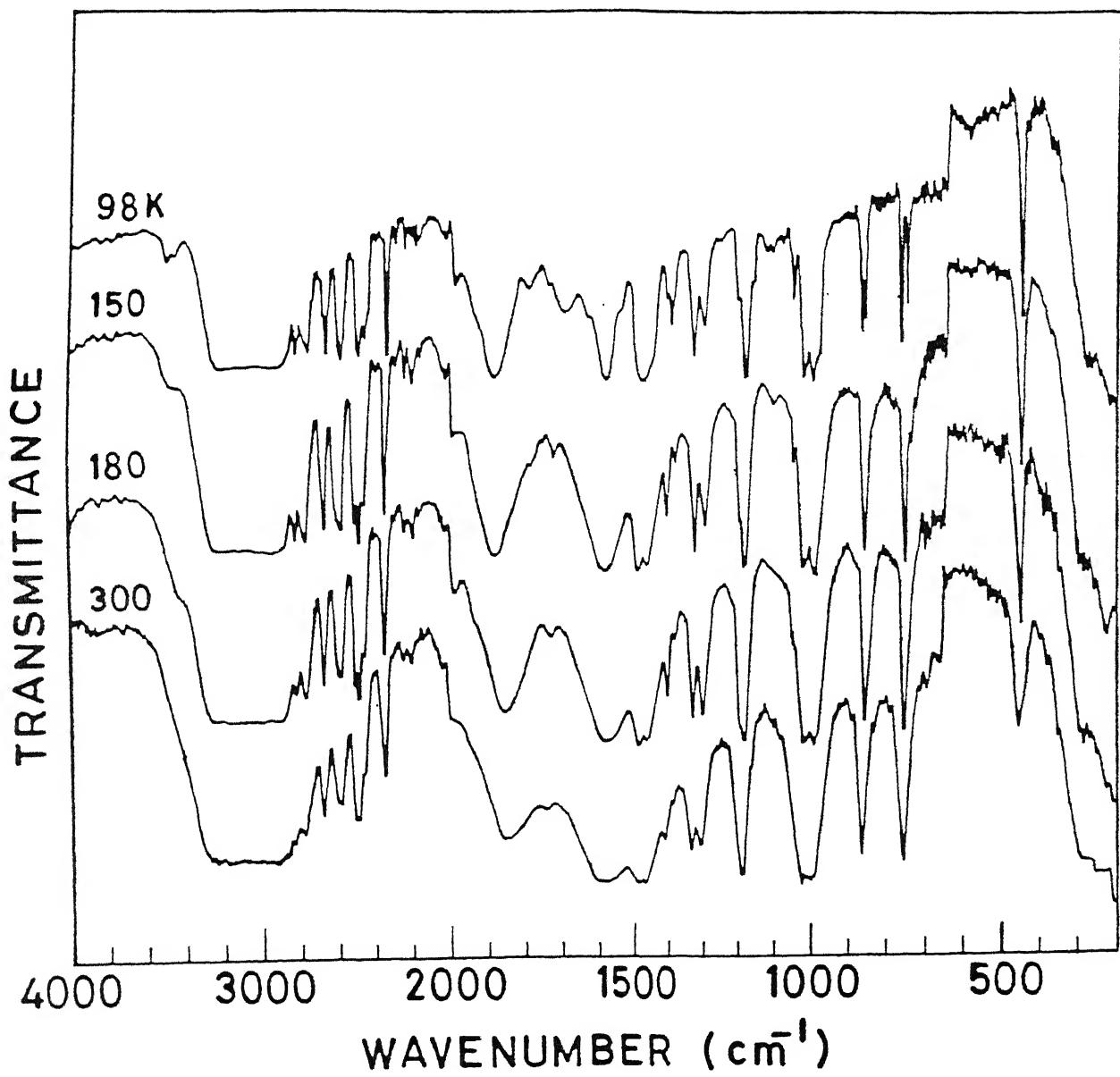
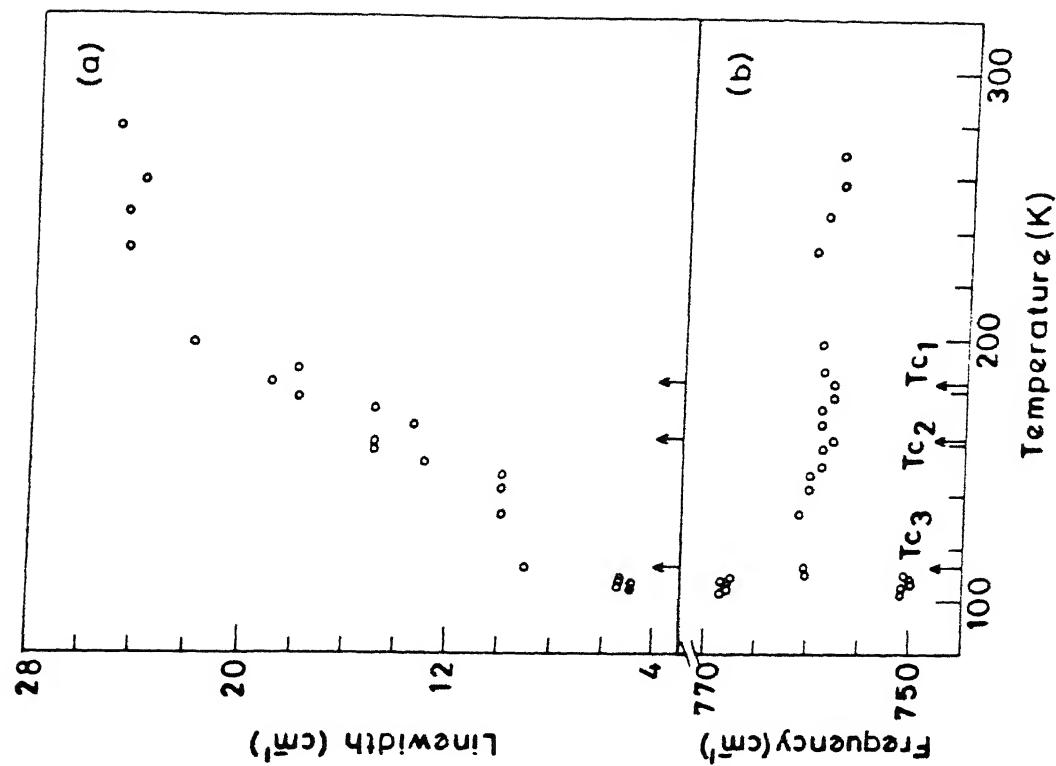Fig 5.13 IR spectra of C_3CdCl .in different phases.

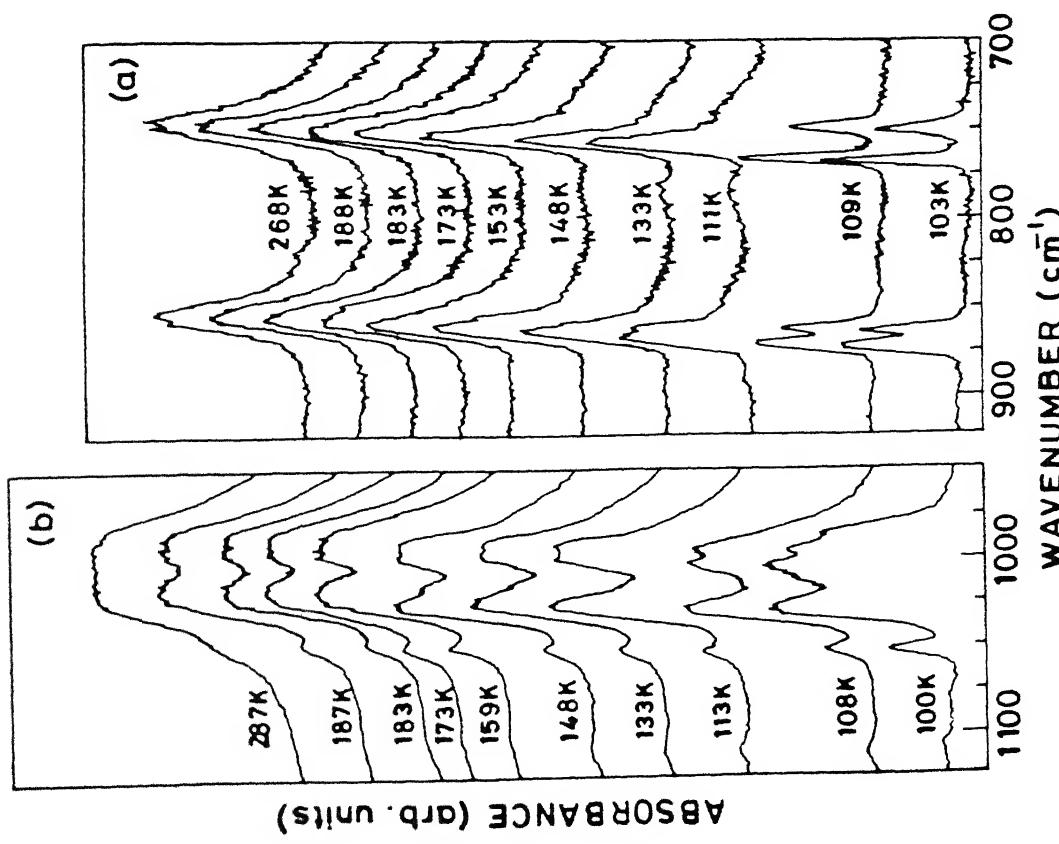Fig 5.15 Spectral parametric variations of $\rho(CH_2)$ mode of C_3CdCl.

Fig 5.14 Thermal evolution of IR modes of C_3CdCl in 700–1120 cm^{-1} range.
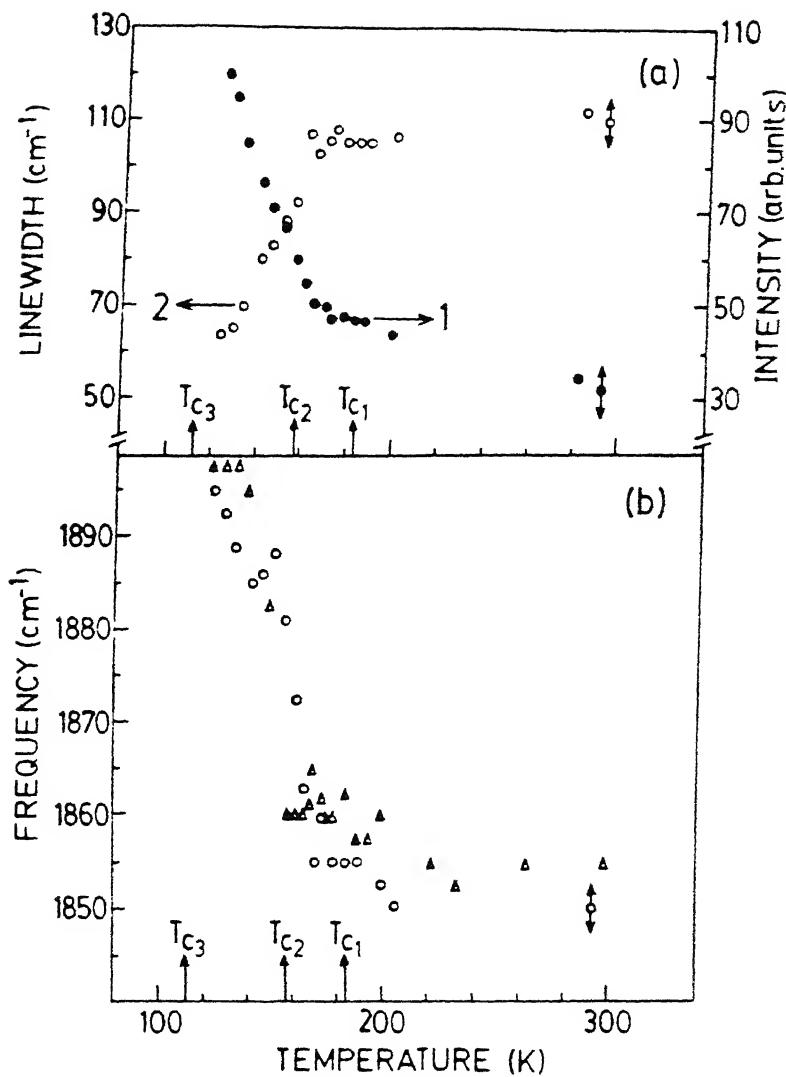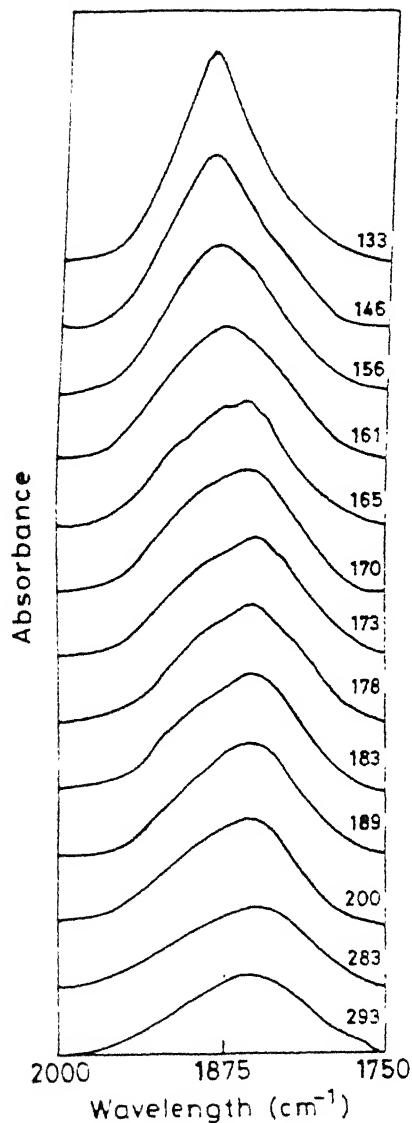
Fig 5.16 Recorded IR spectra in 1750-2000 cm^{-1} region of C$_3$CdCl.

Fig 5.17 Spectral parameter variations for δ_{asy}(NH$_3$)+τ(NH$_3$) mode in 110-300 K range.

CHAPTER VI

CONCLUDING REMARKS

In this thesis a detailed investigation of vibrational spectra of the compounds of the family $(C_nH_{2n+1}NH_3)_2MCl_4$ (abbreviated as C_nMCl) with M = Cd, Zn and Hg have been reported. Marginal shifts in the internal modes of methylammonium groups in C_1MCl with M = Cd, Zn and Hg crystals suggest that they are weakly linked with the inorganic layer. This kind of similarity has also been observed in $C_2H_5NH_3Cl$ and $C_3H_7NH_3Cl$ with their corresponding cadmium compounds $i.e.$, C_2CdCl and C_3CdCl. This particular observation corroborates the weak linkage between the two parts of the crystal. Further evidence of it is from its morphological appearance. The crystallization is difficult, specially in C_nCdCl systems. These crystals are very easily cleavable along XY plane.

Study in these perovskite type layered compounds is very interesting because they show several structural phase transitions (SPTs) in 500-77 K region. The mechanism of the SPTs is very complex. However, in short chain compounds many of the transitions are because of the reorientational motion of alkylammonium ions. The C_1MCl (with M = Cd, Zn and Hg) crystals show transitions in which the effect of reorientational motion can be easily observed through spectral variations. The rocking

modes of CH_3 and NH_3 groups in C_1CdCl at 160 K show anomalous variations reflecting the fact that a soft mode is coupled to them. Extremely sharp $\nu(CN)$ mode corroborates the fact that crystal is in orientationally ordered state. Estimated activation energy of 0.04 eV compares well with the NMR results. The transitions in C_1ZnCl and C_1HgCl are essentially due to the reorientational motion of methylammonium ions. Simultaneous variations in $\nu(MCl)$ (M = Zn and Hg) mode in these compounds also suggest that the inorganic layer has been significantly affected by the transition. Crystallographic studies would further throw light on the transitions.

Vibrational studies in $C_2H_5NH_3Cl$ and $(C_2H_5NH_3)_2CdCl_4$ crystals in the present study clearly corroborate the SPTs reported earlier. The transition at 345 K in C_2Cl induces many variations in the Raman spectra and could be classified as an order-disorder type. However, the transition at 221 K has not provided convincing spectral evidences. A careful structural investigation would prove to be important before proceeding with a detailed investigation. The transitions at 216 K in C_2CdCl has conveniently been attributed to an order-disorder type. Entire ethylammonium group seems to participate in the reorientational motion. The calculated activation energy from the spectral evolutions of few IR and Raman modes (0.06 eV) closely matches with the NMR results.

The Raman investigation in $C_3H_7NH_3Cl$ proves beyond doubt that the crystals undergo an order-disorder type

transition at 188 K. Anomalous increase in the Raman intensity of few skeleton modes indicates that the long range interactions dominate in lower temperature phase. A symbiotic study in C_3CdCl gives a convincing evidence that the transition at 158 K, which is thermodynamically equivalent to the 216 K transition in C_2CdCl, is not due to the ordering of propylammonium chain. This transition is triggered mainly due to the variation in hydrogen bonding strength.

The thermal variation observed for $\delta_{asy}(NH_3) + \tau(NH_3)$ mode in all C_nCdCl (n=1,2,3) systems indicate the strengthening of hydrogen bond in the ordered phase. Study of partially deuterated (NH_3 ends) samples would provide valuable information regarding the role of hydrogen bonding in the phase transition mechanism. Quantitative estimation of the variation in the strength of H-bonding would be an interesting problem from a theoretical point of view.

To improve the knowledge about these systems a detailed crystallographic studies are needed, specially in TLT phase of C_1CdCl. Likewise, the other well known SPT studies in C_1ZnCl and C_1HgCl systems will provide greater insight into the transition mechanism. The present study has provided sufficient indications about the transitions in C_2Cl and C_3Cl. However, lack of information about the crystal structure in other phases makes the vibrational analysis difficult. A detailed study using single crystals (difficult to grow) would certainly make the interpretation easier. In C_3CdCl, no convincing

spectroscopic evidence was observed for the reported incommensurate phase in 183-158 K range. A comparative study with other propyl compounds of the same family could provide some insight into the transition.

In this thesis a careful experimental investigation of SPTs in some perovskite type layered compounds is reported. The observed spectral variations are interpreted in the light of known SPTs. Very sharp changes have been observed during the order-disorder transitions. The order parameter exponent value is calculated in some crystals using the well established models. The calculated activation energies in few systems are in excellent agreement with the previous NMR results.

LIST OF PUBLICATIONS

i) **Journals**

1. Raman Spectroscopic Study of $(CH_3NH_3)_2HgCl_4$ in the High-Temperature Range, PSR Prasad, S Sathaiah and HD Bist, Chem Phys Lett., **142**, 341 (1987).

2. Vibrational Spectroscopic Study of the Structural Phase Transitions in Perovskite Laser Compounds $(CH_3NH_3)_2CdCl_4$, PSR Prasad and HD Bist, J Phys Chem Solids, **50**, 1033 (1989).

3. Vibrational Spectroscopy Study of Order-Disorder Transition in Ethylammonium Tetrachloro Cadmate, PSR Prasad and HD Bist, Phys Stat Sol., **116a**, 275 (1989).

4. Raman Investigation of Order-Disorder Transition in n-Propylammonium Chloride, PSR Prasad and HD Bist, Solid State Commu., **00**, 000 (1990).

ii) **Conferences**

1. Phase transitions in Bis (Propylammonium) Tetrachlorocadmate (PACC): An IR study, PSR Prasad and HD Bist, Proc. Solid State Symp. **30C**, 335 (1987).

2. Reorientational motion of Ethylammoniumchloride studied by Raman spectroscopy, PSR Prasad and HD Bist, Proc.Int.Conf. on Raman spectrosc. XI (London), 457 (1988).

3. Structural phase transitions in the Layer crystals of $(CH_3NH_3)_2CdCl_4$: Raman study, PSR Prasad and HD Bist, Int.Conf. on Raman spectrosc. (Calcutta), **abs** 59 (1988).

4. Raman spectroscopic study of $(CH_3NH_4)_2HgCl_4$ crystal near the phase transition, PSR Prasad and HD Bist, Int.Conf.on Raman spectrosc. XII 492 (1990).

PHY - 1990 - D - PRA - VIP